LIBRARY

INTERNATIONAL ATOMIC ENERGY AGENCY
UNITED NATIONS EDUCATIONAL, SCIENTIFIC AND CULTURAL ORGANIZATION

INTERNATIONAL CENTRE FOR THEORETICAL PHYSICS
34100 TRIESTE (ITALY) - P.O.B. 586 - MIRAMARE - STRADA COSTIERA 11 - TELEPHONES: 224281/2/3/4/5/6
CABLE: CENTRATOM - TELEX 460392-1

SMR/115 - 11

WINTER COLLEGE ON LASERS, ATOMIC AND MOLECULAR PHYSICS

(21 January - 22 March 1985)

OPTICAL BISTABILITY

L. LUGIATO
Dipartimento di Fisica
Università degli Studi
Via Celoria, 16
20133 Milano
Italy

These are preliminary lecture notes, intended only for distribution to participants.
Missing or extra copies are available from Room 229.

CONTEMP. PHYS., 1983, VOL. 24, NO. 4, 333–371

Optical Bistability

LUIGI A. LUGIATO

Istituto di Fisica dell'Università, Via Celoria 16, 20133 Milano, Italy

ABSTRACT. Optical bistability is a phenomenon that arises in the transmission of light by an optical cavity filled with a medium which presents saturable absorption or nonlinear dispersion. From the theoretical viewpoint, optical bistability is a remarkable example of cooperative behaviour in an open system driven far from thermal equilibrium. From the practical viewpoint, optical bistability offers the possibility of realizing memory elements that may perhaps be used to construct an optical computer. We illustrate the basic physical principles of optical bistability at steady state, and the main features of the transient behaviour. The role and the effects of fluctuations (noise) are described in general.

Particular attention is devoted to the situations in which the output of the system is not stationary in time, but oscillatory (self-pulsing behaviour), so that the system works as a converter of continuous wave light into pulsed. It is shown that, according to the values of the external parameters, the oscillations can be either periodic in time or completely aperiodic (optical turbulence). The state of the art in the problem of optical bistability is briefly discussed.

1. Introduction

1.1. *What is optical bistability?*

The subject of optical bistability (OB) has raised remarkable and continuous interest in the community of scientists working in Quantum Optics since Gibbs, McCall and Venkatesan reported its first observation (Gibbs *et al.* 1976). In this introduction, I shall try to explain in simple terms what OB is and why it focused such an enthusiastic attention both from theoreticians and experimentalists, including those mainly interested in technological aspects.

First, let us consider a resonant optical cavity, such as the Fabry–Pérot cavity shown in fig. 1 (*a*). The two mirrors M_1 and M_2 have transmissivity coefficient T which means that when a light beam of intensity I impinges one of these mirrors a fraction TI is transmitted while a fraction $(1-T)I$ is reflected. The function of an optical cavity is essentially that of selecting precise frequencies of the electromagnetic field. In fact only suitable modes of the field, with well defined spacial structures and well defined frequencies, can steadily oscillate in the cavity.

Now, let us inject into the cavity the light beam emitted by a laser operating in a continuous wave (c.w.) regime, a beam whose intensity I_1 is constant in time. The incident field frequency is assumed to be resonant or quasi-resonant with one of the cavity frequencies.

Let us consider first the case of the empty cavity (fig. 1 (*a*)). The incident beam is partly transmitted (I_T) and partly reflected (I_R). When we inject the incident beam there will be a transient stage during which the light enters into the cavity, but after a suitable time the system reaches a stationary or steady-state regime in which I_T and I_R are constant in time. In this regime, the transmitted intensity is proportional to the incident intensity, so $I_T = \mathcal{T} I_1$, where the proportionality constant $\mathcal{T}$, which is never larger than unity, depends on the transmissivity coefficient T and on the degree of resonance

FABRY-PEROT CAVITIES

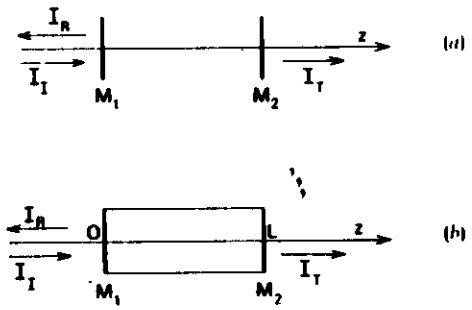

Fig. 1. (*a*) Empty Fabry Pérot cavity. I_I is the incident intensity; I_T and I_R are the transmitted and reflected intensities, respectively. (*b*) Fabry-Pérot cavity filled by an absorber.

between the incident field and the cavity (fig. 2(*a*)). In particular, for perfect tuning (i.e. resonance) one has that $\mathcal{T} = 1$.

The interesting case is when the cavity is filled with absorbing material, resonant or nearly resonant with the incident field. In this situation, part of the incident energy is absorbed by the medium. In turn, part of this absorbed energy is dissipated into heat, and part is reemitted as fluorescent light in all directions.

As we see in fig. 1 (*b*), a sample of length L is placed between the mirrors. We indicate by α the absorption coefficient per unit length of the material. In this case, the steady-state transmitted intensity becomes a *nonlinear* function of the incident intensity. The crucial parameter that determines the stationary behaviour of the system is the ratio between the total absorption αL that the light undergoes during each pass through the medium and the transmissivity coefficient T†

$$C = \frac{\alpha L}{2T} \tag{1}$$

Increasing C, we find that the steady-state curve of transmitted versus incident intensity first develops a portion in which the so-called 'differential gain', the derivative dI_T/dI_I, is larger than unity (fig. 2(*b*)). In this condition, the system works as an optical transistor. Let us modulate the incident field intensity sufficiently slowly to allow the system to follow the steady-state curve (adiabatic variation of the incident intensity). Hence this modulation is transferred to the transmitted beam and, as we see from fig. 2(*b*), the modulation depth turns out to be larger in the transmitted than in the incident field. This is precisely the transistor action, in which the incident intensity plays the role of the battery.

† The quantities α and C differ from those indicated by the same symbols in (Lugiato 1983) by a factor $1 + A^2$ (see (13)).

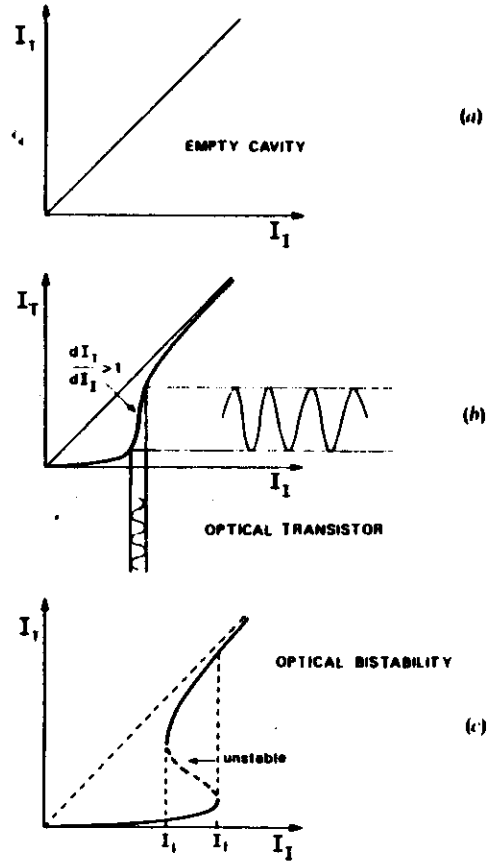

Fig. 2. (*a*) Transmitted intensity versus incident intensity for an empty cavity. (*b*) Optical transistor operation. (*c*) Bistable operation.

If we further increase the ratio $\alpha L/T$, the steady-state curve develops a portion with negative slope and becomes s-shaped (fig. 2(*c*)). Hence in this case I_T is a multivalued function of I_I. In fact, in the range of values $I_1 < I_I < I_2$ the system has three stationary solutions. However, the one which lies in the part with negative slope is unstable and therefore the system is *bistable*. If we adiabatically increase the incident field intensity, when we arrive at I_2 the system is forced to jump discontinuously to the higher transmission branch. If we now slowly decrease the incident intensity, the system remains in the upper branch until we reach the value I_1, at which the system returns discontinuously to the lower transmission branch. Thus, we obtain a *hysteresis cycle*. As we shall see in the following sections, the bistable behaviour arises essentially from

two ingredients: the nonlinearity of the atom field interaction, and the presence of mirrors. In fact, if we remove the mirrors the transmitted intensity is always a single-valued function of the incident intensity and therefore the bistability disappears. The function of the mirrors is to produce a feedback action on the electromagnetic field. When the incident beam arrives at the exit mirror M_2, part of it is reflected back and gives rise to a counterpropagating beam. When this second beam impinges on the other mirror M_1, a part of it is in turn reflected and hence feeds back the primary beam. The threshold value of the parameter C for which one gets bistability depends on several quantities and features such as the degree of resonance between the incident field, the material and the cavity, the atomic linewidth, the type of cavity and so on.

As is well known, when a light-beam goes through a medium one has basically two kinds of effect, absorption and dispersion, the latter being induced by the refractive index of the material. When the incident field is in perfect resonance with the atomic line the dispersion of the light plays no role, so that one has *purely absorptive bistability*. Otherwise, one has the mixed absorptive and dispersive case. When the difference between the frequency of the incident field and absorption by the material is so large that absorption becomes negligible one has *purely dispersive bistability*.

The systems we have described are usually called *all-optical (or intrinsic) bistable systems*. On the other hand, there are also the so-called *hybrid electro-optical systems*, which have been devised in many variants. A typical device of this type is obtained by replacing the absorber by an electro-optic crystal, which is monitored by the output field and produces changes in refractive index proportional to the output power. In this article, we shall consider only the all-optical systems.

From our brief description it is immediately evident that our optically bistable systems have a large technological interest. We have already seen that in the non-bistable regime they can work as optical transistors. On the other hand, in the bistable situation they can work as *optical memories*, in which information can be stored. In fact, in the range $I_1 < I_1 < I_1$ (fig. 2(c)) the lower and the upper states are the 0 and the 1 of a memory element, and by suitably varying the incident field intensity one can switch from one state to the other as illustrated in fig. 3. Of course, in order to build an optical computer one must assemble a very large number of elements of this type, so each element must be miniaturized. Therefore there is a big effort towards the construction of practical, miniaturized and fast operating bistable optical devices of this kind. These devices can also work as pulse shapers that tailor the incident light pulses in many different ways, by amplifying part of them and eliminating others, suppressing the noisy parts (clippers, discriminators, limiters and so on). Finally, as we shall see later, these systems can work as converters of c.w. coherent light into pulsed light.

On the other hand, OB has also raised wide theoretical interest, renewing in part the enthusiasm that in the sixties was devoted to the laser. In fact, OB is a remarkable example of cooperative behaviour in an open system far from thermal equilibrium, and therefore it naturally receives a chapter of Haken's *Synergetics* (Haken 1977) and of Prigogine's theory of dissipative structures (Nicolis and Prigogine 1977). First of all, the steady-state hysteresis cycle of OB suggests an immediate analogy to *first-order phase transitions* in equilibrium systems. Furthermore, by controlling the incident intensity one can induce the emergence of *spontaneous pulsations* in the system, in which the transmitted intensity is no longer stationary in time, but is given by an undamped sequence of pulses. According to the external control parameters, this sequence can be either perfectly periodic in time (*regular self-pulsing behaviour*) or completely irregular (*chaotic behaviour* or *optical turbulence*).

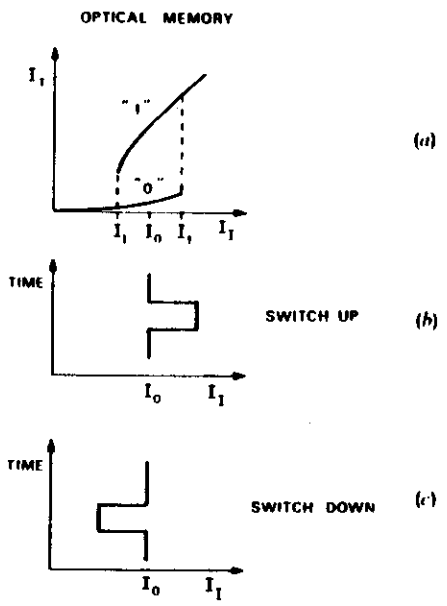

Fig. 3. (*a*) Optical memory. I_0 is the holding intensity. (*b*) Switch up operation. The system is initially in the lower branch at $I_1 = I_0$. By the pulse shown in the figure, the system switches to the upper branch. Eventually the system is in the upper branch at $I_1 = I_0$. (*c*) Switch down operation. The system is initially in the upper branch at $I_1 = I_0$. By the pulse shown in the figure, the system switches to the lower branch. Eventually the system is in the lower branch at $I_1 = I_0$.

1.2. *A brief historical sketch*

The complete history of OB is very lengthy, so I will restrict myself to a short description of the first basic stages of this story.

Absorptive OB was first theoretically predicted by Szöke and collaborators (1969). Some years later McCall (1974) proved that under suitable conditions the same system can show differential gain larger than unity with transistor action and on the other hand treated absorptive OB in a Fabry–Pérot cavity by numerical analysis of the so-called Maxwell–Bloch equations. This work suggested the experiments of Gibbs *et al.* (1976) in Na, in which both transistor operation and bistability were observed. The analysis of the data showed that the observed bistability was of dispersive type, with few exceptions. The mechanism which produces dispersive OB was explained with the help of a simple cubic model.

Felber and Marburger (1976) gave an analytical treatment of dispersive OB in a Kerr medium. Bonifacio and Lugiato (1976) initiated a theoretical treatment of OB which is both from first principles and analytical, with particular emphasis on the cooperative behaviour and on the analogy with first-order phase transitions. Smith and Turner (1977) proposed and demonstrated the operation of an electro-optic bistable device. All these results stimulated some very active research, both theoretical and

experimental, that split into two distinct directions. The first channel is mainly technological and devoted to the device aspects, using both all-optical and electro-optical systems. The other channel is devoted to the fundamental aspects of OB and related phenomena.

1.3. *Plan of the article*

In this article I shall try to give an elementary description of OB and of the phenomena that are directly related to it. For further details, I refer the reader to the recent review articles by Abraham and Smith (1982 b) and by Lugiato (1983). Other shorter reviews can be found in articles by Gibbs *et al.* (1979 b, 1980) Lugovoi (1979), Collins and Wasmundt (1980), Bonifacio (1982), Abraham and Smith (1982 a). Collections of papers on optical bistability can be found in the Proceedings of the Asheville Conference edited by Bowden *et al.* (1981) and in the special issue of IEEE *Journal of Quantum Electronics* edited by Smith (1981).

In Section 2, I describe in detail the various elements (incident field, cavity, atomic system) that enter into optical bistability. Section 3 gives an extensive description of optical bistability at steady state, emphasizing the main physical principles and encompassing both dispersive and absorptive OB. In particular, in Section 3.3 I work out the analogy with first-order phase transitions in equilibrium systems. Section 4 is devoted to the treatment of the transient approach to steady state, with particular emphasis on the so-called critical slowing down. In Section 5, I deal with noise and outline the quantum statistical treatment of OB, thereby completing the analogy with first-order phase transitions. Section 6 illustrates the main features of the pulsed behaviour in OB, including both regular self-pulsing and chaotic behaviour (optical turbulence). Finally, in Section 7 I outline briefly the state of the art in the problem of constructing a practical optical bistable device which can be the basic element for the future realization of an optical computer.

2. The elements of the OB systems

The essential ingredients of OB are the incident field, the optical cavity and the atomic (or molecular) system.

2.1. *The incident field*

The incident field comes from an external laser which operates in a c.w. regime. As is well known, laser light is coherent. Roughly speaking, this means that the light is monochromatic and its intensity is perfectly constant in time. Actually, in real lasers the stituation is not so ideal. The intensity exhibits some small fluctuations around its mean value. The phase of the field is not fixed but undergoes random jitters which bears the consequence that the light has a finite linewidth or is not perfectly monochromatic. In the following treatment I shall neglect these features for the sake of simplicity and assume that the incident light is perfectly coherent.

If we consider a section of the laser beam, we can see that its intensity decreases from the centre of the beam, following a Gaussian law. Again for reasons of simplicity, I shall neglect this radial variation of the electric field and assume that this field is a plane wave with respect to the transverse directions. In fact, this approximation changes the results quantitatively whereas most qualitative features remain basically unchanged. Hence, if we call z the direction of propagation of the incident beam (see fig. 1), the electric field will in general depend on z as well as on the time variable t, but will be independent of the transverse variables x and y.

2.2. *The cavity*

By suitably arranging a number of mirrors, we build an optical cavity. In accord with our plane wave assumption, we consider only plane mirrors. The most common type of cavity is the Fabry–Pérot with plane parallel mirrors, as in fig. 1. Another type is the ring cavity shown in fig. 4, in which the incident beam $\mathcal{E}_I$ enters from the left. The injected beam is in part reflected ($\mathcal{E}_R$) and in part propagates in the medium. At the exit mirror 2, the light is in part transmitted ($\mathcal{E}_T$) and in part returns to the entrance mirror 1 after reflection on mirrors 3 and 4. I shall assume that mirrors 3 and 4 have 100% reflectivity, and call T the transmissivity coefficient of mirrors 1 and 2. Also, I indicate by R the reflectivity coefficient $R = 1 - T$.

As is well known, an optical cavity supports only well-defined frequencies. In the case of a ring cavity, the circular frequencies are $2\pi cn/\mathscr{L}$, where $n = 0, 1, 2, \ldots$, c is the velocity of light and $\mathscr{L}$ is the total length of the ring cavity ($\mathscr{L} = 2(L+l)$), (see fig. 4). In the case of Fabry–Pérot cavity the circular frequencies are $\pi cn/L$ (see fig. 1). In both cases the cavity modes are equally spaced. From the viewpoint of theory, the ring cavity is easier to treat because the light propagates in only one direction, whereas in a Fabry–Pérot cavity one has counterpropagating beams. For this reason, we shall restrict ourselves to the case of ring cavity. If we indicate the amplitude of the electric field by $\mathcal{E}(z, t)$ and look at fig. 4, we realize that the field $\mathcal{E}(0, t)$ at $z = 0$ arises from two different contributions: the incident field $\mathcal{E}_I$ transmitted by mirror 1 and the field $\mathcal{E}(L, t)$ at $z = L$ successively reflected by all the mirrors of the cavity

$$\mathcal{E}(0, t) = \sqrt{(T)}\mathcal{E}_I + R\mathcal{E}(L, t - \Delta t). \tag{2 a}$$

The square root in front of $\mathcal{E}_I$ comes from the fact that T is the transmissivity coefficient of the intensity and the electric field is the square root of the intensity. The factor R in front of the second term comes from the two reflections on mirrors 2 and 1 ($R = \sqrt{R} \cdot \sqrt{R}$). The reflections on mirrors 3 and 4 do not give factors because these mirrors have reflectivity coefficient equal to unity. Finally, the retardation Δt is the time the light takes to travel from mirror 2 to mirror 1 and is equal to $(L + 2l)/c$ (see fig. 4).

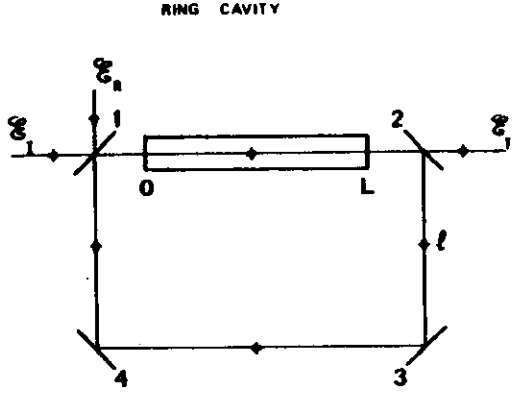

Fig. 4. $\mathcal{E}_I$, and $\mathcal{E}_T$ and $\mathcal{E}_R$ are the incident, transmitted and reflected field amplitudes respectively.

The second term in (2 a) gives a feedback contribution that, as we shall see, is essential for the rise of bistability.

Let us call ω_0 the angular frequency of the monochromatic incident field and $k_0 = \omega_0/c$ the corresponding wave vector. Now, ω_0 is also the central frequency of the electric field inside the cavity and therefore it is suitable to put it in evidence by writing

$$\left.\begin{aligned} &\mathcal{E}(z,t) = E(z,t)\exp[-i(\omega_0 t - k_0 z)] + E^*(z,t)\exp[+i(\omega_0 t - k_0 z)] \\ &\begin{Bmatrix}\mathcal{E}_I\\ \mathcal{E}_T\end{Bmatrix}(t) = \begin{Bmatrix}E_I\\ E_T\end{Bmatrix}(t)\exp(-i\omega_0 t) + \begin{Bmatrix}E_I\\ E_T^*\end{Bmatrix}(t)\exp(i\omega_0 t); \end{aligned}\right\} \tag{3}$$

where $E(z,t)$ varies in space and time much more slowly than the exponential factor, and is therefore called the *slowly varying envelope* of the electric field. Note that contrary to $\mathcal{E}$, which is real by definition, the envelope E is in general complex. The incident field E_I has been assumed real and positive for definiteness. If we now substitute (3) into (2 a), after some calculation we obtain

$$E(0,t) = \sqrt{(T)}E_I + R\exp(-i\delta_0)E(L, t-\Delta t) \tag{2 b}$$

where the cavity detuning parameter δ_0 is given by

$$\delta_0 = \frac{\omega_c - \omega_0}{c/\mathscr{L}} \tag{4}$$

with ω_c being any of the cavity frequencies; for definiteness, we consider the cavity frequency that is nearest to the incident frequency ω_0. Hence in the case of perfect resonance between cavity and incident field one has $\delta_0 = 0$. Another relation that is obvious from simple inspection of fig. 4 is the following

$$E_T(t) = \sqrt{(T)}E(L,t). \tag{5}$$

The relation (2 b) can immediately be reinterpreted in terms of transmission of the *empty cavity*. In fact, in the steady state E does not depend on time and in the case of an empty cavity one has simply $E(0) = E(L)$ Hence by combining (2 b) and (5) and defining the incident and transmitted intensities

$$I_I = E_I^2, \quad I_T = |E_T|^2 \tag{6}$$

one finds after some calculation the following well-known expression for the transmission $\mathscr{T}$ of the cavity

$$\mathscr{T} \equiv \frac{I_T}{I_I} = \frac{1}{1 + \dfrac{4R}{T^2}\sin^2\dfrac{\delta_0}{2}}. \tag{7}$$

If we plot $\mathscr{T}$ as a function of the detuning parameter $\delta_0 c/\mathscr{L}$ we obtain the graph of fig. 5 with peaks and valleys. The peaks correspond to the cavity frequencies; that is, the empty cavity transmits only its own frequencies. The width of each peak is

$$k = \frac{cT}{\mathscr{L}\sqrt{R}} \tag{8}$$

For this reason, k is called the *cavity linewidth*.

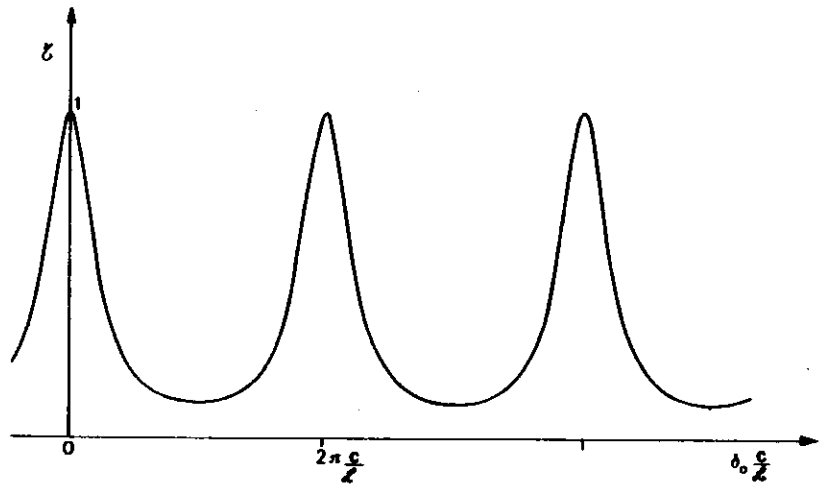

Fig. 5. The transmission of the empty cavity is graphed as a function of the cavity detuning parameter $\delta_0 c/\mathscr{L} = \omega_c - \omega_0$.

2.3. *The atomic system*

Although the absorbing sample can consist of molecules as well as atoms, I shall, for the sake of definiteness, always speak of atoms. In the so-called dipole approximation, the atom-field interaction energy is given by

$$H_{int} = -\mathscr{P}\cdot\mathcal{E} \tag{9}$$

where $\mathscr{P}$ is the total atomic dipole moment (the macroscopic atomic polarization). A point of paramount importance is that, even if (9) is linear in the field variable as well in the atomic variable separately, it is *nonlinear* in the two variables taken simultaneously. This feature implies the nonlinear character of the atom- field interaction, which in turn gives rise to all the interesting phenomena in the field of Quantum Optics, including OB.

Exactly as I did with the electric field, let me introduce a slowly varying envelope for the atomic polarization, by writing

$$\mathscr{P}(z,t) = P(z,t)\exp[-i(\omega_0 t - k_0 z)] + P^*(z,t)\exp[+i(\omega_0 t - k_0 z)]. \tag{10}$$

In the steady state, one has in general

$$P = E\chi(|E|^2), \tag{11}$$

where χ is the dielectric susceptibility of the medium, which is proportional to the absorption coefficient α. For weak fields χ can be taken as constant so that P turns out to be proportional to E. However, in Quantum Optics we consider also intense fields and in this case P becomes in general a nonlinear function of E, which depends of course on the atomic medium. The susceptibility is a complex quantity

$$\chi = \chi_d + i\chi_a, \tag{12}$$

where the real part χ_d affects the *phase* of the electric field and is responsible for dispersion, while the imaginary part χ_a affects the *modulus* of the electric field and is responsible for absorption.

A situation that is particularly simple from the theoretical viewpoint is when the process involves the transition between two energy levels only. In this case we speak of *two-level atoms* (Allen and Eberly 1975), see fig. 6. We indicate by ω_a the Bohr transition frequency $\omega_a = (W_1 - W_0)/\hbar$, where $\hbar$ is Planck's constant and W_i $(i = 0, 1)$ are the energies of the two levels. As is well known, the interaction with the electromagnetic field induces three kinds of processes: spontaneous emission, stimulated emission and absorption.

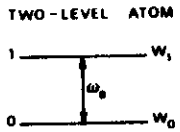

Fig. 6.

Spontaneous emission occurs when the field is in the vacuum state (no photons) and the atom is in the excited state. With a time constant which is called the *natural lifetime*, the atom decays exponentially to the ground state. The main effect of spontaneous emission is that the excited level acquires a finite width termed its *natural linewidth*. This linewidth is increased by any process, such as collisions between atoms, that shortens the lifetime of the excited level. In the following I shall indicate by γ the atomic linewidth, which arises from spontaneous emission and collisions.

Stimulated emission arises when an electromagnetic field with n photons interacts with the atom in the excited level and as a result the atom decays to the ground state emitting one photon more. Finally, one has absorption when the same field impinges on the atom in the ground state and as a consequence the atom performs a transition to the upper state absorbing one photon.

In the case of the laser, one 'pumps' the atoms in order to obtain a situation of population inversion in which the upper level is more populated than the lower level. Hence in the laser stimulated emission overcomes absorption. On the contrary, in the case of OB one does not pump the atoms, the lower level is always more populated, and hence absorption overcomes stimulated emission.

Note that in general the atoms need not all have the same transition frequency. In fact, there are two main mechanisms that can render the atomic transition frequencies unequal. One is the motion of the atoms in gases. In fact, owing to the Doppler effect groups of atoms with different velocity also have different frequencies. The other mechanism is the presence of impurities or defects in solids. Hence in general we have not a single atomic frequency but a frequency *distribution*. In this case, I shall indicate by ω_a the central frequency of this distribution. The width of the distribution is called the *inhomogeneous linewidth* in contrast to the *homogeneous linewidth* γ already discussed. When the inhomogeneous linewidth is small with respect to the homogeneous one, the atomic system is said to be *homogeneously broadened*; otherwise, one speaks of *inhomogeneous broadening*. Finally, we observe that the dispersive part χ_d of

the susceptibility turns out to be proportional to the atomic detuning parameter Δ which is defined by

$$\Delta = \frac{\omega_a - \omega_0}{\gamma} \tag{13}$$

and therefore vanishes when the atomic line is perfectly resonant with the driving field frequency ω_0.

3. The physical principles of optical bistability at steady state

For the sake of simplicity I shall consider the case of the ring cavity.

Let me indicate by ρ and φ the modulus and the phase of the electric field inside the sample

$$E(z, t) = \rho(z, t) \exp[i\varphi(z, t)] \tag{14}$$

In the steady state, ρ and φ obey the differential equations

$$\frac{d\rho}{dz} = -\alpha\rho\tilde{\chi}_a(\rho^2) \tag{15a}$$

$$\frac{d\varphi}{dz} = -\alpha\Delta\tilde{\chi}_d(\rho^2) \tag{15b}$$

where $\tilde{\chi}_a$ and $\tilde{\chi}_d$ are proportional to χ_a and χ_d respectively, and are defined in such a way that the factors α and $\alpha\Delta$ are put in evidence in the two equations; in particular $\tilde{\chi}_a(0) = 1$. The physical interpretation of (15 a) is obvious. In fact, in the limit of small fields $\tilde{\chi}_a = 1$ so that

$$\rho(z) = \rho(0) \exp(-\alpha z) \tag{16}$$

which is the usual Beer's exponential absorption law. Now using (2 b), (5) and (6) one obtains the following general expression for the transmission of a filled ring cavity:

$$\mathcal{T} \equiv \frac{I_T}{I_1} = \frac{T^2}{(\eta - R)^2 + 4R\eta \sin^2 [\frac{1}{2}(\delta_0 - \Delta\varphi)]} \tag{17}$$

where

$$\left.\begin{aligned} \eta &\equiv \frac{\rho(0)}{\rho(L)} \geq 1 \\ \Delta\varphi &\equiv \varphi(L) - \varphi(0). \end{aligned}\right\} \tag{18}$$

When the cavity is empty ($\tilde{\chi}_a = \tilde{\chi}_d = 0$), from (15) we get $\eta = 1$ and $\Delta\varphi = 0$, so that (17) reduces to (7). Note also that in the limit $\tilde{\chi}_a = 1$, η is equal to $\exp(\alpha L)$, see equation (16). The crucial point is that η and $\Delta\varphi$ are in general functions of the transmitted intensity, $\eta = \eta(I_T)$ and $\Delta\varphi = \Delta\varphi(I_T)$. These functions can be explicitly calculated by solving the differential equations (15 a) and (15 b) and taking (5) and (6) into account. If we substitute the expressions $\eta(I_T)$ and $\Delta\varphi(I_T)$ in (17) and solve equation (17) with respect to I_1, we obtain immediately the explicit expression of I_1 as a function of I_T:

$$I_1 = f(I_T)$$

$$f = \frac{I_T}{T^2}\left\{[\eta(I_T) - R]^2 + 4R\eta(I_T)\sin^2[\tfrac{1}{2}(\delta_0 - \Delta\varphi(I_T))]\right\}$$

The function f is single-valued by definition; however if we plot f (fig. 7(*a*)) and if we exchange the axes in order to have a graph of I_T versus I_I (fig. 7(*b*)) we see that the inverse function can be multivalued: the curve of I_T versus I_I can be S-shaped, and in this case we obtain bistability.

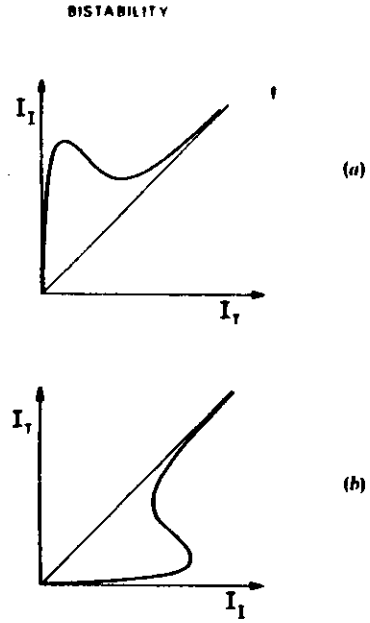

Fig. 7. Graphs of (*a*) incident field intensity as a function of transmitted field intensity and (*b*) transmitted field intensity as a function of incident field intensity.

3.1. *Dispersive bistability in a Kerr medium*

In a Kerr medium, we have

$$\tilde{\chi}_a = 0, \quad \tilde{\chi}_d = c_1 + c_2\rho^2 . \tag{19}$$

Hence from equations (18), (15) and (5) we obtain immediately

$$\eta = 1, \quad \Delta\varphi = a_1 - a_2 I_T \tag{20}$$

where $a_1 = -\alpha\Delta L c_1$, $a_2 = \alpha L \Delta c_2 / T$. Hence using (17) we have

$$\mathcal{F} \equiv \frac{I_T}{I_I} = \left(1 + \frac{4R}{T^2}\sin^2\left\{\tfrac{1}{2}[(\delta_0 - a_1) + a_2 I_T]\right\}\right)^{-1} \tag{21}$$

If we plot $\mathcal{F}$ versus $I' = a_2 I_T$ we obtain (fig. 8) a curve that coincides with the empty cavity graph (7) of $\mathcal{F}$ versus δ_0 (fig. 5), but for a translation by a quantity $\delta_0 - a_1$. The stationary solutions can be found following a simple graphical procedure devised by Felber and Marburger (1976). In fact, we must simply intersect our curve with the

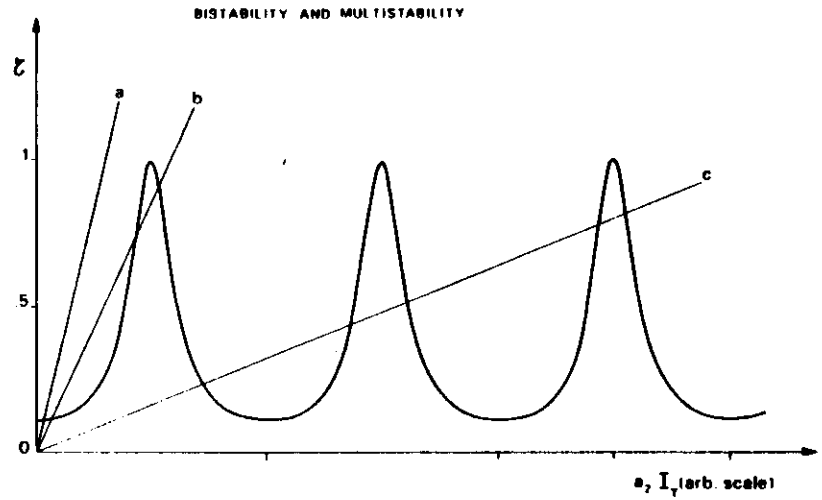

Fig. 8. Graphical calculation of the stationary solution for a Kerr medium. I' is defined as $a_2 I_T$ (see text).

straight line $\mathcal{F} = I_T/I_I = I'/a_2 I_I$, whose slope is inversely proportional to the incident intensity. For small I_I one has only one intersection (line a)). By increasing I_I the intersections become three (line b)), which correspond to a bistable situation because the solution in the middle is unstable. Hence if one plots I_T versus I_I, one finds a hysteresis cycle. For larger values of I_I one obtains multiple solutions (line c)), which lead to multistability and multiple hysteresis cycles. When T approaches unity, the curve (21) flattens and bistability disappears.

3.2. *Absorptive bistability for zero cavity detuning*

Let us now assume that the incident field, the atoms and the cavity are perfectly in resonance so that $\delta_0 = \Delta = 0$ (see equations (4) and (13)). This is a case of purely absorptive OB. Hence at steady state equation (2b) reads

$$E(0) = \sqrt{(T)}E_I + RE(L) \tag{22}$$

and the field E is real, i.e. $\varphi = 0$, $\rho = E$. Now we shall calculate the stationary solution following a graphical method due to Bonifacio and Lugiato (1978a). By solving (15a) one obtains an expression for $E(0)$ as a function of $E(L)$. Let us assume that this curve has the shape shown in fig. 9, as in the case of a homogeneously broadened two-level atomic system. The typical features of this curve for large αL are:

(i) When $E(0)$ is small, $E(L)$ is much smaller than $E(0)$ because there is strong absorption, which follows Beer's law (16).

(ii) For $E(0)$ large, $E(L)$ is practically equal to $E(0)$ (the medium is transparent). In fact, for large fields $\tilde{\chi}_a(E^2) \simeq 0$, hence $dE/dz \simeq 0$. This phenomenon is called *saturation* of the atomic medium. It arises because the electric field also populates the upper level of the (two-level) atoms. For strong fields, the two

(14)

STATIONARY SOLUTIONS

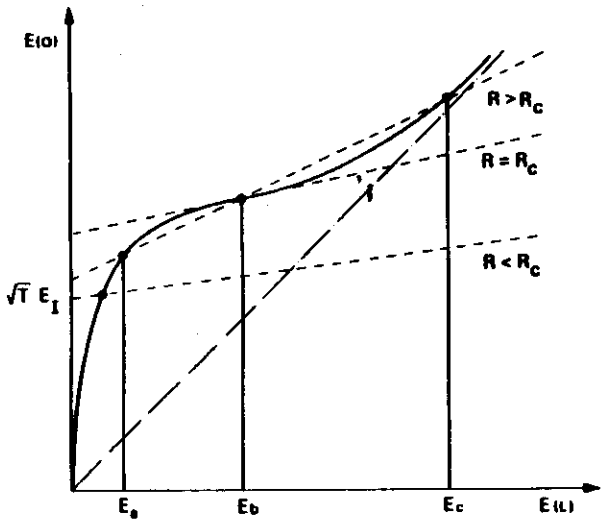

Fig. 9. Graphical calculation of the stationary solutions for absorptive OB with zero cavity detuning. The curve represents the transfer function of the medium.

levels become equally populated, hence the probabilities of stimulated emission and absorption are also equal, which implies transparency.

(iii) Between the strong absorption and the saturation regions, the curve of $E(0)$ versus $E(L)$ has an inflection point. The slope R_c of the tangent at the inflection point is such that $0 < R_c < 1$ and depends only on αL.

The stationary solutions are obtained by intersecting the curve of fig. 9 with the straight line (22) which has a slope R and intercept at $E(L)=0$ equal to $\sqrt{(T)}E_I$. Hence for $R < R_c$ there is only one intersection point for all values of E_I. For $R > R_c$ there is a range of values of E_I for which one finds three intersection points $E_a < E_b < E_c$. Points E_b are unstable; hence there is a bistable situation. If we plot the steady-state values of $E_T = \sqrt{(T(E(L)}$ as a function of the incident field E_I, we obtain an S-shaped curve which leads to a hysteresis cycle.

From this analysis we see that bistability arises from the combined action of the nonlinearity of the transfer function of the medium (fig. 9) and the feedback action of the mirrors (equation (22)). This action is essential because as one sees from fig. 9 there is no bistability for $R=0$ (absence of mirrors).

3.3. *Steady-state equation in the mean-field limit*

The relation which links the incident and the transmitted fields takes a particularly simple analytical form in the limit of small absorption, small transmissivity and small

(15)

cavity detuning, when $\alpha L \ll 1$, $T \ll 1$, $\delta_0 \ll 1$. Mathematically, these conditions are expressed by the limit

$$\alpha L \to 0, \quad T \to 0, \quad \delta_0 \to 0 \tag{23}$$

with

$$C = \frac{\alpha L}{2T} \text{ constant}, \quad \theta = \frac{\delta_0}{T} \text{ constant}.$$

This is called the 'mean-field limit' because for $\alpha L \to 0$ the electric field becomes uniform in space, so that its value at the output face of the atomic sample coincides with its mean value in space. Note that here the phrase 'mean-field' has a different meaning from the one used in other fields of physics such as the Landau theory of equilibrium phase transitions. In the limit (23) one obtains the following 'equation of state', that expresses the incident intensity as a function of the transmitted intensity:

$$I_I = I_T\{[1 + 2C\tilde{\chi}_a(I_T)]^2 + [\theta - 2C\Delta\tilde{\chi}_d(I_T)]^2\} \tag{24 a}$$

Let me now briefly comment on the physical meaning of the limit (23). First, $\alpha L \to 0$ means that the interaction between the electric field and the atoms becomes very weak. If we let $\alpha L \to 0$ but keep T finite, C vanishes and therefore we obtain the empty cavity solution $I_T = I_I/(1+\theta^2)$. By contrast, if we also let $T \to 0$ the bistability parameter C is arbitrary and we obtain the nonlinear terms in equation (24) which produce all the interesting phenomena. The physical meaning of the limit $T \to 0$ is that the mean lifetime $\mathscr{L}/cT$ of the photons in the cavity becomes very long so that the photons experience the interaction with the atoms even when this becomes very weak. Finally the limit $\delta_0 \to 0$, while $\theta = \delta_0/T$ remains finite, means that the cavity detuning $\omega_c - \omega_0$ must be much smaller than the distance $2\pi c/\mathscr{L}$ between the resonant mode and the adjacent modes of the cavity (see equation (4)), but on the other hand it must be of the same order of magnitude as the cavity linewidth (see equation (8)), otherwise nothing could be transmitted. Hence this limit implies that the system operates only with the cavity mode nearest to resonance with the incident field (single mode operation).

In the particular case of a homogeneously broadened, two-level atomic system equation (24 a) reads explicitly

$$I_I = I_T\left\{\left[1 + \frac{2C}{1 + \dfrac{I_T}{(1+\Delta^2)I_s}}\right]^2 + \left[\theta - \frac{2C\Delta}{1 + \dfrac{I_T}{(1+\Delta^2)I_s}}\right]^2\right\} \tag{25 a}$$

where I_s is the so-called 'saturation intensity' of the atomic medium, which depends on the atomic linewidth and on the dipole moment of the transition between the two levels.

On the basis of equations (24 a) and (25 a) we can now discuss the physical mechanisms which give rise to hysteresis in absorptive and dispersive OB. In the absorptive case ($\Delta = 0$), let us consider for simplicity the resonant situation $\theta = 0$ ($\omega_c = \omega_0$). Hence equations (24 a) and (25 a) become respectively

$$I_I = I_T[1 + 2C\tilde{\chi}_a(I_T)]^2 \tag{24 b}$$

$$I_I = I_T\left[1 + \frac{2C}{1 + \dfrac{I_T}{I_s}}\right]^2 \tag{25 b}$$

For small incident intensity, the transmission is small because of the presence of the absorber. Most of the incident light is reflected by the cavity. Increasing the incident field, the absorber begins to saturate. By decreasing absorption, this in turn increases the electric field which again increases the saturation and so on, until the absorber becomes transparent so that $I_T \simeq I_I$ and the system switches to the upper branch of the hysteresis cycle. On the other hand, when the system is in the higher transmission branch and the incident intensity is decreased, the field internal to the cavity is already strong enough to maintain the absorber saturated and therefore the transmitted light switches down at an incident intensity lower than that necessary to switch up, thereby producing hysteresis.

In the case of purely dispersive bistability the mechanism is quite different (Gibbs *et al.* 1976). In this situation, equation (24 a) reduces to

$$I_I = I_T\{1 + [\theta - 2C\Delta\tilde{\chi}_d(I_T)]^2\}. \tag{24 c}$$

In the case of the empty cavity ($C = 0$), the transmission is low because the cavity frequency ω_c is detuned from the incident frequency ω_0. If in the filled cavity the atomic and cavity detunings have the same sign, increasing the incident field (and hence the nonlinear refractive index related to χ_d) changes the effective optical length of the cavity towards resonance. This in turn increases the internal field which further drives the effective cavity frequency $\omega_c' = \omega_c - 2Ck\Delta\tilde{\chi}_d$ towards the incident frequency ω_0 and so on, until resonance is reached so that $I_T \simeq I_I$. On the other hand, when the system is in the higher transmission branch and the incident intensity is decreased, the internal field is already strong enough to maintain resonance, which again produces hysteresis.

3.4. *Cooperative effects and first-order phase transition analogy*

In this section, we focus our attention on the case $\Delta = \theta = 0$. In this situation, by defining

$$x = \sqrt{\frac{I_T}{I_s}}, \quad y = \sqrt{\frac{I_I}{I_s}} \tag{26}$$

equation (25 b) can be rewritten in terms of the normalized incident and transmitted field amplitudes as follows:

$$y = x\left(1 + \frac{2C}{1 + x^2}\right). \tag{27}$$

The field internal to the cavity is in general quite different from the incident field, because there is a reaction field, cooperatively produced by the atoms, which counteracts the incident one. The nonlinear term $2Cx/(1 + x^2)$ arises from the reaction field and hence from atomic cooperation, which is measured by the parameter C.

For very large x, equation (27) reduces to the empty cavity solution $x = y$ (that is, $I_T = I_I$). The atomic system is saturated, hence the medium is transparent. In this situation each atom interacts with the incident field as if the other atoms were not there; this is the noncooperative situation and in fact the quantum statistical treatment shows that atom–atom correlations are negligible.

On the other hand for small x equation (27) reduces to $y = (2C + 1)x$ which is again linear. Here the linearity arises simply from the fact that for small driving field the response of the system is linear as usual. In this situation the atomic system is unsaturated; for large C the atomic cooperation is dominant and one has relevant atom–atom correlations.

Optical Bistability, a phenomenon which occurs in a system driven far from thermal equilibrium by the external field, bears an immediate analogy with first-order phase transitions in equilibrium systems. In fact, the curves $y(x)$ obtained by varying C are analogous to the Van der Waals curves for the liquid–vapour phase transition, with y, x and C playing the role of pressure, volume and temperature respectively (fig. 10). For $C < 4$, y is a monotonic function of x, so that there is no bistability but only the possibility of transistor action (compare fig. 2 (*b*)). For $C = 4$ (critical curve) the graph has an inflection point with horizontal tangent. Finally for $C > 4$ the curve develops a maximum and a minimum, which corresponds to bistability. In fact, for $y_m < y < y_M$ (fig. 10) one finds three stationary solutions $x_a < x_b < x_c$, and solutions x_b are unstable. Hence by exchanging the axes x and y we immediately obtain the hysteresis cycle of transmitted versus incident light. Since atomic cooperation is relevant in the states x_a and negligible in the states x_c we shall call x_a 'cooperative stationary state' and x_c 'one atom stationary state' (Bonifacio and Lugiato 1976).

When in a two-level atomic system the upper level has a nonvanishing population, the system emits fluorescent light (spontaneous emission) in all directions and the total fluorescent intensity I_F is proportional to the population of the upper level. One can show that when the system is in the one-atom branch I_F is, as usual, proportional to the number of atoms. On the contrary, when the system is in the cooperative branch, I_F scales in an anomalous way, namely I_F turns out to be *inversely proportional* to the number of atoms. This is a clear manifestation of the cooperative behaviour of the atoms.

The analogy of OB with first-order phase transitions will be further illustrated in Section 5, in connection with the quantum statistical treatment of OB.

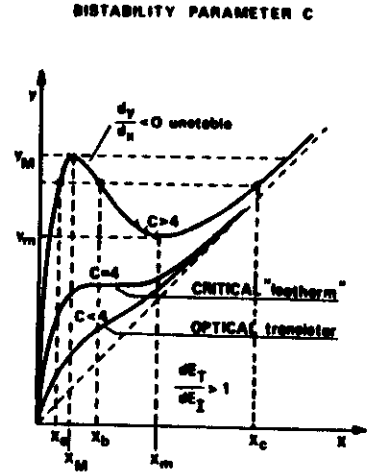

Fig. 10. Plot of the mean-field state equation (27) for purely absorptive bistability with $\theta = 0$, for different values of the bistability parameter C.

4. Transient behaviour

Up to this point, we have considered only the stationary behaviour of the system. The steady-state hysteresis cycle of OB can be experimentally observed by sweeping the incident field back and forth in an extremely slow (adiabatic) fashion, in such a way that the system can continuously adapt itself to each new value of the incident field.

In this section, we consider the transient approach of the system to the steady state. This approach is ruled by its characteristic time constants. In the case of a homogeneously broadened two-level system, the atomic time constants are the inverse of the atomic linewidth γ and the relaxation time of the population difference between the lower and the upper level. In the absence of collisions or when the collisions are inelastic the population relaxation time is one half the inverse of the atomic linewidth. Otherwise it is more than one half by an amount which is proportional to the elastic collision rate. The last characteristic time of the system is the cavity relaxation time. In fact, when we inject a coherent field this builds up in the cavity in a time equal to the inverse of the cavity lindewidth k (see equation (8)).

Let us now restrict ourselves to the purely absorptive case $\Delta = \theta = 0$ in the mean field limit conditions $\alpha L \ll 1$, $T \ll 1$. Furthermore, let us assume that the atomic relaxation times are much shorter than the cavity relaxation time. In this situation, the dynamics of the system is ruled by the following equation for the transmitted field amplitude (26)

$$\frac{dx}{dt} = k\left(y - x - \frac{2Cx}{1+x^2}\right) \tag{28}$$

and hence is governed by the cavity relaxation time k^{-1}. Clearly, in the steady state ($dx/dt = 0$) one recovers the state equation (27).

An intuitive picture of the behaviour of the system can be obtained by rewriting equation (28) in this compact form:

$$k^{-1}\frac{dx}{dt} = -\frac{dV_y(x)}{dx} \tag{29 a}$$

$$\left.\begin{aligned} -V_y(x) &= \int dx\left(y - x - \frac{2Cx}{1+x^2}\right) \\ &= yx - \frac{x^2}{2} - C\ln(1+x^2). \end{aligned}\right\} \tag{29 b}$$

In this way, (28) becomes identical to the equation that rules the overdamped one-dimensional motion of a classical particle. In fact, let us consider a particle of mass m that moves in a potential V and is subjected to friction with friction constant f. Its equation of motion is

$$m\frac{d^2x}{dt^2} + f\frac{dx}{dt} = -\frac{dV}{dx}. \tag{30}$$

When f is large enough, one can neglect the inertial term md^2x/dt^2 and hence (30) takes the form of (29 a).

By definition, the extrema of the 'potential' $V_y(x)$ defined by (29 b) coincide with the stationary solutions. The shape of $V_y(x)$ depends on the incident field y (fig. 11). For those values of y for which we have only one stationary solution $\bar{x}$, the potential has a

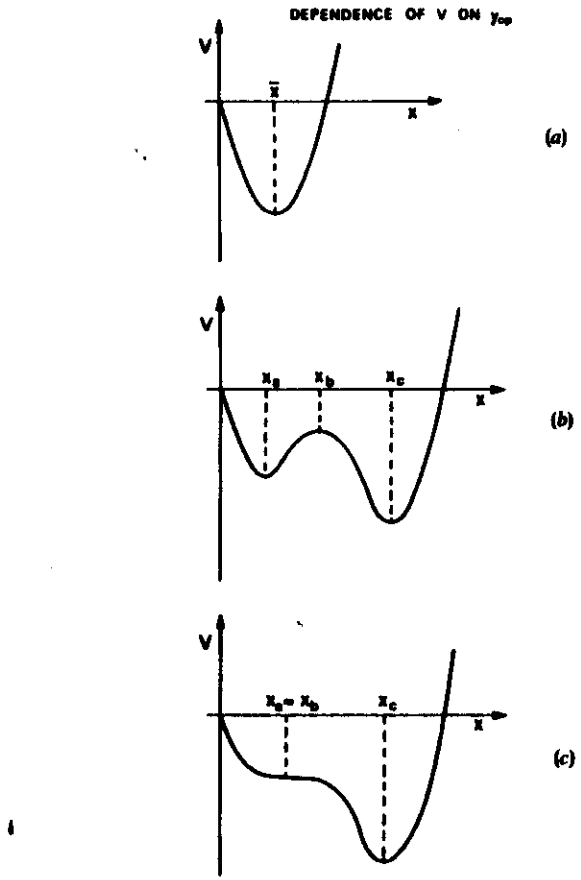

Fig. 11. The shape of the potential $V_y(x)$ depends on the value of the normalized incident field y. (a) y_{op} changed to a value $\gg y_M$; (b) y_{op} changed to a value $< y_M$ and $> y_m$; (c) y changed to critical value just equal to y_M.

single minimum at $x = \bar{x}$ (fig. 1 (a)). When, instead, we have three stationary solutions $x_a < x_b < x_c$ (fig. 10) V_y has two minima for $x = x_a$, $x = x_c$ and one maximum corresponding to the unstable stationary solution $x = x_b$ (fig. 11 (b)). Let us now consider the following experiment. Let us assume that initially the system is in a steady state with zero external field, so that $x(0) = 0$. At this point, we abruptly switch the incident light on to some operating value y_{op} larger than the upper bistability threshold y_M (see fig. 10). Hence the transmitted field approaches the stationary value $\bar{x}$ in the high transmission branch corresponding to the value y_{op} of the incident field. Equation (28) can be solved analytically, and gives the picture shown in fig. 12. Clearly, the approach shows a kind of 'lethargy', and the time the system takes to reach steady state becomes

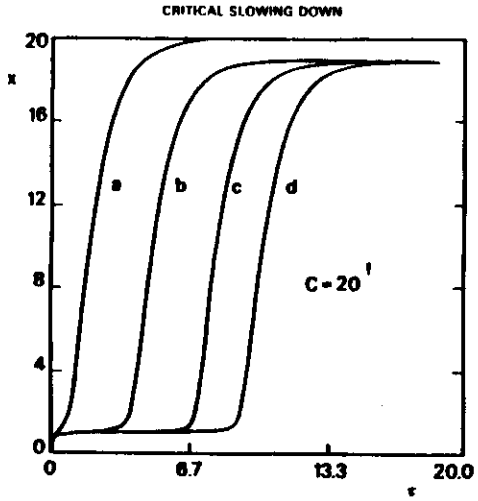

Fig. 12. Time evolution of the transmitted field showing 'lethargy' and critical slowing down. C has the value 20 and (*a*) $y_{0p}=22$; (*b*) $y_{0p}=21{\cdot}1$, (*c*) $y_{0p}=21{\cdot}04$; (*d*) $y_{0p}=21{\cdot}04$. Time is expressed in units k^{-1}. The value of y_M is 21·0264.

longer and longer as y_{0p} approaches y_M from above and diverges for $y_{0p}\to y_M$. This behaviour is called 'critical slowing down' and has been experimentally observed (Garmire *et al.* 1979, Barbarino *et al.* 1982). This phenomenon can be intuitively understood on the basis of equation (29 a). In fact, when y_{0p} is only slightly larger than y_M the potential $V_{y_{0p}}$ presents a flat part (fig. 11 (*c*)) that the system takes a long time to cover. As y_{0p} approaches y_M, this part becomes flatter and flatter (in fact, for $y_{0p}=y_M$ the curve $V_{y_{0p}}(x)$ has an inflection point with horizontal tangent) and hence the time of approach to steady state becomes longer and longer.

This analysis shows that owing to the critical slowing down, which arises from the nonlinearity of the dynamics of the system, the time of approach to the stationary state can be much longer than the relaxation times of the system. This implies that, in order to observe the steady-state hysteresis cycle, the incident field must be swept back and forth in a time that is 100 to 1000 times longer than the largest characteristic time in play. If the incident field intensity is swept more rapidly, the cycle turns out to be rounded and the transitions from the lower to the upper branch and vice versa are no longer discontinuous (Weyer *et al.* 1981).

5. Fluctuations

The theory I have described so far is completely deterministic. In fact, it is based on differential equations, so that once given the initial conditions the following time evolution is univocally determined. However, in such a treatment we neglect the *fluctuations* that are present in this as in all macroscopic systems. In fact, fluctuations are a manifestation of the microscopic structure that underlies a macroscopic system. We can control the macroscopic variables of the system, but we cannot control the microscopic variables which make themselves manifest just via the fluctuations, the uncontrollable noise of the system.

In the case of a bistable system, the analysis of fluctuations is particularly important because noise can induce the system to perform spontaneous and random jumps from one to the other branch of the hysteresis cycle. Hence the two branches are not absolutely stable but only metastable.

Of course, this phenomenon is an undesired effect because if we use our system as a memory element, clearly the memory is lost as soon as the system jumps. On the contrary, the operating value of the incident intensity must be chosen in such a way that the jumping probability is minimal. This corresponds to the so-called 'holding intensity' of the system (see fig. 3). In OB noise can have three different origins:

(i) it can be external noise, e.g. noise coming from the fluctuations of the incident field;
(ii) it can be thermal noise;
(iii) it can be 'intrinsic' or 'quantum' noise, originating from the intrinsic quantum nature of the system. Roughly speaking, intrinsic noise comes from spontaneous emission.

In order to take fluctuations into account, one must give a *statistical* description, in which the state of the system is not assigned by simply giving a number (the value of the electric field at time t), but by giving a whole *probability distribution* (the probability distribution of the electric field at time t). The time evolution of this distribution is governed by a suitable equation, called the Fokker–Planck equation. It is beyond the scope of this paper to discuss this equation here; we only mention that the Fokker–Planck equation contains one parameter in addition to those which already appear in the fluctuationless theory. This parameter, q, which is inversely proportional to the volume of the system, measures the 'strength' of the fluctuations and therefore we shall call it the 'fluctuation parameter'. Let us now describe qualitatively the results of the statistical treatment, obtained for $\Delta=\theta=0$, in the mean field limit $\alpha L\ll 1$, $T\ll 1$ and assuming (as in Section 4) that the atomic relaxation times are much shorter than the field relaxation time. We indicate by $P(x,t)$ the probability distribution of the electric field at time t so that $P(x,t)\,dx$ is the probability that at time t the normalized transmitted field amplitude (26) has a value between x and $x+dx$. Hence one has the normalization condition

$$\int_0^\infty dx\,P(x)=1.$$

For $t\to\infty$, $P(x,t)$ approaches a stationary probability distribution $P_{st}(x)$ which, since P is positive, can always be written in the following exponential form:

$$P_{st}(x)=\exp\left(-\frac{U_y(x)}{q}\right). \tag{31}$$

The function $U_y(x)$, defined in this way, plays the role of a *generalized free energy* in this system, which lies far from thermal equilibrium, and allows us to establish a connection with the Landau theory of equilibrium phase transitions, exactly as was done for the laser by Degiorgio and Scully (1970) and Graham and Haken (1970). When the thermal and external noise dominates the quantum noise, the free energy U_y turns out to coincide with the potential V_y discussed in previous section. Otherwise U_y is different from V_y. However, the extrema (minima and maxima) of both functions always correspond to the stationary solutions $x_a<x_b<x_c$ of the fluctuationless theory (see fig. 10). What makes U_y in general different from V_y is the depth of the two minima (see

fig. 11(*b*)), which is an important feature because it determines the relative degree of stability of the two states of the bistable system. The deeper the minimum of U_y, the more stable is the stationary state which corresponds to that minimum. Using (31) we can rephrase all of this in terms of probabilities instead of degree of stability. In fact, the minima of the generalized free energy U_y correspond to peaks, of the stationary probability distribution. The deeper a minimum, the higher is the corresponding peak. Hence more stable is equivalent to more probable. For those values of y for which the fluctuationless theory gives only one stationary solution $\bar{x}$, the probability distribution $P_{st}(x)$ has a single peak at $x=\bar{x}$ (fig. 13(*a*)). On the other hand, when the fluctuationless theory gives three stationary solutions $x_a<x_b<x_c$, $P_{st}(x)$ has two peaks for $x=x_a$ and $x=x_c$ and one local minimum corresponding to the unstable state $x=x_b$ (fig. 13(*b*)).

The fluctuation parameter q governs the width of the peaks; the smaller the value of q the narrower are the peaks. When q is small, the two peaks have comparable size only in a very small range of values of the normalized incident field y in the bistable region $y_m<y<y_M$ (fig. 10), whereas in all the remaining part of this region the peak at $x=x_a$ is dominant over the one at $x=x_c$ or vice versa.

Using the probability distribution $P_{st}(x)$, one can calculate the mean value $\langle x\rangle$ of the transmitted field defined as follows:

$$\langle x\rangle=\int_0^\infty dx\, x P_{st}(x). \tag{32}$$

It is interesting to plot $\langle x\rangle$ as a function of the incident field y, and compare this curve with the S-shaped curve given by the fluctuationless theory. In fig. 14. we see the two curves for $C=20$, $q=10^{-2}$ when the quantum noise is negligible with respect to the

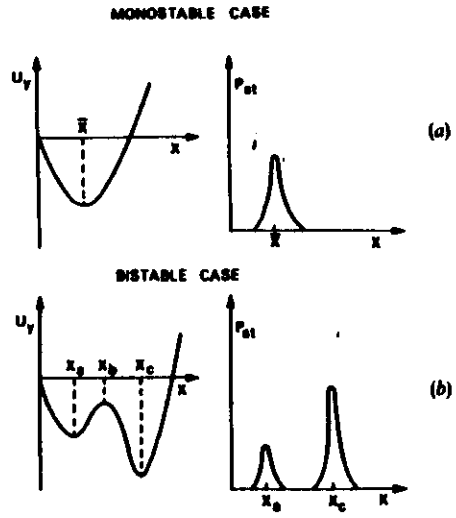

Fig. 13. Shape of the generalized free energy $U_y(x)$ and of the stationary probability distribution $P_{st}(x)$ in (*a*) the monostable case and (*b*) the bistable case.

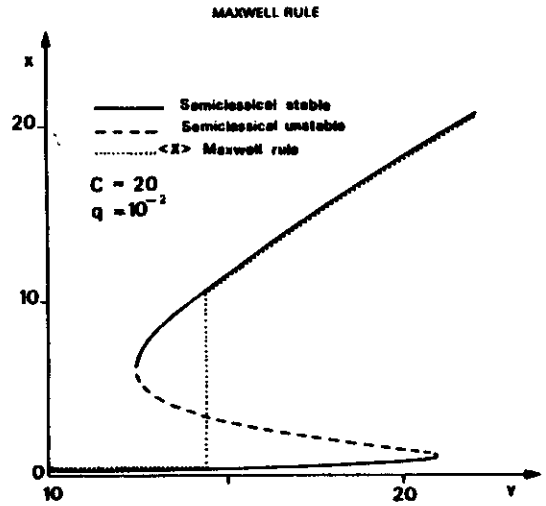

Fig. 14. Case of negligible quantum noise. The S-shaped curve of the fluctuationless theory is compared to the curve of the mean value $\langle x\rangle$ of the transmitted field.

thermal and external noise, so that $U_y(x)=V_y(x)$. The mean value coincides with one of the two branches of the S-shaped bistability curve everywhere, except in a small 'transition region' in which $\langle x\rangle$ passes from the lower to the higher branch. On the scale of this drawing, the passage is so rapid that it seems a discontinuous jump. Actually, by using an expanded scale in y one realizes that the transition is continuous, and becomes discontinuous only in the infinite volume limit, in which $q\to 0$. The shape of the curve of $\langle x\rangle$ shown in fig. 14 can be understood by realizing that it is only in the transition region that the two peaks of the distribution function have comparable size. For values of y below (above) the transition region the peak at $x=x_a(x=x_c)$ is absolutely dominant over the other, and therefore the mean value practically coincides with $x=x_a(x=x_c)$. Figure 14 immediately reminds us of the Maxwell rule of the first-order equilibrium phase transitions. In fact, one can prove that the transition region cuts the S-shaped curve in such a way that one obtains two lobes of equal area. This is no longer true when the intrinsic quantum fluctuations are not negligible. In this case, one obtains a picture quite similar to that of fig. 14, but with a 'generalized Maxwell rule' different from the usual one (fig. 15). This feature arises from the fact that quantum fluctuations depend on the value of the electric field, whereas thermal and external fluctuations do not. Similar deviations from the usual Maxwell rule have also been found in other systems far from thermal equilibrium, for example in chemical reactions.

At this point, it is important to stress that the whole quantum statistical treatment we have described up to now is purely static: it holds in the asymptotic long-time limit. Consider a value of the incident field y which lies in the bistable domain $y_m<y<y_M$ but on the right of the transition region. If our system is initially in the low transmission state, we know that if we wait long enough the system will perform a transition to the more stable high transmission state that corresponds to the same value of the incident field. The crucial question is how long the system takes on the average to make this

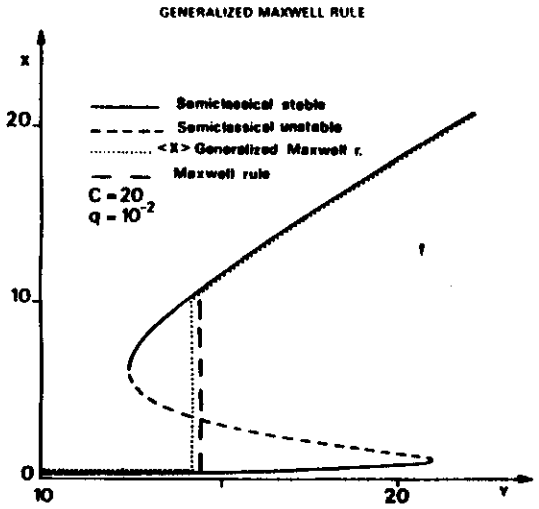

Fig. 15. Same as fig. 14, but with quantum noise dominant over external and thermal noise.

transition. This question can be answered by following a method due to Kramers (1940) and the result is illustrated in fig. 16.

Assume that initially the system is at the bottom of the left-hand well of the free energy, which corresponds to the low transmission state. In order to reach the bottom of the other more stable well, the system must overcome the barrier ΔU which in this problem plays a role similar to that of the activation energy in chemical reactions. The system can overcome this barrier thanks to some suitably large fluctuation. The

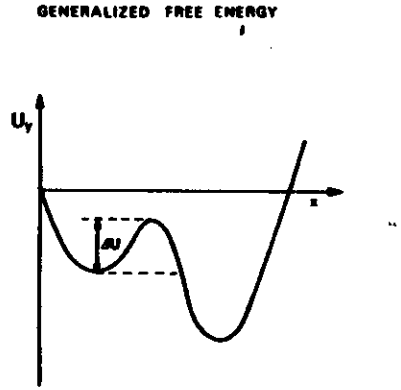

Fig. 16. In order to pass from the lower transmission state (left well) to the higher transmission state, the system must overcome the barrier ΔU.

Kramers procedure shows that the average transition time t_{AV} is proportional to the following expression

$$t_{AV} \propto \exp\left(\frac{\Delta U}{q}\right). \tag{33}$$

Now, when the size of the system is of the order of a centimetre or more, provided the temperature is not too high and the external noise is not large the parameter q turns out to be small, say smaller than 0·01 or 0·001. In this case the transition time is astronomical and the stationary states can be considered as absolutely stable from a practical viewpoint, even if strictly speaking they are metastable. On the other hand, when the external noise increases or the size of the system decreases so that the total number of atoms is on the order of 1000, the time t_{AV} shortens and the influence of fluctuations becomes much more crucial. Note that from a practical viewpoint the problem of constructing miniaturized bistable devices is of outstanding importance in order to reach the ultimate goal of an optical computer (see Section 7).

To end this section, let me mention that fluctuations determine the spectrum of transmitted light, the spectrum of fluorescent light emitted by the system in all directions and the so-called photon statistics of these fields. For a description of these points, I refer the reader to my more detailed article (Lugiato 1983).

6. Self-pulsing and chaotic behaviour

Now let us come back to the fluctuationless theory, by assuming that the fluctuation parameter is so small that the effects of fluctuations are negligible. In this section, we shall discuss the matter of *instabilities* in optical bistability. As usual, a stationary state (or a stationary regime) is said to be unstable when, after displacing the system a little from this state, the system instead of returning to it goes further from it. An unstable state is not physically meaningful because even the slightest perturbation removes the system from it.

Now, optical bistability itself originates from the rise of an instability. In fact, approaching the upper bistability threshold $y = y_M$ from below (see fig. 10) the low transmission state becomes unstable and just for this reason the system jumps to the high transmission branch. The same happens to the high transmission branch when y approaches the lower bistability threshold $y = y_m$.

On the other hand, it is well known (Haken 1977, Nicolis and Prigogine 1977) that in nonlinear systems one can find a whole sequence of instabilities. First the stationary state becomes unstable and the system approaches another steady state, then the new stationary state becomes itself unstable, and so on. This sequence is found by varying the external parameters of the system, that we can control; in OB, the control parameters are the incident field and the length of the cavity. Typically, after a few instabilities the system no longer possesses any stationary state, and in this case it exhibits an oscillatory behaviour: one has the emergence of *spontaneous pulsations* in the system. This oscillatory behaviour can be regular, or perfectly periodic in time, as well as completely irregular and aperiodic, in which case one speaks of *chaotic* or *turbulent* behaviour (see fig. 17).

Two points are of basic importance:

(i) this oscillatory behaviour is not due to external manipulation of the system: it arises when all the parameters of the systems are kept constant. In OB one can

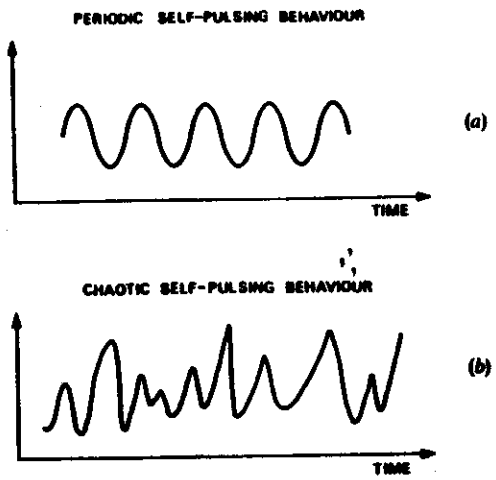

Fig. 17. (*a*) Regular oscillatory behaviour. (*b*) Chaotic oscillatory behaviour.

easily obtain a pulsed behaviour by varying periodically the length of the cavity (for example by using a piezo-electric crystal). This is of course a trivial fact. On the other hand, as we shall show, we can obtain pulsed behaviour even keeping all the external parameters (cavity length, incident field intensity) constant. In this case, the pulsations are spontaneously produced by the self-organization of the system itself and for this reason this behaviour is called *self-pulsing*.

(ii) In the chaotic case (fig. 17(*b*)), if we look at the time plot this immediately reminds us of the irregularities that arise as a consequence of the noise of the system. However, we can find chaotic behaviour even when completely neglecting noise, that is, in the framework of a deterministic (and hence fluctuationless) theory. For this reason, this behaviour is called *deterministic chaos*.

Chaotic behaviour and the various routes that lead the system to chaos have been the object of very active research in recent years, even if we are still far from having a complete classification. The most popular and deeply investigated route to chaos is the so-called 'period doubling route' (Grossmann and Thomae 1977, Feigenbaum 1978, 1979), which is illustrated in fig. 18. We start with the system in a stable regular oscillatory state with a fundamental frequency $\bar{\omega}$. By increasing the control parameter a, at some point this state becomes unstable, and the system approaches a new oscillatory state, which has a doubled period. Note that from the viewpoint of the Fourier transform, that is, of the spectrum, period doubling corresponds to the generation of the subharmonic $\bar{\omega}/2$. By further increasing a, the new state becomes unstable in turn and one has again period doubling, a period of length 4 with respect to the initial period. And so on: by a sequence of instabilities one finds period 8, 16, 32,.... The sequence of values of the control parameter for which one has period doubling get closer and closer according to a geometric law. In fact, the ratio between the interval in which one has period 2^n and the interval in which the period is 2^{n+1} is 4·6692 .... This

number is universal: it holds for all period doubling sequences. Hence quite rapidly the sequence reaches a cumulation point, beyond which the system exhibits chaotic behaviour. In the chaotic domain, the spectrum is no longer given by single lines but has a continuous background. In some systems, the period doubling sequence is found by decreasing the control parameter instead of increasing it.

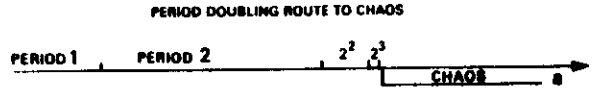

Fig. 18. As the control parameter a is increased, the system undergoes a cascade of period doubling instabilities, which leads finally to chaos.

As I shall show in this section, in OB we can find both periodic and chaotic self-pulsing. I shall distinguish two cases according to the mechanism that gives rise to the instability of the stationary state. As I said in Section 2, the cavity has infinite frequencies (modes). Accordingly, the behaviour of the system can be described in terms of *mode amplitudes*. In the first case, it is the amplitude of the mode resonant with the incident field that goes unstable. In the second case, the instability arises from the off-resonance modes.

6.1. *Resonant mode instability*

This type of instability can arise only in the dispersive case (Ikeda and Akimoto 1982, Lugiato *et al.* 1982), in which a sizable portion of the high transmission branch becomes unstable (see fig. 19). Roughly speaking, the mechanism is the following. In the dispersive situation there is a mismatch between the atomic frequency and the incident field frequency. When this mismatch is large enough, the system is no longer able to adapt itself to the incident frequency and therefore the stationary state becomes unstable and the system begins to oscillate. In this situation, the transmitted light is no longer stationary in time but is given by an undamped sequence of pulses (self-pulsing). From a practical viewpoint, this behaviour is very interesting because it suggests a device to convert coherent stationary light into coherent pulsed light (fig. 20). In this connection, see Bonifacio and Lugiato (1978 b) and McCall (1978).

Let us now look at what happens when the system jumps from the lower to the higher transmission branch. Since the steady state in the higher branch is already unstable, we find immediately a regular sequence of oscillations (fig. 21 (*a*)). Another way of looking at the same behaviour is to consider the plane of the real and imaginary part of the normalized transmitted field. In this case, the trajectory in this plane is a simple limit cycle (fig. 21 (*b*)). If we now decrease the incident field y, which is our control parameter, we find the appearance of a double period (fig. 21 (*c*)), which corresponds to the trajectory shown in fig. 21 (*d*). This trajectory arises from a kind of fission of the limit cycle into two distinct parts. From fig. 21 (*d*) we can also see why one has period doubling. In fact, we see that after one loop the system fails to come back to the initial condition, whereas it succeeds in doing so after two loops; hence the period doubles. A further decrease of y leads to the appearance of period four (figs. 21 (*e*) and (*f*)) and so on. Finally, we enter into the chaotic domain (see figs. 19 and 22 (*a*) and (*b*)), in which the time trace no longer shows any precise periodicity.

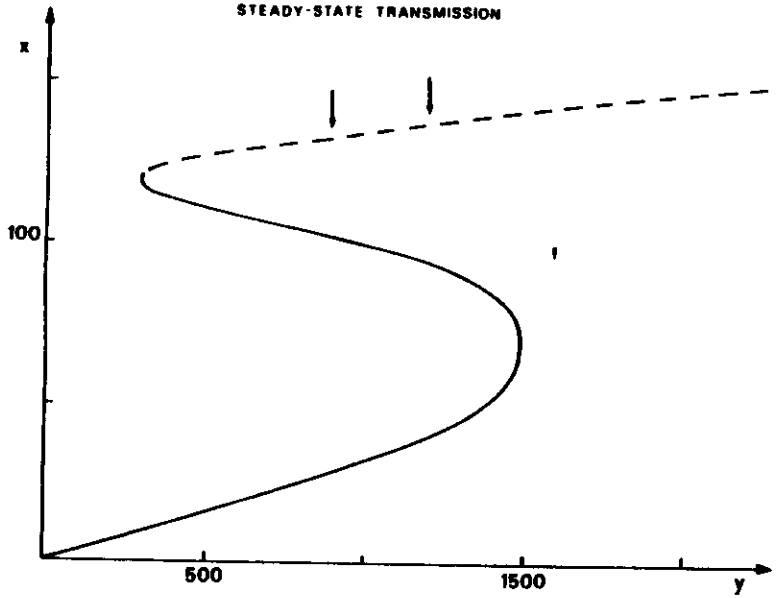

Fig. 19. The horizontal and vertical axes are labelled by the amplitude y and x of the incident and transmitted fields, respectively. The dashed segments denote the instability range that leads to undamped oscillations. The arrows mark the region where chaotic behaviour is found. ($C=0{\cdot}5$, $\Delta=374$, $\theta=340$.)

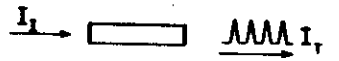

Fig. 20. Converter of c.w. coherent light into pulsed coherent light.

6.2. *Off-resonance mode instability*

This phenomenon arises when the two cavity modes, adjacent to the resonant mode, fall within the absorption line of the atomic medium (fig. 23). This condition can be fulfilled by making the cavity long enough. In this situation, under suitable conditions the adjacent mode amplitudes go unstable, whereas the resonant mode remains stable.

Let us consider first the simplest absorptive case $\Delta=\theta=0$. As we said before, the externally controllable parameters of our system are the incident field y and the total length of the ring cavity $\mathscr{L}$. Instead of y and $\mathscr{L}$ we can use x (which is linked to y by equation (27)) and $\tilde{a}/\gamma=2\pi c/\mathscr{L}\gamma$, which is equal to the frequency difference between the adjacent modes and the resonant mode (fig. 23) divided by the atomic linewidth γ. In fig. 24 we see the plane of the control parameters $\tilde{a}/\gamma$ and x. The stationary state in the high transmission branch becomes unstable when the operating point in this plane lies in the

Regular self-pulsing

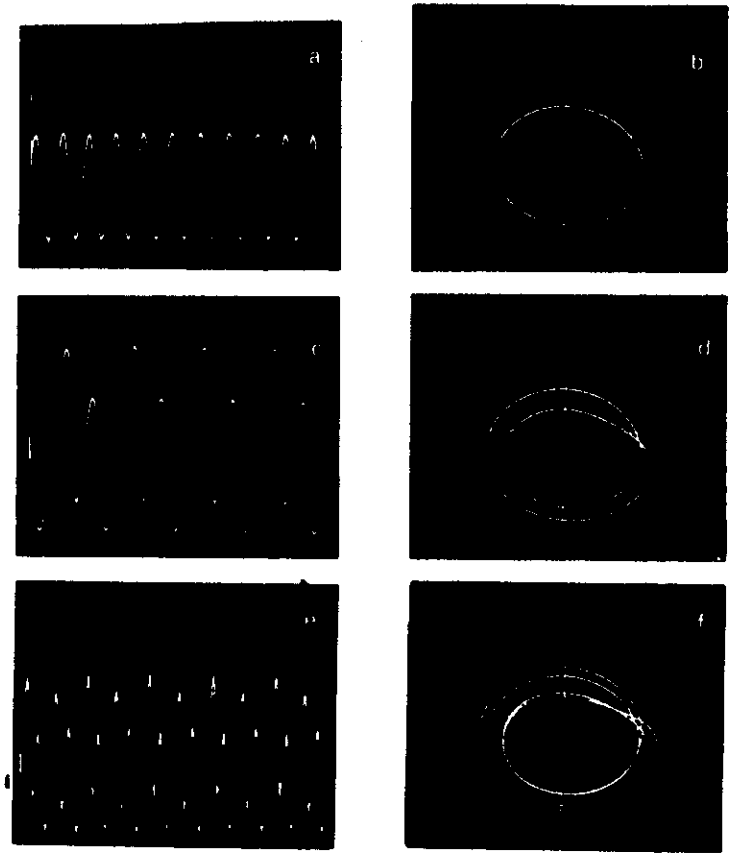

Fig. 21. Self-pulsing oscillations and the corresponding representation in the plane of the real and imaginary parts of the normalized electric field (*a*, *b*) single period; (*c*, *d*) doubled period; (*e*, *f*) quadrupled period. Parameters as in fig. 19. The values of the external field are $y=2000$, 1350, 1225 for the three sets of solutions.

shaded part, which we shall therefore call the instability region. The mechanism which produces the instability in this case is different from the one seen in the previous subsection. It is the same mechanism that one finds in so-called *saturation spectroscopy* (Gronchi *et al.* 1981). In fact, let us consider an atomic sample without any cavity (fig. 25), and let us illuminate it by a strong coherent stationary field, which saturates the medium. Simultaneously, let us irradiate the same sample by a weak probe beam. One finds that for suitable ranges of values of the difference between the frequencies of the probe and of the saturating field, the probe beam experiences not absorption but amplification (gain). The same happens in our system: the resonant cavity mode

Chaotic self-pulsing

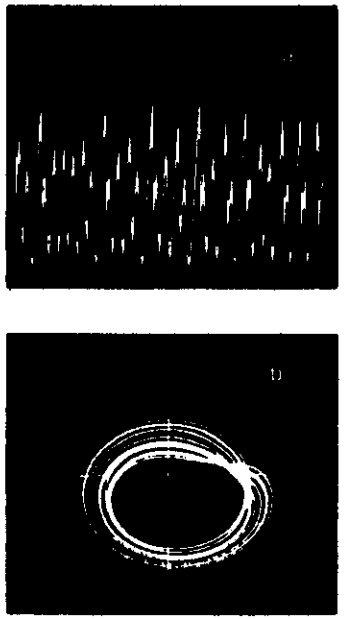

Fig. 22. Typical chaotic self-pulsing behaviour, represented as in fig. 21, for $y=950$ and the remaining parameters as in fig. 19.

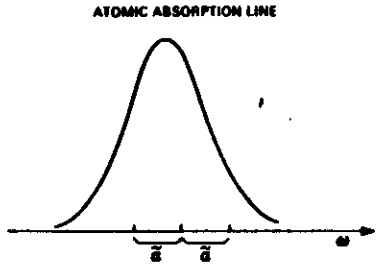

Fig. 23. To illustrate the case where the two cavity modes, adjacent to that nearest to resonance with the incident field, lie within the absorption line of the atomic medium. $\tilde{a}$ is the frequency difference between the adjacent modes and the resonant mode.

saturates the medium, while the adjacent modes work as probe fields. Under suitable conditions, they experience gain and when this gain becomes larger than the losses the adjacent modes go unstable. Hence in this case with respect to the adjacent modes our absorbing system behaves like a laser (amplifying system), but without any population inversion.

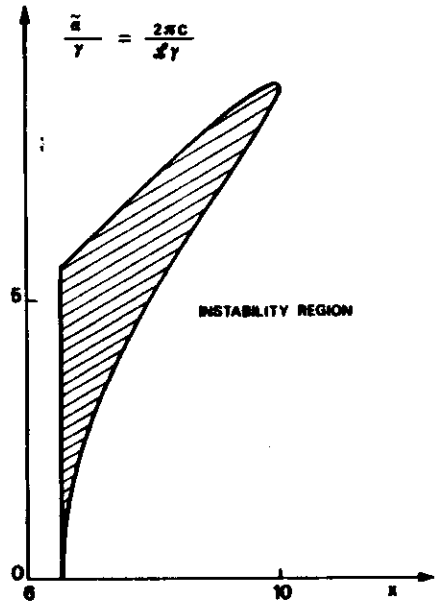

Fig. 24. Instability region in the plane of the control parameters $\tilde{a}/\gamma = 2\pi c/\mathscr{L}\gamma$ and x.

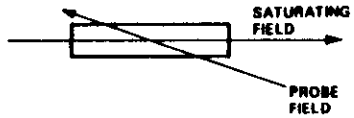

Fig. 25. Typical experiment in saturation spectroscopy.

When the steady state in the higher branch is unstable, the system can exhibit two different kinds of behaviours (Bonifacio and Lugiato 1978 b, Bonifacio *et al.* 1979). In the first case, the system approaches a self-pulsing behaviour, again behaving as a converter of stationary light into pulsed. As we see from fig. 26 (*a*), if the system is initially slightly displaced from the steady state, it begins to show oscillations. The oscillation amplitude increases with time in an exponential way, until a stationary regime is reached, in which the envelope of the oscillations is perfectly horizontal. In this case, the frequency of the oscillations in equal to $\tilde{a}$, which corresponds to a period equal to the transit time $\mathscr{L}/c$ of the photons in the cavity. The second possibility is that the system simply 'precipitates' to the low transmission state that corresponds to the same value of the incident field. In fact, the lower state is always stable. This possibility is illustrated in fig. 26 (*b*), from which we see that the oscillations are first amplified but finally die away, the system precipitating to the low transmission state.

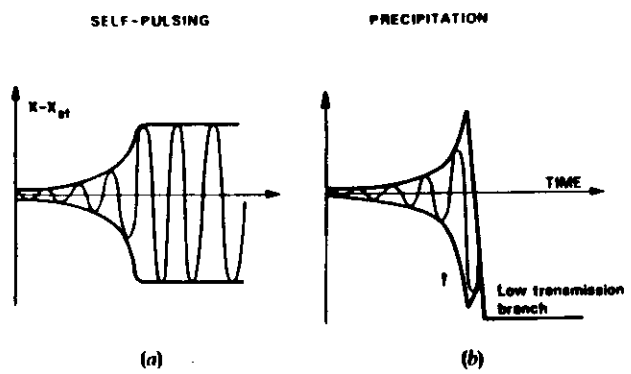

Fig. 26. x_{st} is the value of the normalized transmitted field in the steady state corresponding to the unstable higher transmission state.

In order to treat analytically this self-pulsing behaviour, which is a many-mode phenomenon because it involves both the resonant and the adjacent modes, we developed a formalism called 'dressed mode theory of optical bistability' (see Benza and Lugiato 1982, Lugiato *et al.* 1983 and references quoted therein). This is a development of Haken's theory of generalized Ginzburg-Landau equations for phase transition-like phenomena in open systems far from thermal equilibrium (Haken 1975a, b). This treatment allows us to describe the behaviour of the system in terms of a simple two-dimensional phase space. The two variables are ρ, the half-amplitude of the oscillations, and σ, the difference between the mean value of the oscillations and the unstable steady-state value x_{st} (see fig. 27). The upper and lower envelopes of the oscillations $x_{upper}(t)$ and $x_{lower}(t)$ are simply obtained as follows:

$$x_{\substack{\text{upper}\\\text{lower}}}(t) = x_{st} + \sigma(t) \pm \rho(t) \tag{34}$$

hence the time evolution can be equivalently described in terms of the oscillation envelope or of the trajectory in the phase plane (ρ, σ).

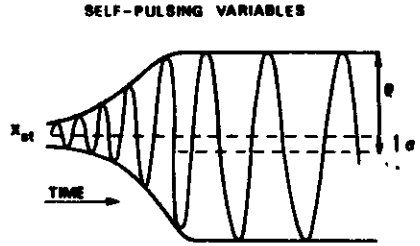

Fig. 27. Definition of the variables ρ and σ.

Using the dressed mode theory, we calculated the self-pulsing state in all its domain of existence, which is shown in fig. 28 and turns out to be very much larger than the

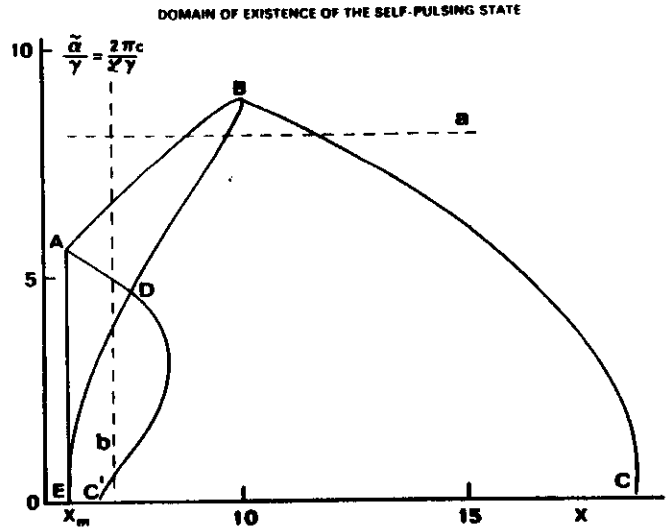

Fig. 28. The whole figure shows the domain of existence of the stable self-pulsing solution for $C = 20$, $\Delta = \theta = 0$. Instability region, ABE; precipitation region, ADE; soft excitation domain, ABD, and hard excitation domain, BCC'D.

instability region ABE. It can be subdivided into the 'soft excitation' domain ABD and a 'hard excitation' domain BCC'D, while the region ADE is the precipitation domain. In the first domain, the self-pulsing state is stable whereas the stationary state is unstable. Hence a small initial deviation from steady state (soft excitation) is enough to let the system approach the self-pulsing state. By contrast, in the second domain one has the simultaneous presence of a stationary and a self-pulsing state, both stable. Which one of the two states is approached by the system is determined by the initial condition. If the initial deviation from steady state is small, the system simply returns to the stationary state itself. In order to reach the self-pulsing state it is necessary to produce a large enough initial deviation from the steady state (hard excitation).

This situation leads to the appearance of hysteresis cycles of a new type. Figure 29 shows the half amplitude of the oscillations for long times $\rho(t = \infty)$ when we vary the incident field along the horizontal line in fig. 28. Upon entering the instability region from the left, a stable self-pulsing state arises. As the incident field is increased, the oscillation amplitude increases and in fact it continues to do so even outside the instability region, until the system returns discontinuously to the stationary state in the high transmission branch. If one now decreases the amplitude of the incident field, the system continues to operate in the stationary high transmission branch until we reach the right boundary of the instability region, where it jumps discontinuously to the self-pulsing regime with a finite amplitude.

Figure 29 can be viewed as representing a second-order phase transition together with a first-order one, the former on the left boundary of the instability domain, the latter tied to the hysteresis cycle that begins at the right boundary of this domain. It is worth stressing that in this case, the bistability involves stationary and self-pulsing states and *not* just stationary states as in the operation of usual bistable systems. This

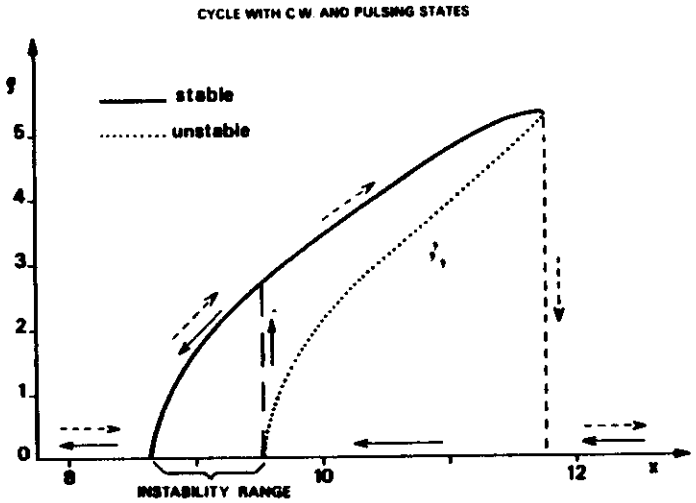

Fig. 29. The half-amplitude of the oscillations in the self-pulsing state is plotted as a function of the stationary value x of the transmitted field in the high transmission branch for $C = 20$, $\bar{a}/\gamma = 8$ (line a of fig. 1). Full (broken) arrows indicate the behaviour of the system when the incident field is decreased (increased).

hysteresis cycle enriches considerably the phenomenology of OB, especially because the new self-pulsing branch is accessible from the usual steady states by suitably varying the external parameters.

An interesting situation occurs also in the neighbourhood of the line AD (fig. 28) that separates the self-pulsing from the precipitation domains. In order to describe this behaviour, let us consider a continuous variation of the cavity length along the line b of fig. 28. As we enter the instability region from above, a stable self-pulsing state develops with a continously growing amplitude. On approaching the line AD (also from above) the time-dependent envelope begins to develop considerable oscillations (fig. 30(*a*)). This behaviour is called 'breathing'. The breathing pattern observed in our case, however, lasts only a finite amount of time. Figure 30(*b*) shows the same phenomenon but from the point of view of the phase-space variables (ρ, σ). The trajectory in the phase plane spirals towards the point corresponding to the self-pulsing state, which behaves as a stable focus. Crossing the line AD, the focus becomes unstable and therefore we have what is usually called a 'Hopf bifurcation' (Marsden and McCracken 1976). As is well known, in a Hopf bifurcation one has the appearance of a limit cycle in the phase plane. In this case the limit cycle is unstable: it repels trajectories instead of attracting them. Hence we have been able to display it only by using a trick, that is, by integrating the time evolution backwards in time, so that the repeller becomes an attractor. Figure 30(*e*) and (*c*) show the backward approach to the limit cycle in the ρ, σ) phase plane, when the starting point is chosen either outside (fig. 30(*e*)) or inside (fig. 30(*c*)) the limiting trajectory. Similarly, figs. 30(*d*) and (*f*) show the backward time evolution of the oscillation envelope of the transmitted field. Now, for long times we have a perfectly periodic breathing regime in which the envelope marks time as a 'regular' clock (but backwards in time). Of course, an unstable limit cycle cannot be observed directly.

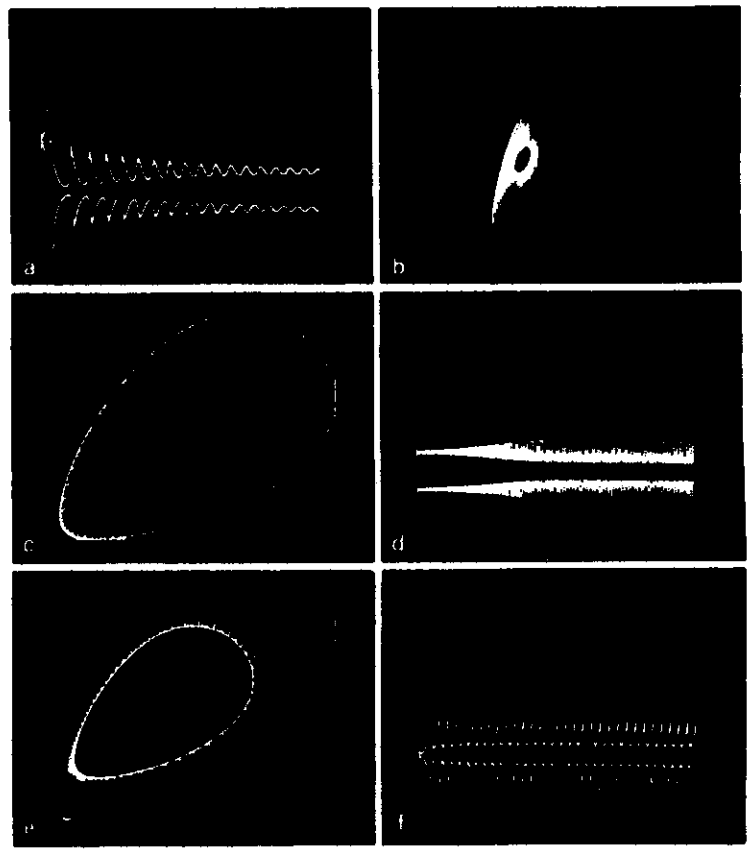

Fig. 30. Envelope breathing and limit cycles in the (ρ, σ) plane for $C = 20$ and $x = 7$. In (*a*) and (*b*), $\bar{a}/\gamma = 4{\cdot}9205$; in (c), (d), (e) and (*f*), $\bar{a}/\gamma = 4{\cdot}92$. The limit cycles and the corresponding time-dependent envelopes have been obtained by integrating the time evolution backwards in time. The initial conditions $\rho(0)$, $\sigma(0)$ were inside the limit cycle for (*c*) and (*d*) and outside the limit cycle for (*e*) and (*f*).

6.3. *Observation of self-pulsing and chaotic behaviour in dispersive OB*

The type of instability described in the previous subsection arises also in the dispersive situation. In this case, as was shown by Ikeda and co-workers (Ikeda 1979, Ikeda *et al.* 1980), the system exhibits a self-pulsing behaviour which can be either periodic with period of the order of twice the cavity transit time $\mathscr{L}/c$ and pulses having a square-wave type shape instead of sinusoidal (fig. 31 (*a*)), or completely chaotic (fig. 31 (*b*)). Again, the chaotic regime is reached via a period-doubling sequence.

A very important fact is that these behaviours, including 'optical turbulence (chaos)' have been experimentally observed (Gibbs *et al.* 1981). More precisely, this experiment

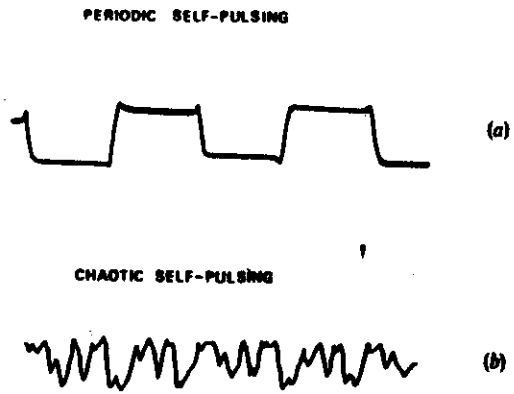

Fig. 31. Experimental observation of self-pulsing in a hybrid system by Gibbs *et al.* (1981).

was not performed with an all-optical but with a hybrid electro-optical system which obeys the same type of time evolution equations (fig. 31).

7. Towards a practical optical bistable device

Optical bistability in all-optical systems has been by now observed in quite a variety of conditions, which range from radio-waves (Meier *et al.* 1982) to the visible, from cavities of more than 10 cm to cavities of the order of 1 μm.

In most experiments the observed bistability is exclusively or mainly of the dispersive type (Gibbs *et al.* 1976, Venkatesan and McCall 1977, Bishofberger and Shen 1978, Grischkowski 1978, Grynberg *et al.* 1980, Sandle and Gallagher 1981). However, more recently a number of experimental investigations of absorptive OB have been made (Weyer *et al.* 1981, Grant and Kimble 1982, Arecchi *et al.* 1982, Gozzini *et al.* 1982).

From a practical viewpoint, the most interesting situation is that of small cavities. In fact, the description of the ideal optical bistable device which would be the basic element for the construction of an optical computer, is the following:

(i) Miniaturization. Both the diameter and the length of the cavity should be smaller than one micron. In this situation, the cavity round-trip time is of the order of 10^{-2} picoseconds.

(ii) Fast response. Both the switch-up and the switch-down time (the time taken to jump from the lower to the upper branch and vice versa) should be of the order of one picosecond.

(iii) Low energy requirement. The holding intensity should be less than one mW/μm^2.

(iv) The device should operate at room temperature.

These conditions have not been reached up to now, so far as I know; however, they have been at least approached by using as absorbing material semiconductors such as GaAs (Gibbs *et al.* 1979 a) or InSb (Miller *et al.* 1979).

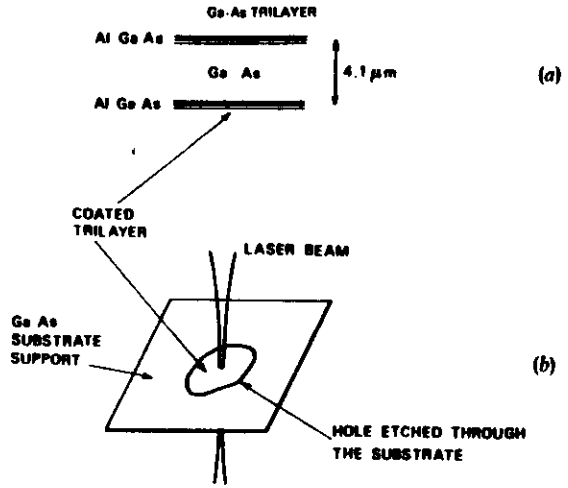

Fig. 32. Miniaturized all-optical bistable system realized using GaAs by Gibbs *et al.* (1979 b).

The device constructed at the Bell Telephone Labs (Murray Hill) by Gibbs, McCall and collaborators consisted of a sample of GaAs, 4·1 μm thick, between two 0·21 μm Al GaAs layers (fig. 32 (*a*)). Reflective coatings with $T = 0{\cdot}1$ were added. This system was supported by a 150 μm GaAs substrate containing a 1–2 mm diameter etched hole to let radiation pass through (fig. 32 (*b*)). Optical bistability of the dispersive type was observed from 5 to 120 K for wavelengths of the order of 0·8 μm. The holding power

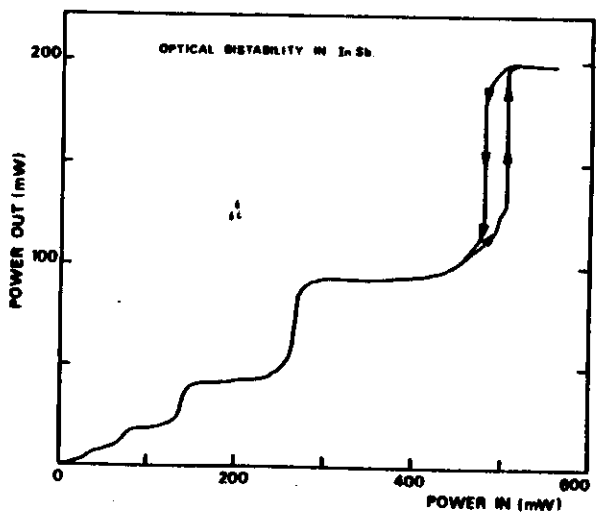

Fig. 33. Observation of optical bistability in InSb by Miller *et al.* (1979).

was about 1 mW/μm^2 and the switching times were smaller than 40 ns. Recently Gibbs, McCall and collaborators (Gibbs *et al.* 1982) obtained bistable operation in GaAs at room temperature. The nonlinear Fabry-Pérot constructed by Miller, S. D. Smith and Johnston using InSb consisted of an uncoated plane-parallel InSb crystal 5 × 5 mm^2 by 560 μm thick. Bistability was observed at 5 K with a stationary CO laser for wavelengths of the order of 5 μm (fig. 33). The holding intensity was only 15 μW/μm^2. Many more details of these systems can be found in Gibbs *et al.* (1980) and Abraham and Smith (1982 a, b).

To end this paper, I wish to observe that bistable behaviour has also been predicted and observed in other all-optical systems that work on the basis of physical principles different from those described in this article. As an example, I mention the optical bistability in reflection at a nonlinear interface predicted by Kaplan (1976) and shown experimentally by P. Smith, Hermann, Tomlinson and Maloney (1979). Details can be found in the books edited by Bowden *et al.* (1981) and by Smith (1981).

References

Abraham, E., and Smith, S. D., 1982 a, *Journal of Physics* E, **15**, 33.
Abraham, E., and Smith, S. D., 1982 b, *Reports on Progress in Physics*, **45**, 815.
Allen, L., and Eberly, J. H., 1975, *Optical Resonance and Two-Level Atoms* (New York: Wiley & Sons).
Arecchi, F. T., Giusfredi, G., Petriella, E., and Salieri, P., 1982, *Applied Physics* B, **29**, 79.
Barbarino, S., Gozzini, A., Longo, I., Maccarrone, F., and Stampacchia, R., 1982, *Nuovo Cimento* B, **71**, 183.
Benza, V., and Lugiato, L. A., 1982, *Zeitschrift für Physik* B, **47**, 79.
Bishofberger, T., and Shen, Y. R., 1978, *Applied Physics Letters*, **32**, 156.
Bonifacio, R., 1982, *Dissipative Systems in Quantum Optics: Resonance Fluorescence, Optical Bistability, Superfluorescence* (Berlin: Springer Verlag).
Bonifacio, R., Gronchi, M., and Lugiato, L. A., 1979, *Optics Communications*, **30**, 129.
Bonifacio, R., and Lugiato, L. A., 1976, *Optics Communications*, **19**, 172.
Bonifacio, R., and Lugiato, L. A., 1978 a, *Lettere al Nuovo Cimento*, **21**, 505.
Bonifacio, R., and Lugiato, L. A., 1978 b, *Lettere al Nuovo Cimento*, **21**, 510.
Bowden, C. M., Ciftan, M., and Robl, H. R., editors, 1981, *Optical Bistability* (Plenum Press).
Collins, Jr., S. A., and Wasmundt, K. C., 1980, *Optical Engineering*, **19**, 478.
Degiorgio, V., and Scully, M. O., 1970, *Physical Review*, A, **2**, 1170.
Feigenbaum, M. J., 1978, *Journal of Statistical Physics*, **19**, 25.
Feigenbaum, M. J., 1979, *Journal of Statistical Physics*, **21**, 669.
Felber, F. S., and Marburger, J. H., 1976, *Applied Physics Letters*, **28**, 731.
Garmire, E., Marburger, J. H., Allen, S. D., and Winful, H. G., 1979, *Applied Physics Letters*, **34**, 374.
Gibbs, H. M., Hopf, F. A., Kaplan, D. L. and Shoemaker, R. L., 1981, *Physical Review Letters*, **46**, 474.
Gibbs, H. M., McCall, S. L., and Venkatesan, T. N. C., 1976, *Physical Review Letters*, **36**, 113.
Gibbs, H. M., McCall, S. L., and Venkatesan, T. N. C., 1979 b, *Optics News*, **5**, 6.
Gibbs, H. M., McCall, S. L., and Venkatesan, T. N. C., 1980, *Optical Engineering*, **19**, 463.
Gibbs, H. M., McCall, S. L., Venkatesan, T. N. C., Gossard, A. C., Passner, A., and Wiegmann, W., 1979 a, *Applied Physics Letters*, **35**, 451.
Gibbs, H. M., Tarng, S. S., Jewell, J. L., Weinberger, D. A., Tai, K. C., Gossard, A. C., McCall, S. L., Passner, A., and Wiegmann, 1982, *Applied Physics Letters*, **41**, 221.
Gozzini, A., Longo, I., Maccarrone, F., 1982, *Nuovo Cimento* D, **1**, 489.
Graham, R., and Haken, H., 1970, *Zeitschrift für* Physik, **237**, 31.
Grant, D. E., and Kimble, H. J., 1982, *Optics Letters*, **7**, 353.
Grischkowski, D., 1978, *Journal of the Optical Society of America*, **68**, 641.
Gronchi, M., Benza, V., Lugiato, L. A., Meystre, P., and Sargent III, M., 1981, *Physical Review* A, **24**, 1419.

Grossman, S., and Thomae, S., 1977, *Zeitschrift für Naturforschung* (a), **32**, 1353.
Grynberg, G., Giacobino, E., Devaud, M., and Biraben, F., 1980, *Physical Review Letters*, **45**, 434.
Haken, H., 1975 a, *Zeitschrift für* Physik B, **21**, 105.
Haken, H., 1975 b, *Zeitschrift für* Physik B, **22**, 69.
Haken, H., 1977, *Synergetics, an Introduction* (Berlin: Springer-Verlag).
Ikeda, K., 1979, *Optics Communications*, **30**, 257.
Ikeda, K., and Akimoto, O., 1982, *Physical Review Letters*, **48**, 617.
Ikeda, K., Daido, H., and Akimoto, O., 1980, *Physical Review Letters*, **45**, 709.
Kaplan, A. E., 1976, *JETP Letters*, **24**, 114.
Kramers, H. A., 1940, *Physica (Utr.)*, **7**, 284.
Lugiato, L. A., 1983, *Progress in Optics*, edited by E. Wolf (to appear).
Lugiato, L. A., Benza, V., Narducci, L. A., and Farina, J., 1983, *Zeitschrift für Physik*, **49**, 351.
Lugiato, L. A., Narducci, L. M., Bandy, D. K., and Pennise, C. A., 1982, *Optics Communications*, **43**, 281.
Lugovoi, V. N., 1979, *Soviet Journal of Quantum Electronics*, **9**, 1207.
McCall, S. L., 1974, *Physical Review* A, **9**, 1515.
McCall, S. L., 1978, *Applied Physics Letters*, **32**, 284.
Marsden, J. E., and McCracken, M., 1976, *The Hopf Bifurcation and its Applications* (Berlin: Springer-Verlag).
Meier, D., Holzner, R., Derighetti, B., and Brun, E., 1982, *Evolution of Order and Chaos* edited by H. Haken (Berlin: Springer-Verlag).
Miller, D. A. B., Smith, S. D., and Johnston, A., 1979, *Applied Physics Letters*, **35**, 658.
Nicolis, G., and Prigogine, I., 1977, *Self-organization in Non-equilibrium Systems: from Dissipative Structures to Order through Fluctuations* (New York: Wiley & Sons).
Sandle, W. J., and Gallagher, A., 1981, *Physical Review* A, **24**, 2017.
Smith, P. W. (ed.), 1981, Special issue on optical bistability, *IEEE Journal of Quantum Electronics*, QE, **17**, N.3.
Smith, P. W., Hermann, J. P., Tomlinson, W. J., and Maloney, P. J., 1979, *Applied Physics Letters*, **35**, 486.
Smith, P. W., and Turner, E. H., 1977, *Applied Physics Letters*, **30**, 280.
Szöke, A., Daneu, V., Goldhar, J., and Kurnit, N. A., 1969, *Applied Physics Letters*, **15**, 376.
Venkatesan, T. N. C., and McCall, S. L., 1977, *Applied Physics Letters*, **30**, 282.
Weyer, K. G., Wiedenmann, H., Rateike, M., MacGillivray, W. R., Meystre, P., and Walther, H., 1981, *Optics Communications*, **37**, 426.

OPTICAL BISTABILITY AND RELATED TOPICS†

L.A. Lugiato
Dipartimento di Fisica, University di Milano
Milano 20133, Italy

L.M. Narducci
Physics Department, Drexel University
Philadelphia, PA 19104 U.S.A.

1. INTRODUCTION

The last decade has witnessed a rapidly growing interest for the general subject of cooperative phenomena in nonequilibrium systems[1,2]. The discovery that such dynamical fireworks as period doubling bifurcations and chaos give evidence of universal features[3,4] has stimulated extensive studies and produced encouraging advances. It is generally known that Quantum Optics has played a major role in the development of Synergetics[1]. Optical Bistability, in particular, has been a center of attraction because of its rich phenomenology and potential usefulness in technological applications. Actually, the field of quantum optics has uncovered more than one system capable of bistable behavior, such as, for example, the laser with a saturable absorber[5-8]. However, the term optical bistability is now commonly used to identify a very specific system; as such, this will be the focus of our attention.

To set the stage for our subsequent discussion, consider the typical layout of an optically bistable device. A coherent, monochromatic field E_I generated by a laser operating in a stationary regime is injected in an optical cavity, such as the Fabry-Perot shown in Fig. 1a. The cavity is adjusted to be resonant or nearly-

† Lectures delivered at the NATO ASI "Nonequilibrium Cooperative Phenomena in Physics and Related Fields", El Escorial (Madrid), Spain, August 1-11, 1983.

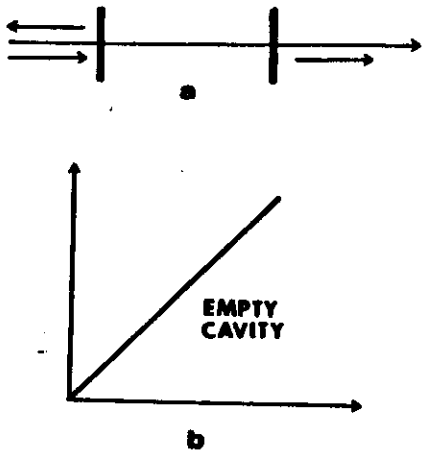

Fig. 1 (a) Empty Fabry-Perot cavity. I_I is the incident intensity; I_T and I_R are the transmitted and reflected intensities, respectively. (b) Transmitted intensity versus incident intensity for an empty cavity.

resonant with the incident field. Obviously, when the cavity is empty, the intensity $I_T = |E_T|^2$ of the transmitted field is proportional to the incident intensity $I_I = E_I^2$ (Fig. 1b), and the constant of proportionality depends on the mirror's transmission coefficient, on the degree of resonance between the incident radiation and one of the empty cavity modes, as well as, in practice, on the quality of the optics that makes up the interferometer.

The physical effects of interest for us arise when the cavity is filled with an absorbing medium, which can also be resonant or nearly-resonant with the incident light (Fig. 2a). In this case, the steady state behavior of the system is governed by the parameter

$$C = \frac{\alpha L}{2T} \qquad (1)$$

where α is the amplitude linear absorption coefficient per unit length, L is the longitudinal dimension of the atomic sample, and

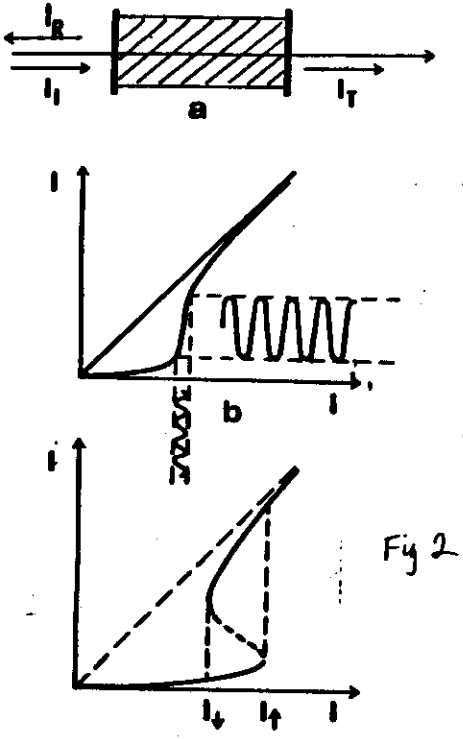

Fig 2

Fig. 2 (a) Fabry-Perot cavity filled by a nonlinear medium; (b) Optical transistor operation: a small modulation of the input intensity is amplified in the range where the differential gain is larger than unity; (c) Bistable operation: the dashed segment with negative slope is unstable; the range $I_\downarrow < I < I_\uparrow$ is bistable.

T is the intensity transmission coefficient of the mirror. For small values of C, the steady state transmission curve that relates the output with the input intensity is single-valued, and generally such that its slope dI_T/dI_I is smaller than unity. On increasing the value of C, a region of the transmission curve develops "differential gain" in the sense that dI_T/dI_I becomes greater than one (Fig. 2b). Under these conditions, the system works as an optical transistor because a slow intensity modulation imposed on the incident field gets amplified at the output. If C is increased even further, the steady state transmission curve becomes S-shaped (Fig. 2c). The segment with negative slope is unstable, while, typically (but not always) the upper and lower branches are stable. One can then find a range of values of the incident intensity for which the system displays a bistable character. With this setting, if we slowly increase the incident intensity from zero to a value beyond the bistable region, and then return to the starting point, the system traces a hysteresis cycle with low and high transmission branches. The two levels of transmission correspond to the logical states "0" and "1", thus suggesting the possibility that bistable devices may eventually form the heart of optical memories.

The threshold value of the parameter C for which bistable action develops depends on several physical parameters such as the degree of resonance between the incident field, the nonlinear medium and the cavity, the atomic linewidth, the type of resonator and so on. As we shall see, the emergence of bistable behavior is essentially tied to two main ingredients: one is the nonlinear nature of the atom-field interaction, and the other is the feedback action of the mirrors.

The existence of optical bistability was predicted in 1969 by Szöke and collaborators[9], but active investigations on this subject did not really begin until after the first experimental observation by Gibbs, McCall and Venkatesan in a sodium filled Fabry-Perot interferometer[10]. Shortly thereafter, Bonifacio and Lugiato formulated a first-principle, analytical description of optical bistability[11] which prompted very active research in two distinct directions, the first mainly concerned with the technological goal of producing practical, miniaturized, room temperature devices, and the second directed to the theoretical understanding of fundamental issues. In fact, the steady state hysteresis cycle of optical bistability exhibits striking analogies to first-order phase transitions in equilibrium systems. Furthermore, by controlling the parameters of the system, one can induce the emergence of spontaneous pulsations in the transmitted intensity. Depending on the choice of the parameters, the output oscillations can be highly periodic (regular self-pulsing behavior) or completely irregular (chaotic behavior, or optical turbulence).

For reasons of space, we have had to omit many interesting details: the reader can retrieve much additional information in the review papers by Gibbs et al.[12], by Abraham and Smith[13], by Arecchi and Salieri[14], by Lugiato[15,16] and in the papers on optical bistability contained in Ref. (17).

2. *A PRACTICAL OPTICAL BISTABLE DEVICE: RECENT ADVANCES*

Optical bistability in all-optical systems has been observed under widely varying conditions and experimental settings, from microwave to visible frequencies, from cavities of macroscopic size (several tens of centimeters) to miniaturized, micron-sized wafers. From a practical point of view, the most interesting situation concerns the smallest possible cavities. In fact, the ideal bistable device to be used as the basic element in a logical system ought to display the following attributes:

i. *Miniaturization.* Both the diameter and the length of the cavity should be in the micron range. In this case, high packing density can be achieved while keeping the cross-talk between neighboring units down to a negligible level, and at the same time, the cavity round-trip time is of the order of 10^{-2} picoseconds.

ii. *Fast response.* Both the switch-up and the switch-down time (i.e., the time required for the system to jump from the lower to the upper branch and viceversa) should be of the order of one picosecond.

iii. *Low energy requirement.* In order to minimise the energy consumption and the cooling requirements, the holding intensity should be less than one mW/μm^2.

iv. *The device should operate at room temperature.*

While these stringent conditions have not been entirely satisfied by the existing prototypes, great progress has been made in recent times using semiconductor materials such as GaAs[18] and InSb[19]. The situation is likely to improve rapidly even as these notes are being prepared. One of the devices constructed by Gibbs, McCall and collaborators at the Bell Telephone Laboratories (Murray Hill, NJ) consisted of a sample of GaAs, with a thickness of 4.1 μm, sandwiched between two AlGaAs layers (Fig. 3a) and reflecting coatings with a transmittivity of 10%. This system was supported by a 150 μm thick substrate of GaAs with a hole of 1-2 mm etched on it, to let the incident radiation through (Fig. 3b). Optical bistability, primarily due to the dispersive component of the medium's index of refraction was observed over a temperature range from 5 to 120°K for an incident wavelength of about 0.8 μm. The holding power of this device was about 1mW/μm^2 and the switching times were smaller than 40 nsec. More recently, bistable operation at room temperature has been reported with a GaAs-AlGaAs multiple quantum well structure[20].

The nonlinear Fabry-Perot constructed by Smith, Miller and collaborators[19] using InSb consisted of an uncoated plane-parallel crystal of dimensions 5x5 mm^2 by 560 μm. Bistability was observed at 5°K using as the input source a CO laser with an output wavelength of about 5 μm (Fig. 4). The holding intensity for this device was only 15 μW/μm^2. For InSb also, room temperature bistability has been reported recently[21].

3. THEORY OF OPTICAL BISTABILITY IN A RING CAVITY

A convenient setting for the analysis of a bistable optical system is a ring cavity because the incident light can be forced to propagate in only one direction. As shown in Fig. 5, a sample of length L and volume V containing N>>1 two-level atoms is placed in a ring cavity of total length $\mathcal{L}$. The incident field amplitude

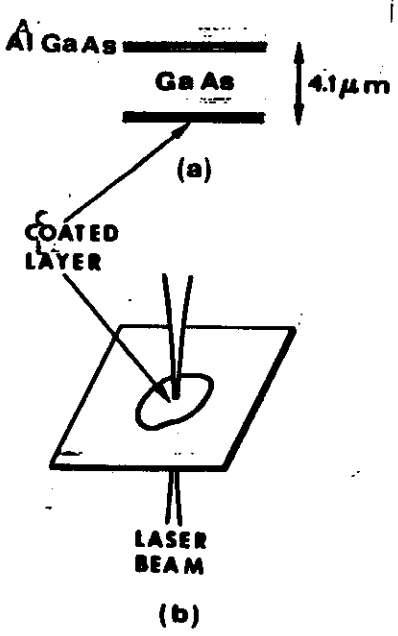

Fig. 3 (a) Miniaturized all-optical bistable system; a 4μm wafer of GaAs is sandwiched between two layers of AlGaAs. (b) GaAs substrate with a hole etched in the center to let the laser beam through.

is labelled $\mathcal{E}_I$, while $\mathcal{E}_T$ and $\mathcal{E}_R$ denote the transmitted and reflected amplitudes respectively. The upper mirrors have a reflectivity coefficient R = 1-T while the lower mirrors are assumed to have 100% reflectivity. We denote by $\mathcal{E}(z,t)$ and $\mathcal{P}(z,t)$ the electric field amplitude and the macroscopic atomic polarization inside the resonator. The field obeys the boundary conditions

$$\mathcal{E}(0,t) = \sqrt{T}\,\mathcal{E}_I + R\,\mathcal{E}(L,t-\Delta t) \qquad (2)$$

where T is the transmittivity coefficient of mirrors 1 and 2 and Δt is the light transit time from mirror 2 to mirror 1

$$\Delta t = \frac{\mathcal{L}-L}{C} \qquad (3)$$

The second term in Eq. (2) is responsible for the feedback mechanism which, as we mentioned, is essential for the emergence of bistability. We now let ω_0 and $\kappa_0 = \omega_0/C$ denote the radian frequency and the wave

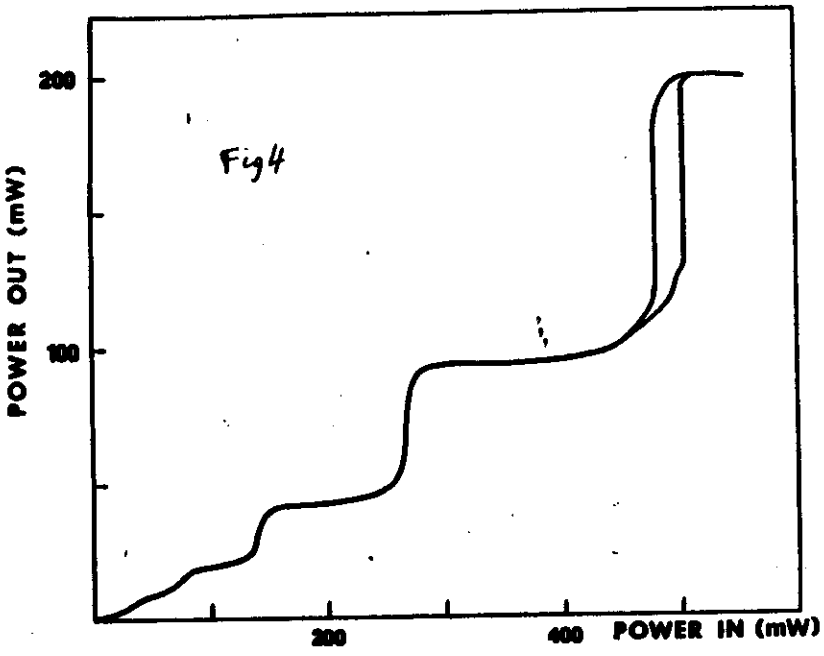

Fig. 4 Bistable action in InSb.

vector of the light field and set

$$\mathcal{E}(z,t) = E(z,t)\exp\left[-i(\omega_0 t - K_0 z)\right] + c.c. \qquad (4a)$$

$$\begin{Bmatrix}\mathcal{E}_I\\ \mathcal{E}_T\end{Bmatrix}(t) = \begin{Bmatrix}E_I\\ E_T\end{Bmatrix}(t)\exp(-i\,\omega_0 t) + c.c. \qquad (4b)$$

$$\mathcal{P}(z,t) = P(z,t)\exp\left[-i(\omega_0 t - K_0 z)\right] + c.c. \qquad (4c)$$

where $E(z,t)$ and $P(z,t)$ are the slowly varying field and polarization envelopes, respectively. After substituting Eq. (4a) into Eq. (2), we obtain

$$E(0,t) = \sqrt{T}\,E_I + R\,e^{-i\delta_0}E(L,t-\Delta t) \qquad (2')$$

where δ_0 is the cavity detuning parameter

$$\delta_0 = \frac{\omega_c-\omega_0}{c/2\mathcal{L}} \qquad (5)$$

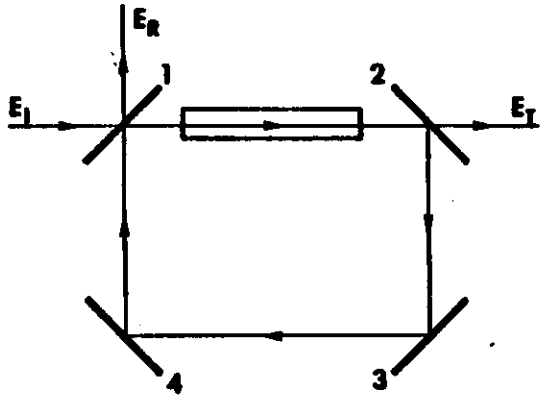

Fig. 5 Schematic layout of a ring cavity. $\mathcal{E}_I$, $\mathcal{E}_T$ and $\mathcal{E}_R$ are the incident, transmitted and reflected field amplitudes, respectively.

and ω_c is the empty cavity resonance which lies nearest to ω_0 (we recall that in a ring cavity the eigenfrequencies are given by $2\pi cm/2\mathcal{L}$, m=1,2,...). In addition to Eq. (2'), we have the obvious relation

$$E_T(t) = \sqrt{T}\,E(L,t) \qquad (6)$$

As the incident field propagates through the sample, the medium reacts back on it. The coupled atom-field dynamics is described by the so-called Maxwell-Bloch equations[22]. In the case of homogeneously broadened, two-level atomic systems, these equations take the form

$$\frac{\partial E}{\partial t} + c\frac{\partial E}{\partial z} = -\,g\,P \qquad (7a)$$

$$\frac{\partial P}{\partial t} = \frac{\mu}{\hbar}E\,D - \gamma_\perp(1+i\Delta)\,P \qquad (7b)$$

$$\frac{\partial D}{\partial t} = \frac{-\mu}{2\hbar}(E^*P+EP^*) - \gamma_\parallel(D-N/2) \qquad (7c)$$

where D is half the population difference of the lower and upper level, μ is the modulus of the atomic dipole moment of the atoms, g is the coupling constant

$$g = \frac{4\pi\omega_0}{V}\mu \tag{8}$$

$\gamma_\parallel$ and $\gamma_\perp$ are the longitudinal and transverse atomic relaxation rates, and in particular $\gamma_\perp$ coincides with the atomic linewidth. The parameter Δ measures the atomic detuning

$$\Delta = \frac{\omega_a - \omega_0}{\gamma_\perp} \tag{9}$$

and ω_a labels the atomic transition frequency. Δ controls the dispersive effects: in particular, for $\Delta=0$ no dispersion in present and the bistability effect is called purely absorptive. In the presence of dispersion, it is common practice to refer to the effect as dispersive bistability, even though the absorptive part of the atomic polarization may be entirely nonnegligible.

3.1 *STEADY-STATE BEHAVIOR IN ABSORPTIVE OPTICAL BISTABILITY WITH ZERO CAVITY DETUNING*[23]

This is the simplest situation that one can encounter from a mathematical point of view. When $\Delta=0$, Eqs. (7b,c) in steady state ($\partial/\partial t = 0$) yield

$$P(z) = \frac{N}{2}\sqrt{\frac{\gamma_\parallel}{\gamma_\perp}}\,\frac{F(z)}{1+F^2(z)}$$
$$D(z) = \frac{N}{2}\,\frac{1}{1+F^2(z)} \tag{10}$$

where F(z) is the scaled field amplitude

$$F(z) = \frac{\mu E(z)}{\hbar\sqrt{\gamma_\perp\gamma_\parallel}} \tag{11}$$

If we now substitute Eq. (10) into Eq. (7a), the stationary field equation takes the form

$$\frac{dF}{dz} = -\alpha\frac{F}{1+F^2} \tag{12}$$

where α is the linear absorption coefficient per unit length (at the atomic line center)

$$\alpha = \frac{\mu g N}{2\hbar c\gamma_\perp} \tag{13}$$

In terms of the normalized incident and transmitted field y and x

$$y = \mu E_I/\hbar\sqrt{\gamma_\perp\gamma_\parallel T}$$
$$x = F(L) = \mu E_T/\hbar\sqrt{\gamma_\perp\gamma_\parallel T} \tag{14}$$

the boundary conditions (2') with $\delta_0 = 0$, can be rewritten in the form

$$F(0) = Ty + Rx \tag{15}$$

and Eq. (12) can be integrated at once with the result

$$\ln(F(0)/x) + \frac{1}{2}\left[F^2(0)-x^2\right] = \alpha L \tag{16}$$

Finally, on combining Eqs. (15) and (16) we obtain the exact relation between the transmitted field x and the incident field y

$$\ln\left[1+T\left(\frac{Y}{x}-1\right)\right] - \frac{x^2}{2}\left\{\left[1+T\left(\frac{Y}{x}-1\right)\right]^2 - 1\right\} = \alpha L \tag{17}$$

Figure 6 shows the transmission curve x=x(y) for $C \equiv \alpha L/2T=10$ and several values of αL and T. An important feature is that, if T becomes too large, the bistable behavior disappears. In particular this is always so for T=1, regardless of the values of the other system parameters. This result shows that in order to achieve bistability, one needs not only a nonlinear medium, but also feedback action (i.e., good mirrors).

3.2 *THE EFFECT OF DISPERSION - KERR MEDIUM*

Consider first the case of an empty cavity in steady state. Because in this case we have $E(0)=E(L)=E_T/\sqrt{T}$, Eq. (2') yields the well known Airy transmission function

$$\mathcal{T} \equiv \frac{I_T}{I_I} = \left[1 + \frac{4R}{T^2}\sin^2\frac{\delta_0}{2}\right]^{-1} \tag{18}$$

The dependence of $\mathcal{T}$ on $\delta_0 = \omega c/\mathcal{L}$ displays the usual resonances shown in Figure 7. The peaks of the resonances coincide with the empty cavity eigenfrequencies. Each resonance has a width

$$\kappa = cT/\mathcal{L} \tag{19}$$

which is commonly denoted as cavity linewidth. When the cavity is filled with a nonlinear medium, it is useful to represent the internal field in terms of its modulus and phase:

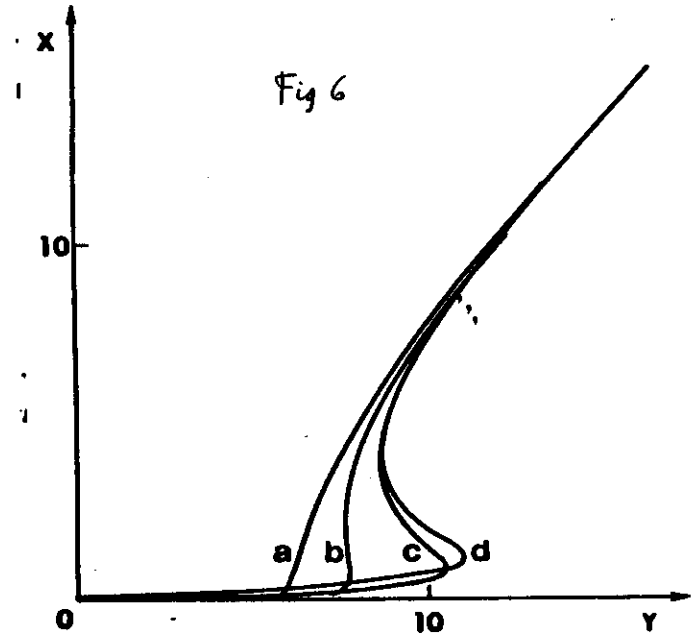

Fig. 6 Steady state transmitted field x as a function of the input field y for $\Delta=\delta_0=0$. All the segments with negative slope are unstable. The parameter $C = \alpha L/2T$ is held fixed and equal to 10. (a) $\alpha L=20$, $T=1$, (b) $\alpha L=10$, $T=0.5$, (c) $\alpha L=2$, $T=0.1$, (d) mean field limit $\alpha L \to 0$, $T \to 0$ with $C=10$.

$$E(z,t) = \rho(z,t)\, \exp(i\phi(z,t)) \tag{20}$$

In steady state, the space dependence of ρ and ϕ can be easily derived from Eqs. (7)

$$-\frac{d\rho}{dz} = -\alpha\, \rho\, \chi_a(\rho^2) \tag{21a}$$

$$\frac{d\phi}{dz} = -\alpha\, \chi_d(\rho^2) \tag{21b}$$

where χ_a and χ_d represent the absorptive and dispersive parts of the nonlinear dielectric susceptibility of the medium, i.e.,

$$\chi_a = \frac{1}{1+\Delta^2+\rho^2}\,, \quad \chi_d = \Delta\chi_a \tag{22}$$

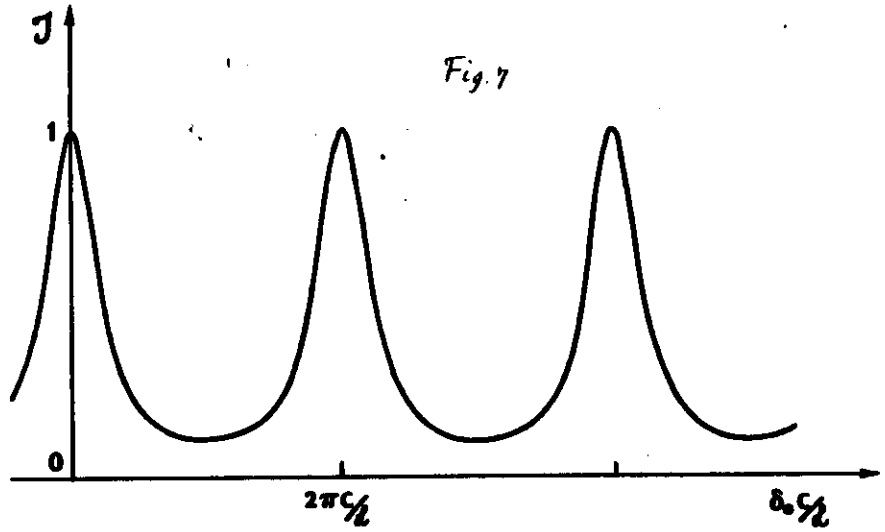

Fig. 7 The transmission function of the empty cavity is plotted as a function of the cavity detuning parameter $\delta_0 c/\mathcal{L} = \omega_c - \omega_0$.

Equation (21a) leads to a well known physical consequence in the limit when the field amplitude is sufficiently small ($\rho^2 \ll 1+\Delta^2$). After approximating χ_a with $(1+\Delta^2)^{-1}$, Eq. (21a) can be integrated at once to yield

$$\rho(z) = \rho(0)\exp(-\bar{\alpha}z), \quad \bar{\alpha} \equiv \frac{\alpha}{1+\Delta^2} \tag{23}$$

where $\bar{\alpha}$ is the out of resonance linear absorption coefficient. This result is known in optics at the Beer absorption law.

More generally, the boundary conditions (2') and Eq. (6) lead to the following general expression for the transmission of a ring cavity in steady state

$$\mathcal{I} \equiv \frac{I_T}{I_T} = \frac{T^2}{(\eta-R)^2 + 4R\eta\, \sin^2[\frac{1}{2}(\delta_0 - \Delta\phi)]} \tag{24}$$

where

$$\eta \equiv \frac{\rho(0)}{\rho(L)} \geq 1$$

$$\Delta\phi \equiv \phi(L) - \phi(0) \tag{25}$$

In the limit of an empty cavity, i.e., when $\alpha=0$, Eqs. (21) lead to $\eta=1$ and $\Delta\phi=0$, so that the transmission function (24) reduces to the form given by Eq. (18), as expected. Note also that, in the small field limit, η is given by $\exp(\bar{\alpha} L)$.

It is important to observe at this point that Eqs. (21) are much more general than one might surmise from the present discussion. If the nonlinear medium is not made up of homogeneously broadened two-level atoms, the nonlinear dielectric susceptibility functions are no longer given by Eq. (22) and depend, of course, on the specific medium. The crucial point, however, is that, in all instances, η and $\Delta\phi$ *depend* on the transmitted intensity, i.e., $\eta = \eta(I_T)$ and $\Delta\phi = \Delta\phi(I_T)$. In our case, these functions can be calculated explicitly by solving the differential equations (21) while taking Eq. (6) into account. Thus, the interferometer transmission function (24) provides an explicit expression for the incident intensity I_I as a function of I_T

$$I_I = f(I_T)$$

$$f = \frac{I_T}{T^2}\left\{[\eta(I_T)-R]^2 + 4R\eta(I_T)\sin^2\left[\frac{1}{2}(\delta_0-\Delta\phi(I_T))\right]\right\} \tag{26}$$

The function f is single-valued by definition; however, if we plot I_I as a function of I_T, and exchange the horizontal with the vertical axis, we see that I_T can be a multivalued function of I_I (Fig.8). In this case, the s-shaped form of the transmitted intensity curve gives the clue for the existence of bistability.

When the atomic detuning is large ($\Delta^2 \gg 1+\rho^2$), the absorptive component of the susceptibility becomes negligible with respect to the dispersive part, and bistability becomes, properly, of the dispersive type. As a concrete example of the analysis developed in this subsection, we focus on the case of dispersive bistability in a Kerr medium in which

$$\chi_a=0,\ \chi_d = c_1+c_2\,\rho^2 \tag{27}$$

From eqs. (25), (21) and (6) we easily obtain

$$\eta=1,\ \Delta\phi = a_1 - a_2\, I_T \tag{28}$$

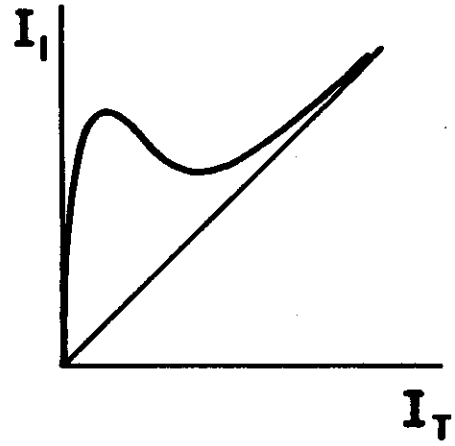

Fig. 8 Incident intensity plotted as a function of the transmitted intensity.

where $a_1 = -\alpha\Delta L c_1$, $a_2 = \alpha L \Delta c_2/T$ (*Note:* the appearance of the absorption coefficient should not be interpreted as a contradiction of the statement $\chi_a=0$; the Kerr limit can be obtained by detuning the incident field from the atomic resonance to the point that the absorption at the selected frequency is negligible, while, of course, the line center absorption coefficient is different from zero). In this case, Eq. (24) leads to the following transmission function

$$\mathcal{T} \equiv \frac{I_T}{I_I} = \frac{1}{1+\frac{4R}{T^2}\sin^2\left\{\frac{1}{2}\left[(\delta_0-a_1) + a_2\, I_T\right]\right\}} \tag{29}$$

If we plot $\mathcal{T}$ as a function of $I' \equiv a_2\, I_T$, we obtain Figure 9, a curve that coincides with the empty cavity curve ($\mathcal{T}$ vs. δ_0, Fig.7) apart from a translation of the horizontal axis by an amount $-a_1$. The stationary solutions of the system can be found with the help of a simple graphical procedure devised by Felber and Marburger[14] which consists of looking for the intersects of Eq. (29) with the

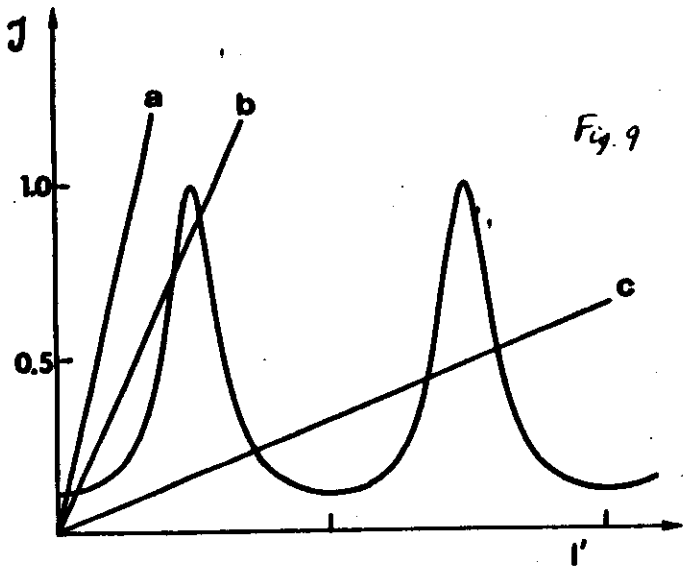

Fig. 9

Fig. 9 Graphical search of the stationary solutions for a Kerr medium. I' is defined as $a_2 I_T$ (see text).

straight lines $\mathcal{J} = I_T/I_I = I'/a_2 I_T$ whose slope is inversely proportional to the incident intensity. For small values of I_I, one has only one intersect (line a). On increasing the strength of the incident intensity, three intersections develop (line b) which correspond to a bistable situation because the intermediate solution is unstable. Hence, if one plots I_T as a function of I_I, one finds a hysteresis cycle. For larger values of I_I, one obtains multiple solutions (line c) which lead to multi-stability and multiple limit cycles. When T approaches unity, the curve (29) flattens out and bistability disappears.

4. *THE MEAN FIELD MODEL OF OPTICAL BISTABILITY*

The description of our system takes a particularly simple form in the limit of small absorption, small transmittivity coefficient and small cavity detuning

$$\alpha L \ll 1, \quad T \ll 1, \quad \delta_0 \ll 1 \tag{30a}$$

as long as the following ratios remain finite, but otherwise arbitrary

$$C \equiv \frac{\alpha L}{2T}, \quad \text{constant and arbitrary} \tag{30b}$$

$$\theta \equiv \frac{\delta_0}{T}$$

This situation is called "mean field limit" because when L approaches zero, the internal field becomes spacially uniform, so that its value at the output mirror coincides with its mean value in space. Note that here the words "mean field" have a different meaning from that which is commonly understood in the context of equilibrium phase transitions (e.g., in the Landau theory).

In the limit (30), the time evolution is governed by the so-called "mean field model", first proposed by Bonifacio and Lugiato[11].

$$\kappa^{-1} \dot{x} = -i\theta x - (x-y) - 2Cp \tag{31a}$$

$$\gamma_\Delta^{-1} \dot{p} = xd - (1+i\Delta)p \tag{31b}$$

$$\gamma_\parallel^{-1} \dot{d} = -\frac{1}{2}(xp^* + x^*p) - d + 1 \tag{31c}$$

The dot denotes derivative with respect to time and

$$p = \left(\sqrt{\frac{\gamma_\parallel}{\gamma_\perp}}\,\frac{N}{2}\right)^{-1} P, \quad d = \left(\frac{N}{2}\right)^{-1} D$$

The steady state solution of Eqs. (31) is easily calculated and it leads to the state equation

$$y^2 = |x|^2 \left\{(1+2C\chi_a(|x|^2))^2 + (\theta - 2C\chi_d(|x|^2))^2\right\} \tag{32}$$

where χ_a and χ_d are given by Eq. (22). If, in particular, one sets $\theta = \Delta = 0$, it is easy to prove that the state equation reduces to

$$y = x\left[1 + \frac{2C}{1+x^2}\right] \tag{33}$$

which coincides with the limit of Eq. (17) when $\alpha L \to 0$, $T \to 0$ and $C = \alpha L/2T$ = constant. This result is displayed graphically in Figure 6.

The limit $\delta_0 \ll 1$ implies that the operation of the system is restricted to the resonant cavity mode at frequency ω_c. Hence, the mean field model is a *single-mode* model. It has played an important role in quite a number of investigations on the transient properties

of Optical Bistability.

5. *SELF-PULSING AND CHAOTIC BEHAVIOR*

In this section we discuss the matter of *instabilities* in Optical Bistability. As usual, a stationary state (or a stationary regime) is said to be unstable when, as a result of a perturbation, the system departs exponentially from its initial configuration. Of course, an unstable state is never realized, in practice, because even the slightest perturbation removes the system from it.

The existence of optical bistability is itself a manifestation of the existence of an instability. In fact, on approaching the upper bistability threshold $I_\uparrow$ from below (see Fig. 2c) the low transmission state becomes unstable and precisely for this reason the system jumps to the high transmission branch. The same process in reverse is responsible for the downward transition at the lower bistability threshold $I_\downarrow$.

It is well known, on the other hand, that nonlinear systems usually display sequences of successive instabilities where a steady state becomes unstable, thus driving the system to another stable steady state, which in turn becomes unstable, and so on. This sequence can be identified by varying the control parameters of the system (for example, in optical bistability, the intensity of the incident field or the length of the cavity). Typically, after a few instabilities the system runs out of stationary states and develops an oscillatory behavior with the emergence of spontaneous pulsations. The oscillations can be regular, i.e., perfectly periodic in time, as well as completely irregular and aperiodic. In the latter case, one speaks of chaotic or turbulent behavior.

Two points are of basic importance:

(a) The oscillations are not induced by external manipulations. They arise even when all the external parameters are constant in time. It is not unexpected, for example, that pulsed behavior should be produced in a bistable system by modulating the cavity length; this is a rather trivial fact. It is a different story, instead, when time-independent external parameters produce spontaneous pulsations because this is indicative of the existence of self-organization from within the system itself (for this reason, a behavior of this type is called self-pulsing).

(b) In the chaotic case, the time-dependent output intensity is often reminiscent of the type of behavior that may be expected of a system which has been contaminated by a noise source. In the situations of interest to us, chaotic behavior persists even without any external noise perturbation; because its origin resides in the differential equations themselves it is often called <u>deterministic chaos</u>.

Chaotic self-pulsing and the various routes by which this effect is produced have been the object of very active research in recent years, although our understanding of these phenomena is still far from being satisfactory. The best understood and most frequently occurring route to chaos in quantum optical systems is the so-called "period-doubling route"[3,6]. This begins with the system in a stable oscillatory state characterized by a fundamental frequency $\bar{\omega}$ (in point of fact, $\bar{\omega}$ usually varies slowly as a function of the external parameters, but this is not important for this discussion). As one varies a selected control parameter, at some point the oscillatory state becomes unstable, and the system approaches a new stable state of oscillation whose period is twice as long as the previous one. In this case, the power spectrum of the observable variables develops a component at the subharmonic frequency $\bar{\omega}/2$. By further changing the control parameter, a subsequent instability develops which then leads to a new periodic oscillation whose period is four times as large as the original one. This process goes on indefinitely (again, we must stress that because of the slow dependence of $\bar{\omega}$ on the control parameters, it is not exactly true that the period of, say, the nth bifurcation is 2^n times longer than the original period. What is rigorously true, however, is that the power spectrum of the nth bifurcation displays a string of subharmonic frequencies components $\bar{\omega}_n/2^n$ where $\bar{\omega}_n$ is the fundamental oscillation frequency of the new stable solution). The values of the control parameter at which period doubling is observed get closer and closer according to a geometrical law, such that the ratio between the intervals in which period 2^n and period 2^{n+1} are observed approaches the value 4.6692..., as n approaches infinity. This value is universal in the sense that it characterizes all period doubling sequences. Hence, very rapidly, the sequence reaches an accumulation point beyond which the system exhibits chaotic behavior. In the chaotic regime, the power spectrum is no longer a simple line spectrum, but it displays a continuous background.

As shown in this section, optical bistability displays both periodic and chaotic self-pulsing. We shall distinguish two cases according to the mechanism which is responsible for the emergence of an instability in the stationary state. The optical cavity is characterized by an infinite number of possible excitation frequencies (modes); accordingly the behavior of the system can be described in terms of *mode amplitudes*. In the two cases to be discussed, the amplitude of the resonant mode becomes unstable (case 1); in the second case, the instability arises from the off-resonance modes.

6.1 *RESONANT-MODE INSTABILITY*

This type of instability can arise only in the dispersive case[25,26]. The stability analysis of the mean field model (31) shows[26] that under appropriate conditions, a sizeable segment of the high transmission branch becomes unstable (see Fig. 10). Roughly speaking, the mechanism of the instability can be described as follows. In the dispersive situation, the atomic and the incident field frequency are mismatched. When the mismatch is sufficiently large, the system is no longer able to adapt itself to the driving field; the stationary state becomes unstable and the output begins to develop oscillations in the form of an undamped sequence of pulses. From a practical point of view, this behavior is very

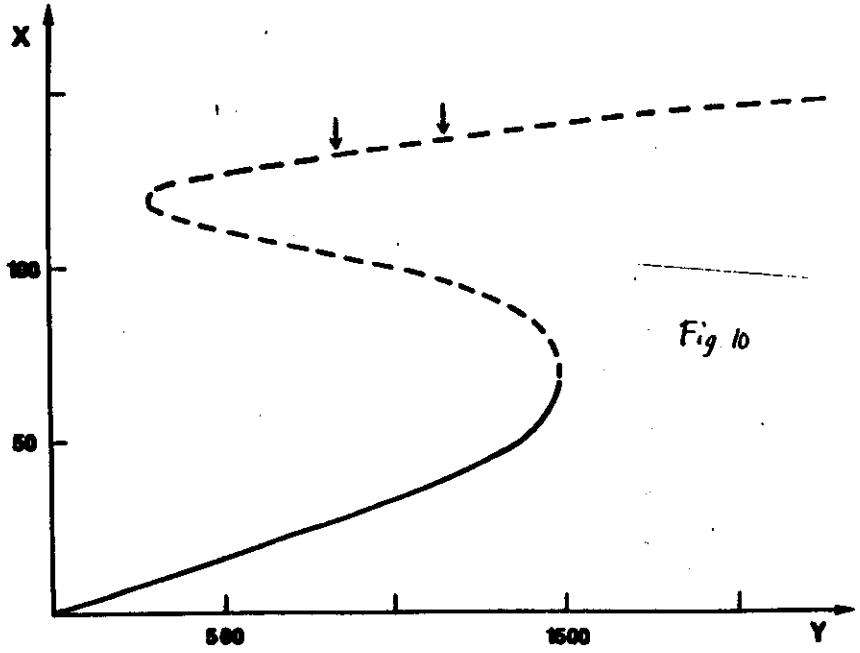

Fig. 10 Steady state transmission curve for C=70,000, Δ=374 and θ=340. The dashed segment is unstable. The arrows mark the region of the upper branch where chaotic behavior is found.

interesting, as it suggests the possibility that an optical device may convert a coherent constant intensity beam into coherent pulsed light.

Consider now what happens when the system jumps from the lower to the higher transmission branch. Since, in the case illustrated in Figure 10, the higher branch is unstable at the switching point, one expects immediately the appearence of a regular sequence of oscillations (Fig. 11a). Another way of looking at the same behavior is to consider the plane of the real and imaginary parts of the normalized transmitted field. In this case, the trajectory in this plane is a simple limit cycle (Fig. 11b). If one now decreases the incident field strength (the control parameter), the system undergoes a period doubling bifurcation (Fig. 11c) which corresponds to the trajectory shown in Fig. 11d. This trajectory arises from a kind of fission process of the limit cycle into two distinct parts. A further decrease of y leads to the appearence of period four (Figs. 11e,f) and so on. Finally, the system enters the chaotic domain (Figs. 10,11g,h) with the time trace displaying no remnant of periodicity.

6.2 *OFF-RESONANCE MODE INSTABILITY*

This phenomenon arises when two cavity modes, other than the resonant one, fall below the power broadened absorption line of the atomic medium. This condition can be fulfilled, for example, by increasing the length of the cavity, thus decreasing the intermode spacing. In this situation, under suitable conditions, the off-resonant mode amplitudes become unstable, while the resonant mode remains stable (in the sense of linear stability) analysis.

Consider first the simplest absorptive case $\Delta=\theta=0$. The external parameters of practical interest are the incident field y and the total length $\mathcal{L}$ of the ring cavity. Instead of y and $\mathcal{L}$, it is more convenient to use x, which is linked to y by Eq. (33), and $\tilde{a}/\gamma_\perp = 2\pi c/\mathcal{L}\gamma_\perp$ which is the spacing of two adjacent cavity modes in units of atomic linewidth $\gamma_\perp$. In Figure 12, we display the plane of the control parameters $\tilde{a}/\gamma_\perp$ and x. The stationary state of the high transmission branch becomes unstable when the operating point lies in the hatched part of the plane, which will be called instability region.

The mechanism that produces the instability in this case is different from the one discussed in the previous subsection. It is, instead, similar to what one finds in the so-called saturation spectroscopy[27] where an atomic sample is illuminated by a strong coherent stationary field which saturates the medium, and sampled by a weak probe beam (see Fig. 13). In this case, one finds that for suitable ranges of values of the frequency detuning between

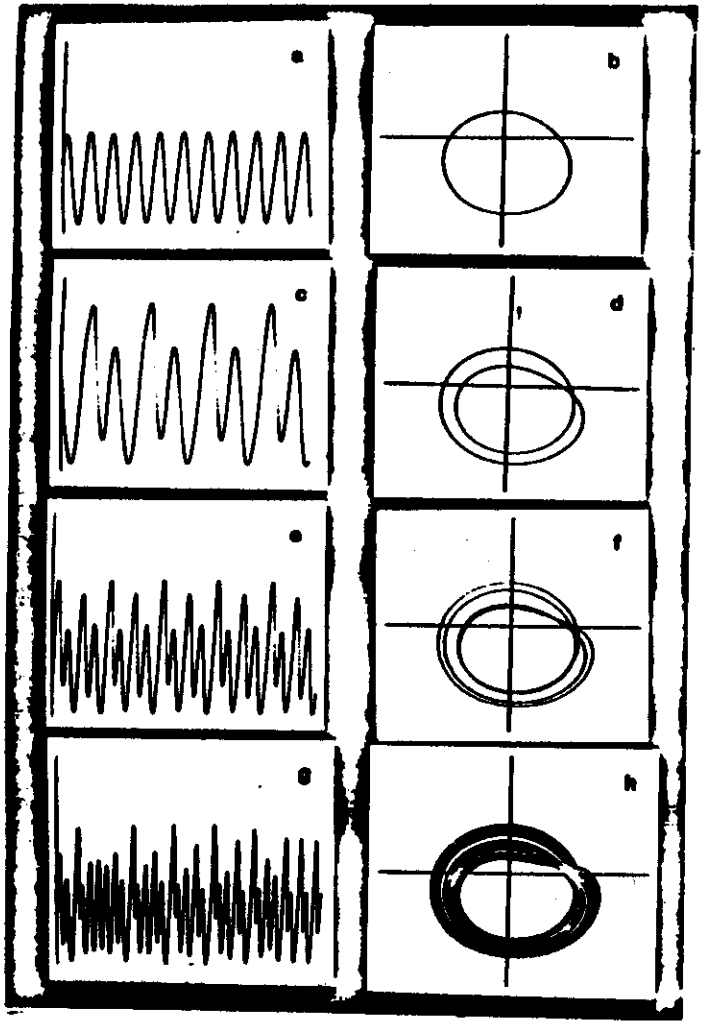

Fig. 11 Self-pulsing oscillations and corresponding phase-space trajectories in the plane of the real and imaginary parts of the normalized electric field for solutions of the type: period 1 (a,b), period 2 (c,d), period 4 (e,f), and chaotic (g,h), respectively. The values of the external field are y=2000, 1350, 1225 and 950 for the four sets of solutions.

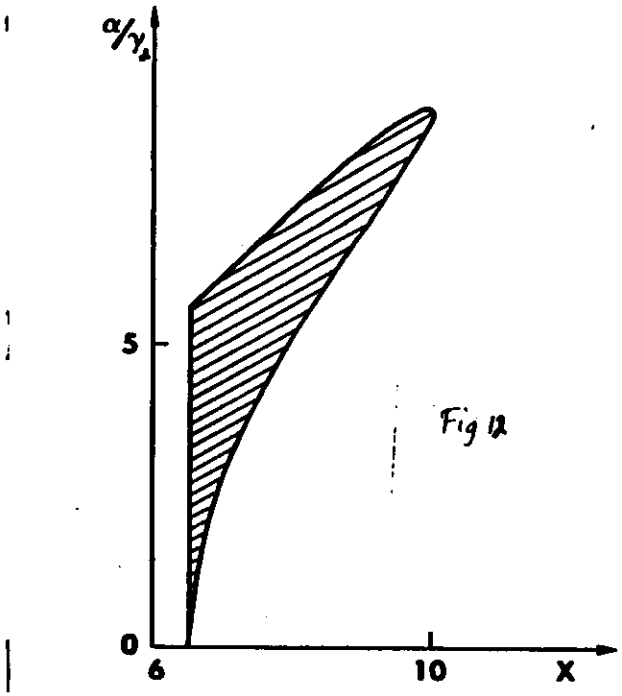

Fig 12

Fig. 12 Instability region in the plane of the control parameters $\tilde{a}/\gamma_\perp$ and x.

saturating and probe beam, the probe experiences gain instead of loss (as one might expect, because the sample under study does not have a population inversion). The same happens in our system: the resonant cavity mode saturates the medium, while the neighboring modes play the role of the probe fields. Under appropriate conditions, some of the sidebands may experience gain, and when the gain becomes larger than the loss the sidebands become unstable. In some sense, the absorbing medium behaves as a laser with respect to the sidebands even without a built-in population inversion.

When the steady state in the higher branch is unstable, the system can exhibit two different kinds of evolutions[27,28]. In the first case, the system approaches a self-pulsing behavior; as we see from Fig. 14a, if the system is initially slightly displaced from steady state, it will begin to develop an oscillatory behavior. The amplitude of the oscillations increases with time, until a stationary regime is reaches, as evidenced by the flat shape of the self-pulsing envelope. The self-pulsing frequency in this case is equal to $\tilde{a}$ which corresponds to a period equal to the transit time,

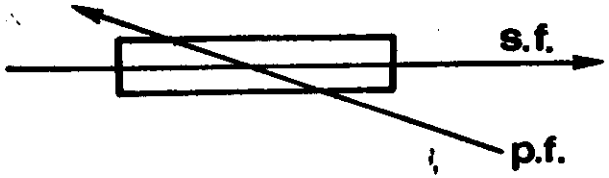

Fig. 13 Typical set-up of a saturation spectroscopy experiment. sf = saturating field; pf = probe field.

$\mathcal{E}/c$, of the photons in the cavity. The second possibility is that the system, after a transient self-pulsing action, simply precipitates to the low transmission state corresponding to the same value of the incident field. This possibility is illustrated in Fig. 14b from which we see that the oscillations are amplified, at first, but that eventually they die off as the system precipitates to the low transmission state.

The analytical treatment of this self-pulsing behavior, which is a multi-mode phenomenon, as it involves not only the resonant but also some of the sidebands, has been carried out in terms of a procedure called the "dressed mode theory of Optical Bistability"[29,31]. In the case of only two unstable sidebands (i.e., only three resonator modes altogether) this treatment is capable of handling the behavior of the system in terms of a simple two-dimensional description. The only two relevant variables are *(i) the half-amplitude of the oscillations, ρ, and (ii) the displacement, σ, of the mean value of the oscillations from the unstable steady state value x_{st}.* The upper and lower envelopes of the oscillations $x_{upper}(t)$ and $x_{lower}(t)$ are obtained as follows:

$$x_{\substack{upper\\lower}}(t) = x_{st} + \sigma(t) \pm \rho(t) \qquad (34)$$

Hence, the time evolution can be described in equivalent ways by the envelope of the oscillations or by a trajectory in the phase-space (ρ,σ).

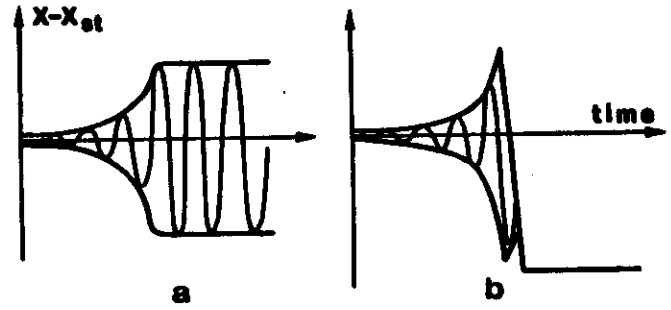

Fig. 14 Self-pulsing (a) and precipitation (b). x_{st} is the value of the normalized transmitted field at steady state in correspondence to the high transmission state.

Using the dressed mode theory, we can follow the behavior of the self-pulsing state over its entire domain of existence. This domain is shown in Figure 15 and is quite a bit wider than the instability region ABE. It can be subdivided into a "soft excitation" domain ABD, and a "hard excitation" domain BCC'D. The region ADE, instead, is the precipitation domain. The region bounded by the lines ABD corresponds to values of the control parameters $(x,\tilde{\sigma}/\gamma_\parallel)$ for which the self-pulsing state is stable, while the stationary state is unstable. Hence, a small initial deviation from steady state (soft excitation) is enough to push the system into the self-pulsing state. In the domain BCC'D, one encounters coexisting stationary and self-pulsing states, both being stable. Exactly which of the two stable states will be occupied by the system depends on the initial conditions; thus, if the initial fluctuation away from steady state is small, the system simply returns to the stationary state. The self-pulsing state is reached, instead, after a sufficiently large initial fluctuation (hard excitation).

Fig 15

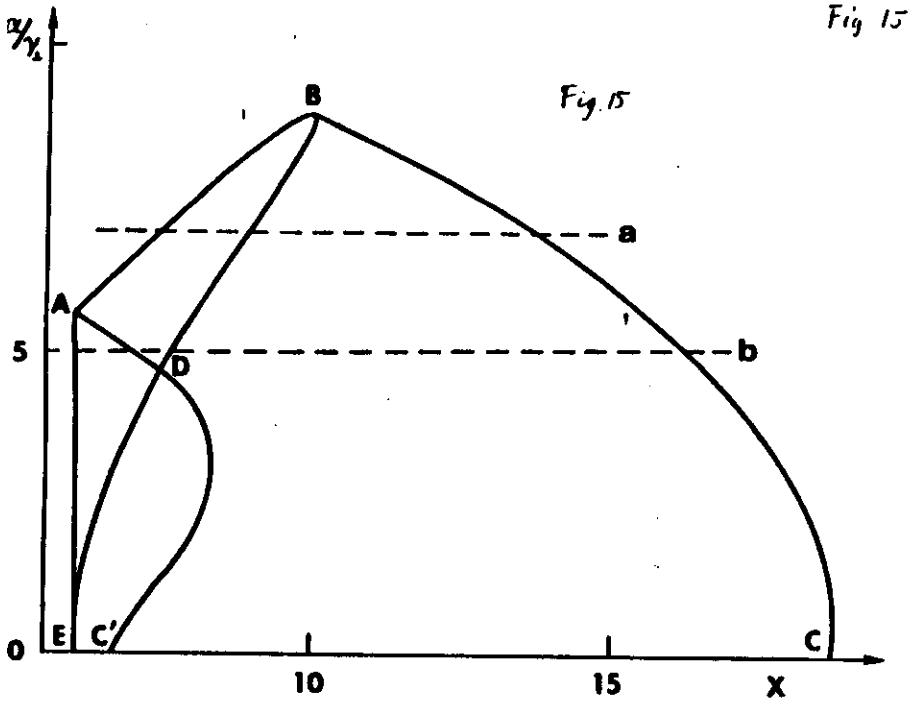

Fig. 15 Instability region, precipitation region and domain of existence of the stable self-pulsing solution for C=20, Δ=θ=0 in the mean field limit.

This situation leads to the appearance of a hysteresis cycle of new type. Figure 16 shows the half amplitude of the oscillations for long times, $\rho(t^{\infty})$, upon varying the incident field along the horizontal line a of Fig. 15. On entering the instability region from the left, a stable self-pulsing state develops. As the incident field is increased, the amplitude of oscillation also increases, and, in fact, it continues to do so even outside the instability region, until the system returns discontinuously to the stationary state in the high transmission branch. If one now decreases the amplitude of the incident field, the system continues to operate in the stationary high transmission branch until we reach the right boundary of the instability region, where it jumps discontinuously to the self-pulsing regime with a finite amplitude.

The diagram of Figure 16 can be viewed as representing a second and first order phase transition simultaneously. The second order transition occurs on the left boundary of the instability domain. The first order transition is tied to the hysteresis cycle that

Fig

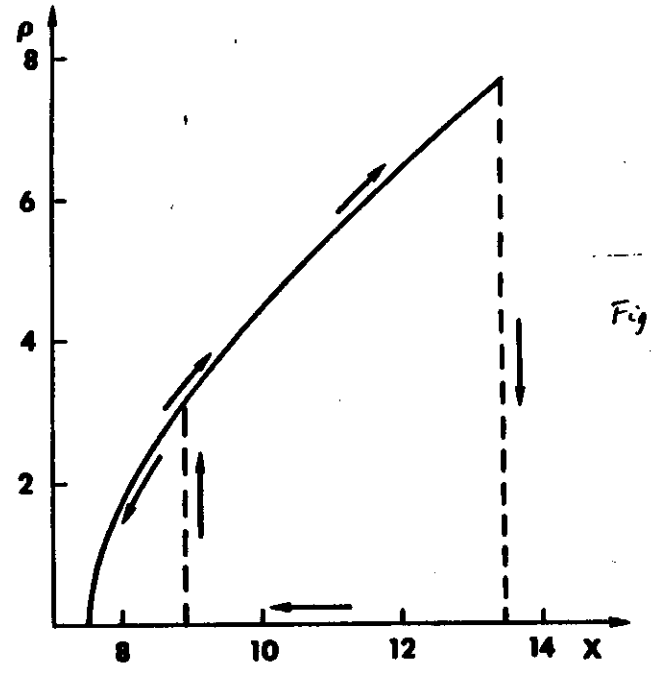

Fig. 16 The half-amplitude of the oscillations in the self-pulsing state is plotted as a function of the stationary value x of the transmitted field in the high transmission branch for C=20, $\bar{\alpha}/\gamma_{\perp}$=7 (line a of Fig. 15). The arrows indicate the behavior of the system when the incident field is decreased or increased.

begins at the right boundary domain. It is worth stressing that in this case the bistability involves stationary and self-pulsing states, and not just stationary states as in the operation of usual bistable systems. This hysteresis cycle enriches the phenomenology of optical bistability, especially because the new self-pulsing branch is accessible from the usual steady states by suitably varying the external parameters.

An interesting situation occurs in the neighborhood of the line AD (Fig. 15) that separates the self-pulsing from the precipitation domains. In order to describe this behavior, consider a continuous variation of the cavity length along the line b of Fig. 15. On approaching the line AD from the right, the time-dependent envelope begins to develop considerable oscillations (Fig. 17a). This behavior is usually called "breathing". The breathing pattern observed in our case, however, lasts only a finite amount of time

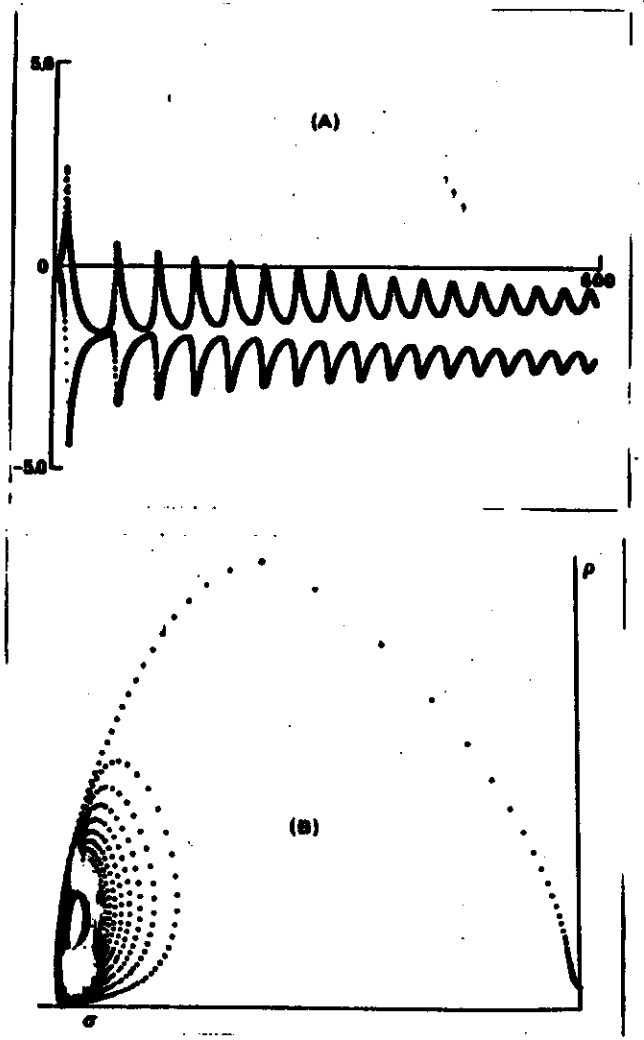

Fig. 17(a,b) Envelope breathing and phase trajectory in the (ρ,σ) plane for C=20, $\tilde{\alpha}/\gamma_{\perp}$=5, and x = 6.867.

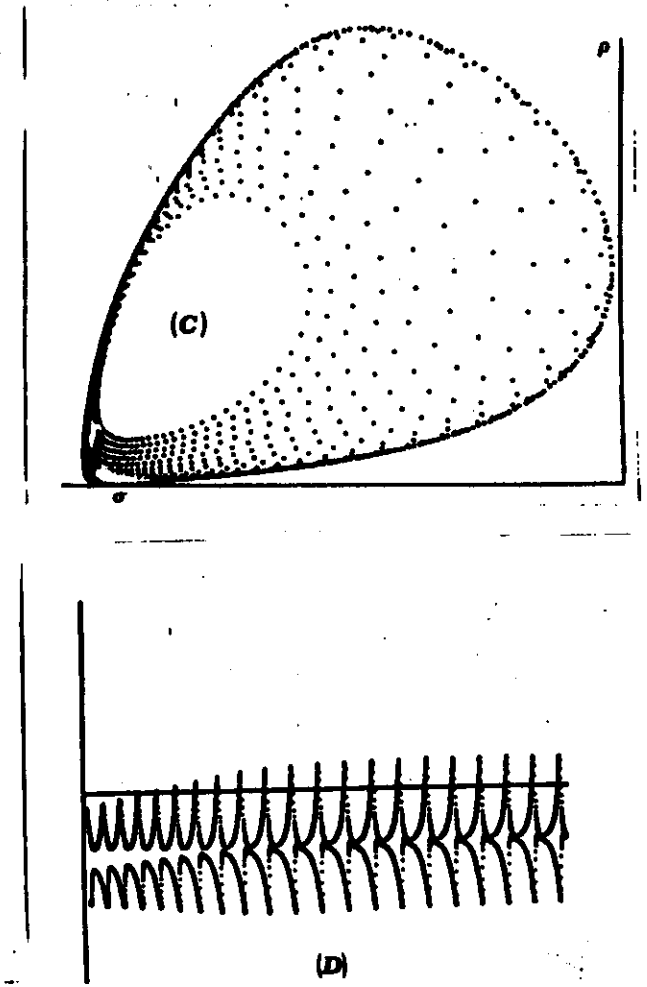

Fig. 17(c,d) Envelope breathing and limit cycle in the (ρ,σ) plane for C=20, $\tilde{\alpha}/\gamma_{\perp}$=5, and x = 6.8669. The limit cycle and the corresponding time dependant envelope have been obtained by integrating the equations of motion backward in time.

before eventually the envelope settles down to a steady asymptotic value. Figure 17b shows the same phenomenon, but from the point of view of the phase-space variables (ρ,σ). The trajectory in phase space spirals towards the point corresponding to the self-pulsing state, which behaves as a stable focus. After crossing the line AD, the focus becomes unstable through a Hopf bifurcation. In this case, one expects the appearance of a limit cycle in the phase space, which can be stable or unstable, depending on the nature of the Hopf bifurcation. The limit cycle that accompanies the crossing of the boundary line AD is unstable, i.e., it repels nearby trajectories. In order to display its presence, we have used a trick; by integrating the time evolution backward in time, the repeller becomes an attractor. Figure 17c shows the backward approach to the limit cycle in the (ρ,σ) phase-plane. Similarly, Figure 17d shows the backward time evolution of the envelope of oscillations of the transmitted field. Now for long times we have a perfectly periodic breathing regime in which the envelope marks time as a "regular" clock (but backwards in time). Of course, unstable limit cycles, just as unstable steady states, cannot be observed directly.

ACKNOWLEDGEMENTS

The research described in this review was partially supported by the Italian National Research Council (CNR), by a contract with the U.S. Army Research Office and by a grant from the Martin-Marietta Research Laboratories. We are grateful to Mrs. Debbie DeLise-Hughes for her skillful handling of this manuscript.

REFERENCES

1. H. Haken, *Synergetics - An Introduction*, Springer-Verlag, Berlin, 1977.
2. G. Nicolis and I. Prigogine, Self-Organization in Non-Equilibrium Systems: From Dissipative Structures to Order Through Fluctuations", Wiley and Sons, NY 1977.
3. S. Grossman and J. Thomae, Z. Naturforsch. 32a, 1353 (1977).
4. M.J. Feigenbaum, J. Stat. Phys. 19, 25 (1978) and 21, 669 (1979).
5. L.A. Lugiato, P. Mandel, S.T. Dembinski, and A. Kossakowski, Phys. Rev. A18, 238 (1978).
6. J.C. Antoranz, J. Gea, M. Velarde, Phys. Rev. Lett. 47, 1895 (1981); J.C. Antoranz, L.L. Bonilla, J. Gea, M. Velarde, Phys. Rev. Lett. 49, 35 (1982).
7. T. Erneux and P. Mandel, Z. Physik 44B, 353 and 365 (1982).
8. E. Arimondo, F. Casagrande, L.A. Lugiato and P. Glorieux, Appl. Phys. 30B, 57 (1983).
9. A. Szöke, V. Daneu, J. Goldhar and N.A. Kurnit, Appl. Phys. Lett. 15, 376 (1969).
10. H.M. Gibbs, S.L. McCall and T.N.C. Venkatesan, Phys. Rev. Lett. 36, 113 (1976).
11. R. Bonifacio and L.A. Lugiato, Opt. Comm. 19, 172 (1976).
12. H.M. Gibbs, S.L. McCall and T.N.C. Venkatesan, Opt. Eng. 19, 463 (1980).
13. E. Abraham, S.D. Smith, Rept. Progr. Phys. 45, 815 (1982).
14. F.T. Arecchi and P. Salieri, Physics Bull. 33, 20 (1982).
15. L.A. Lugiato, in *Progress in Optics*, Vol. XXI, edited by E. Wolf, North-Holland (in press).
16. L.A. Lugiato, Contemporary Physics (in press).
17. R. Bonifacio, Editor, *Dissipative Systems in Quantum Optics: Resonance Fluorescence, Optical Bistability, Superfluorescence*, Springer-Verlag, Berlin (1982).
18. H.M. Gibbs, S.L. McCall, T.N.C. Venkatesan, A.C. Gossard, A. Passner, and W. Wiegmann, Appl. Phys. Lett. 35, 451 (1979); S.S. Tarng, K. Tai, J.L. Jewell, H.M. Gibbs, A.C. Gossard, S.L. McCall, A. Passner, T.N.C. Venkatesan, and W. Weigmann, Appl. Phys. Lett. 40, 205 (1982).
19. D.A.B. Miller, S.D. Smith, C.T. Seaton, IEEE J. Quant. Elect. QE17, 312 (1981).
20. H.M. Gibbs, S.S. Tarng, J.L. Jewell, D.A. Weinberger, K.C. Tai, A.C. Gossard, S.L. McCall, A. Passner and W. Wiegmann, Appl. Phys. Lett. 41, 221 (1982).
21. S.D. Smith, Topical Meeting on Optical Bistability, Rochester (1981).
22. L. Allen and J.H. Eberly, *Optical Resonance and Two-Level Atoms*, Wiley and Sons, NY 1975.
23. R. Bonifacio and L.A. Lugiato, Lett. al. Nuovo Cimento, 21, 505 (1978).

(55)

References (contd.)

24. P.S. Pelber and J.H. Marburger, Appl. Phys. Lett. 28, 731 (1976).
25. K. Ikeda and O. Akimoto, Phys. Rev. Lett. 45, 709 (1980).
26. L.A. Lugiato, L.M. Narducci, D.K. Bandy and C.A. Pennise, Opt. Comm. 43, 281 (1982).
27. M. Gronchi, V. Benza, L.A. Lugiato, P. Meystre and M. Sargent III, Phys. Rev. A24, 1419 (1981).
28. R. Bonifacio and L.A. Lugiato, Lett. al Nuovo Cimento 21, 510 (1978).
29. L.A. Lugiato, V. Benza, L.M. Narducci and J.D. Farina, Zeit. Phys. B49, 351 (1983).
30. H. Haken, Zeit. Phys. B21, 105 (1975); ibid. B22, 69 (1975).
31. J.E. Marsden and M. McCracken, The Hopf Bifurcation and its Applications, Springer-Verlag, Berlin (1976).

(56)

From: COHERENCE AND QUANTUM OPTICS V
Edited by Leonard Mandel, and Emil Wolf
(Plenum Publishing Corporation, 1984)

SELF-PULSING, BREATHING AND CHAOS IN OPTICAL BISTABILITY AND IN A LASER WITH INJECTED SIGNAL

L.A. Lugiato
Dipartimento di Fisica, Universita' di Milano
via Celoria 16, Milano, Italy

L.M. Narducci
Physics Department, Drexel University
Philadelphia, PA 19104 USA

1. INTRODUCTION

Six years ago, two contributions on Optical Bistability were delivered at the Fourth Rochester Conference on Coherence and Quantum Optics[1], which, was apparently the first international meeting to include in its program an invited paper on this subject. Since then, the growth of interest in bistability has been so rapid to justify a second topical conference, following the 1980 meeting in Asheville[2].

Actually, despite the pioneering work by Szöke, Daneu, Goldhar, and Kurnit[3], Seidel[4] and others, widespread interest in Optical Bistability did not become obvious until after the experimental observation of this phenomenon by Gibbs, McCall and Venkatesan[5], almost exactly one year before CQO4. The early investigations were mostly focused on the description of the steady state, on the switching properties of the system, and on the identification of the optimal parameters for practical devices. Undoubtedly, we shall learn about the many recent technical advances from several other contributions in this Conference. Here we shall focus on one aspect of the theoretical development.

In 1978, two papers by McCall[6] and by Bonifacio and Lugiato[7] opened an entirely new line of investigation by showing that instabilities and spontaneous pulsations could occur in bistable systems. It is now well established that Optical Bistability can lead to a wide variety of time-dependent behaviors that need to be properly characterized, either because one may wish to avoid unwanted

oscillations in practical devices, or, perhaps, because these features are to be exploited for communication and signal modulation purposes.

This optical effect is directly connected to the general problem of the unstable and chaotic behavior displayed by all kinds of nonlinear systems in Physics and other disciplines[8,9]. In the specific case of Optical Bistability, wide excitement was created by Ikeda's prediction[10] of chaotic self-pulsing (optical turbulence).

In this paper, we focus our attention on the general subject of periodic and chaotic self-pulsing in optically bistable systems, and in the laser with injected signal, which represents the active counterpart of a bistable device (the absorbing medium is replaced by one with population inversion). In Section 2, we review the main results that have been obtained from the analysis of the Maxwell-Bloch equations for a unidirectional ring cavity. Section 3 contains a discussion of more recent findings concerning the instabilities that arise in the mean field model of mixed absorptive and dispersive bistability. Finally in Section 4, we provide examples of the rich variety of behaviors which are typical of the laser with injected signal.

2. MULTI-MODE SELF-PULSING BEHAVIOR IN OPTICAL BISTABILITY

Interest in the unstable behavior of quantum optical systems was stimulated, in the mid-sixties, by Haken and collaborators with their analyses of the single-mode[11] and multi-mode[12] homogeneously broadened ring laser. The possibility of pulsed behavior in Optical Bistability was mentioned in Ref. 3 for the first time. Later McCall[6] showed that pulsing can be produced when the nonlinearity of the medium originates from contributions having opposite signs and very different time constants. He also reported the observation of regenerative pulsations in a hybrid electro-optic system and proposed that the same phenomenon could be observed in a intrinsic all-optical device in which switching is produced by fast electronic effects, but where slower thermal drifts prevent either of the two states of transmission from being stable. In fact, a behavior of this type has been observed recently[13], with a pulsation period of the order of several microseconds.

Throughout this paper, we shall restrict ourselves to the case of a homogeneously broadened two-level atomic sample of length L, contained in a unidirectional ring cavity of length $\mathscr{L}$. We review the instabilities that have been predicted from the analysis of the Maxwell field equations, within the slowly varying envelope and plane wave approximations, and of the optical Bloch equations. This section, in particular, describes the nature and the origin of instabilities that involve more cavity modes than just the resonant

(or quasi-resonant) one. For additional details, the reader should consult the original papers or the recent review cited in Ref. 14.

(a) Bonifacio-Lugiato Self-Pulsing

The stability analysis of Ref. 7 proved for the first time that under appropriate conditions a stationary state of the system can become unstable because some of the off-resonance modes develop an instability. These modes act in a similar way to the probe field in saturation spectroscopy[15], in the sense that they may experience gain instead of attenuation. When the gain exceeds the cavity losses, these modes become unstable, and any initial fluctuation will be able to trigger their growth. The unstable mode amplitudes grow until the system reaches a new steady state regime, which can be stationary (the self-pulsing is quenched by the presence of another stable stationary state), or pulsed. In the latter case, the output displays undamped oscillations which, because of their spontaneous emergence within the system, are properly referred to as self-pulsing oscillations.

In order to achieve this off-resonance mode instability, it is necessary that at least one cavity mode, other than the resonant one, fall below the power-broadened absorption line of the atomic medium, $c/\mathscr{L} < \gamma_\perp \sqrt{1+I_T/I_S}$, where $\gamma_\perp$ is the homogeneous linewidth, I_T the transmitted intensity and I_S is the saturation intensity, respectively. This condition implies that the total length $\mathscr{L}$ of the ring cavity must be suitably large.

The Maxwell-Bloch equations predict this kind of self-pulsing both in the absorptive[7,15] and in the mixed absorptive-dispersive cases[10,16]. In the absorptive situation, the off-resonance mode instability arises only in the presence of bistability[7], while, in the general case, it can emerge even when the steady state transmission function is single-valued[16]. Furthermore, the Maxwell-Bloch equations predict the occurrence of self-pulsing both in the case of small or large values of the absorption coefficient, αL, and of the mirror transmittivity, T. When, in particular, the "mean field limit" conditions

$$\alpha L \ll 1, \quad T \ll 1, \quad \text{with } C = \frac{\alpha L}{2T} = \text{constant}, \tag{1}$$

are satisfied (C is the bistability parameter, which remains arbitrary in this limit) the period of self-pulsing becomes equal to the cavity transit time $t_R = \mathscr{L}/c$. The shape and the duration of each pulse depends on αL, and of course, on the number of unstable modes.

A particularly simple setting is provided by absorptive optical bistability in the mean field limit (1), when only the nearest neighbors of the resonant mode are unstable. In this case, the

pulsations are very nearly sinusoidal, and can be calculated in an essentially analytic way using the so-called "dressed mode theory of optical bistability"[17,18], which is a spin-off of Haken's theory of the generalized Ginzburg-Landau equations for phase-transition-like phenomenatin systems far from thermal equilibrium[19]. By this procedure, we have identified the entire domain of existence of the self-pulsing state in the plane of the external control parameters, which are the incident field intensity and the length of the cavity.

A surprising result was the observation that the domain of existence of the self-pulsing state extends well beyond the small signal instability domain. In fact, we have identified a region in the plane of the control parameters where two stable steady-state solutions coexist with a stable self-pulsing state. This situation gives rise to hysteresis cycles of a different kind that involve self-pulsing states along one of the branches.

(b) Ikeda Chaotic Behavior

Roughly one year after publication of Ref. 7, Ikeda[10] reconsidered the problem of instabilities in the Maxwell-Bloch equations, with an emphasis on the dispersive limit, for large values of αL (i.e., quite far from the mean field conditions (1)). He also assumed that the transit time inside the cavity was much longer than the atomic characteristic decay times, or to be more precise, that $c/\mathscr{L} \ll \gamma_\perp$, $\gamma_\parallel$, where $\gamma_\parallel$ is the relaxation rate of the atomic population inversion. In this situation, all atomic variables can be eliminated adiabatically, and the dynamics, including the boundary conditions, can be recast in terms of finite difference equations with the transit time t_R playing the role of the elementary time step. The stability analysis of these equations, or of the equivalent Maxwell-Bloch equations, after adiabatic elimination of the atomic variables[20], shows that under appropriate conditions, all the stationary solutions are unstable, and the system exhibits self-pulsing. In this case, the pulses acquire a square wave shape with a period equal to $2t_R$. By suitably varying the incident intensity, the period becomes successively equal to $4t_R$, $8t_R$, etc., i.e. the system undergoes a cascade of period-doubling bifurcations as in the general theory of discrete maps[21-24].

Beyond the accumulation point of this bifurcation sequence, the system exhibits chaotic behavior. This picture was shown to occur also in the case of optical bistability with a Kerr medium[25]. In addition, this paper proposed the possibility of constructing a hybrid electro-optic device that would allow the observation of these effects without the need for very large interferometric structures. A device of this type was assembled by Gibbs, Hopf, Kaplan and Shoemaker, who observed, indeed, periodic self-pulsing, period-doubling and chaos, in general agreement with the theory[26].

The connection between the Bonifacio-Lugiato and the Ikeda instability was discussed in Ref. 20, where, in particular, the Ikeda instability was shown to disappear in the mean field limit (1). Here we comment only on the reason why the period of oscillation of the Bonifacio-Lugiato self-pulsing is half as large as the one predicted for the Ikeda oscillations. (This point was not discussed in Ref. 20.) To this purpose, consider the eigenvalues λ of the linearized Maxwell-Bloch equations. In all cases when it is possible to calculate them analytically, the eigenvalues have the structure

$$\lambda_n = \frac{c}{\mathscr{L}} \left\{ 2\pi i n + \ell n \, (1 + A_n) \right\} \tag{2}$$

where the index $n = 0, \pm 1, \pm 2, \ldots$ labels the cavity modes. The index $n=0$ corresponds to the mode that is resonant with the incident field (or quasi-resonant, in the dispersive case). The quantity A_n, when expanded in a power series of αL and T, turns out to be of the order of αL or T. In the case of the Bonifacio-Lugiato instability, and in the mean field limit, the term $\ell n \, (1 + A_n) \approx A_n$ is of the order of $T \ll 1$, and therefore $\mathrm{Im}(\lambda_n)$ is approximately given by $2\pi n \, c/\mathscr{L}$. This is the origin of the oscillations with period $\mathscr{L}/c = t_R$. On the other hand, in the case of the Ikeda instability, αL is large and the second term gives a meaningful correction to the empty cavity frequency $2\pi n c/\mathscr{L}$. In this situation, one finds that $1 + A_n$ is real and negative for the unstable modes, and $\mathrm{Im}(\lambda_n) = 2\pi(2n+1)(c/2\mathscr{L})$; this is the origin of the oscillations with period $2\mathscr{L}/c = 2t_R$. Clearly, no fundamental physical fact lies behind this difference, which, in our opinion, has been overemphasized, at times.

3. SINGLE-MODE SELF-PULSING IN OPTICAL BISTABILITY

Even if the single-mode laser model of Optical Bistability was proposed several years ago[27], only recently it has been shown to display such dynamical fireworks as self-pulsing and chaos. Ikeda and Akimoto[28] first demonstrated these effects in the case of purely dispersive optical bistability with a Kerr medium, while Lugiato, Narducci, Bandy and Pennise[29] analyzed the full optical Bloch equations, including absorption and saturation. The mean field model equations of optical bistability for a ring cavity are[27,30]

$$\kappa^{-1} \dot{x} = -i\theta x - (x-y) - 2Cp \tag{3.1}$$

$$\gamma_\perp^{-1} \dot{p} = xd - (1+i\Delta) \, p \tag{3.2}$$

$$\gamma_\parallel^{-1} \dot{d} = -\frac{1}{2}(xp^* + x^*p) - d + 1 \tag{3.3}$$

where x, y, p and d are the normalized output and input fields, the atomic polarization and population difference, respectively; $\kappa = cT/\mathscr{L}$ is the empty cavity linewidth; Δ and θ, the atomic and

cavity detuning parameters, are defined as follows:

$$\Delta = (\omega_a - \omega_o)/\gamma_\perp \tag{4.1}$$

$$\theta = (\omega_c - \omega_o)/\kappa \tag{4.2}$$

where ω_o is the frequency of the incident field, ω_a the atomic transition frequency and ω_c the frequency of the cavity mode nearest ω_o (resonant mode). The model (3) is valid in the mean field limit (1), and describes the dynamics of the resonant mode whose evolution develops over a time scale much longer than the cavity transit time t_R. Evolutions over times of the order of t_R become important only when some off-resonance modes are unstable, as in the case discussed in the previous section. While, in that situation, the delay in the feedback loop of the ring cavity plays a crucial role, here it does not.

As it is well known[27,38], the steady-state solution of (3) has the form

$$y^2 = |x|^2 \left\{ \left[1 + \frac{2C}{1+\Delta^2+|x|^2} \right]^2 + \left[\theta - \frac{2C}{1+\Delta^2+|x|^2} \right]^2 \right\}. \tag{5}$$

We have analyzed eqs. (3) both in the limit of the adiabatic elimination of the polarization (i.e., p=0) and with the full set of dynamical variables. We have found that when the bistability parameter C is sufficiently large, and the detuning constants Δ and θ are chosen appropriately, a large segment of the high transmission branch can become unstable (Fig. 1). The leftmost part of the instability domain that lies around the upper turning point of the state equation leads to precipitation into the low transmission state; the rest of the unstable segment produces undamped oscillations. For $C > 5000$, the instability range include a segment of chaotic oscillations. On approaching this segment *from both sides*, one finds a sequence of period doubling bifurcations, as illustrated in Fig. 2. In the regime of aperiodic oscillations, we have examined the chaotic nature of the solutions by means of suitable Poincare maps and tests of exponential divergence (sensitivity to initial conditions). As usual, in situations of this type, we have found "windows" in the chaotic domain where the output itensity again acquires a periodic behavior. Figure 3 shows a map of the instability domain in the plane of the parameters y and $\kappa/\gamma_\parallel$ for the case of the adiabatic elimination of the polarization. If y_i denotes the value of the driving field in correspondence of which a bifurcation occurs from period i to period 2i, for a fixed value of $\kappa/\gamma_\parallel$ the first four ratios $\delta_i = (y_i - y_{i+1})/(y_{i+1} - y_{i+2})$ are compatible with the universal Feigenbaum number $\delta = 4.6692...$[24]. As shown in Fig. 2 at each period doubling bifurcation, each loop of the phase space trajectory undergoes a kind of fission process in which it separates into two distinct loops. We have evaluated the separation of each

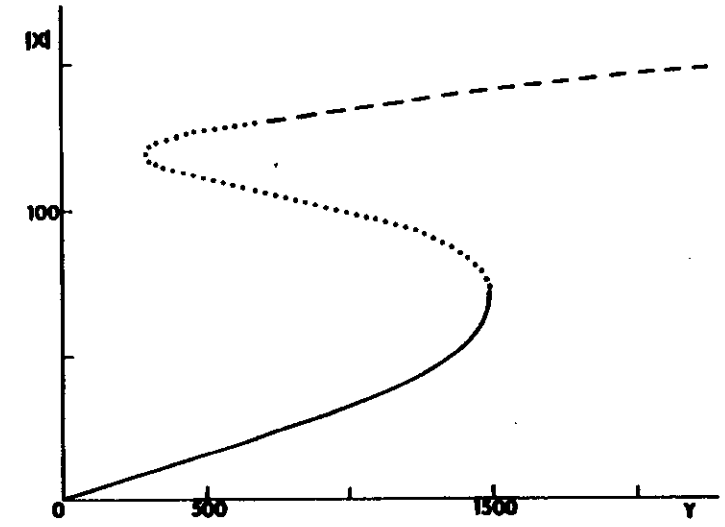

Fig. 1. Steady state transmission curve for an optically bistable system for $C = 70{,}000$, $\Delta = 374$, $\theta = 340$ (eq. 5). The horizontal and vertical axes are labelled by the amplitudes y and $|x|$ of the incident and transmitted fields, respectively. This figure shows the stability range of the steady state for $\kappa/\gamma_\parallel = 0.25$. The dotted part of the upper branch denotes the unstable region which leads to long-term precipitation; the dashed segment denotes the instability range that leads to self-pulsing. The arrows mark the approximate domain of chaotic oscillations. The results shown in Figs. 1-3 have been obtained in the limit $\kappa/\gamma_\perp \to 0$, $\gamma_\parallel/\gamma_\perp \to 0$ of adiabatic elimination of the atomic polarization.

pairs of loops beyond the bifurcation points as a function of the control parameter y, and found that each distance D is well fitted by the power law

$$D = \text{const} \; |y - y_i|^{1/2}. \tag{6}$$

This is reminiscent of the behavior of the order parameter in the Landau theory of second order phase transitions. When y approaches a critical value y_i, the time evolution of the system exhibits critical slowing down. Our numerical analysis shows that the rate of approach to the limit cycle is compatible with the power law

$$\gamma = \text{const} \; |y_i - y| \tag{7}$$

in agreement with the analytical result by Hao[31] in the case of one dimensional discrete maps.

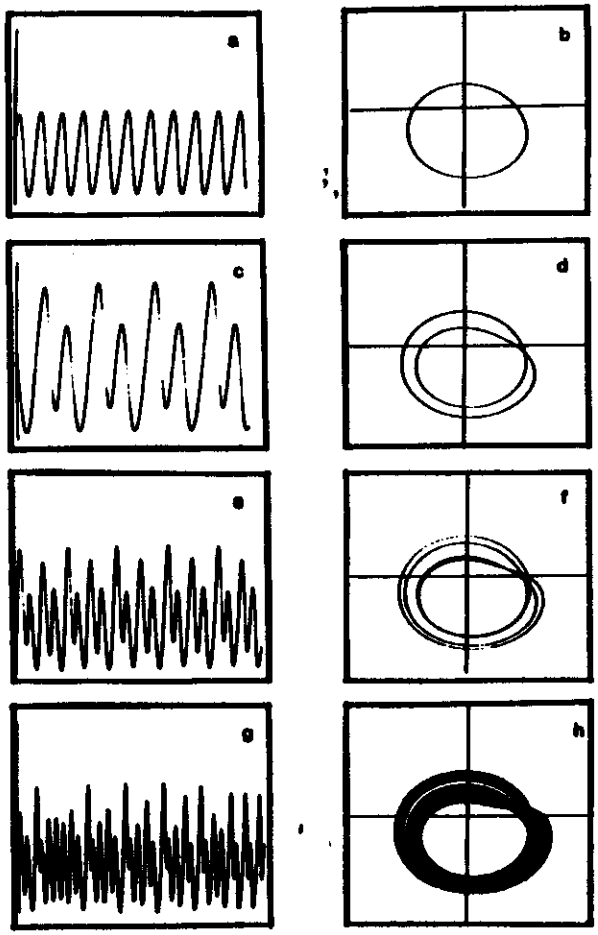

Fig. 2 Self-pulsing oscillations and corresponding phase space representations on the (Re x, Im x) plane for solutions of the type 1P(a,b), 2P(c,d), 4P(e,f) and chaotic (g,h), respectively. The parameters are the same as in Fig. 1. The values of the incident field are y=2000, 1350, 1225, and 950, for the four sets of solutions.

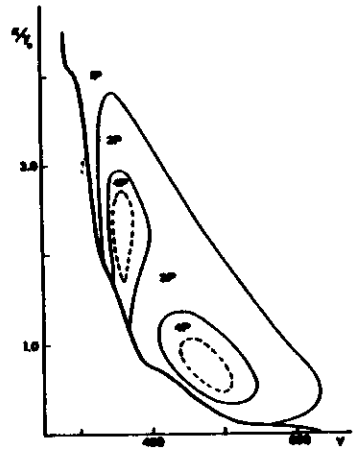

Fig. 3 Instability domain for an optically bistable system corresponding to C = 5000, $\Delta = \theta = 70$. The heavy line on the left separates the precipitation from the stable self-pulsing regions. The dashed lines encircle the chaotic domains.

As we said, chaotic behavior is found here only for very large values of Δ and θ. On the other hand, periodic pulsations and even modulation of the train of pulses are predicted for much more accessible values of the parameters. By numerical integration of eqs. (3), *without* adiabatic elimination of the polarization, we have shown that for C = 75, $\Delta = 0$, $\theta = 10$, $\gamma_\perp/\gamma_\parallel = 2$ and $\kappa/\gamma_\perp = 0.5$, one obtains regular self-pulsing with a period of the order of κ^{-1}. It is interesting to note that this selection of parameters corresponds to absorptive bistability because $\Delta = 0$. As this example shows, it is usually enough that θ be sufficiently different from zero in order to obtain self-pulsing. On the other hand, as we well know, if both Δ and θ are equal to zero, the positive slope segments of the state equation are always stable[27].

A final example of interest corresponds to the parameters C = 200, $\Delta = -3$, $\theta = 5$, $\gamma_\perp/\gamma_\parallel = 2$ and $\kappa/\gamma_\perp = 10$, where a range of incident field values can be found for which the envelope of the oscillations acquires long term modulation (breathing).

4. CHAOS, BREATHING AND SPIKING IN THE LASER WITH INJECTED SIGNAL

If the atoms contained in the resonant cavity are pumped to a state of population inversion, the optically bistable system becomes a laser with injected signal. Single mode operation in this system is governed by eqs. (3) with C negative (this implies that the absorber has been turned into an amplifier). In the resonant case, $\Delta = \theta = 0$, the laser with injected signal is not bistable[32], while, if one allows for detuning, one can find narrow ranges of bistability[33], under appropriate conditions. In this paper, however, we shall not consider bistable situations. Spencer and Lamb[33] were the first to show that the output of a laser with injected signal can exhibit undamped oscillations. Yamada, Graham and collaborators[34] pointed out that this system can also display chaotic behavior, and analyzed this regime in detail. The results discussed in Ref. 34 have been obtained in the limit of adiabatic elimination of all the atomic variables (i.e., after setting $\beta = \partial = 0$ in eqs. (3)) and assuming that the incident field and the pump parameter are sinusoidally modulated. Here, instead, we take *all* the external parameters as *constant* in time[35].

We assume that the atomic and cavity frequencies, ω_a and ω_c, coincide (hence $\Delta/\theta = \kappa/\gamma_\perp$), and that the laser is pumped above threshold ($|C| > 1/2$). The carrier frequency ω_0 of the incident field, instead, is different from ω_a; hence, there is a mismatch between the external and the laser frequencies. This is the origin of the competition that produces the instabilities and, as we shall show, the chaotic behavior. Fig. 4 shows the steady-state curve as obtained from eq. (5). The entire segment OAB is unstable for the chosen parameters. In the absence of the external field (y=0) the system oscillates with the laser frequency ω_a and produces the stationary output $|x|^2 = 2|C| - 1$. On the other hand, for $y > y_{thr}$, the laser is slaved by the external field, and oscillates with the frequency ω_0 (injection locking), again producing a stationary output.

We have analyzed the behavior of the system over the entire range of values of the incident field from y=0 to the injection locking threshold y_{thr}. As the external field is turned on, the output intensity begins to oscillate with the beat-note frequency $|\omega_a - \omega_0|$. The amplitude of the oscillations grows from zero in a continuous way, as the incident intensity level is increased, while the oscillation frequency remains essentially constant. For sufficiently large values of the external field strength, the output oscillations begin to display irregularities (Fig. 5a). The system here enters a chaotic regime where nearby phase-space trajectories separate from each other exponentially in time. The chaotic character of the oscillations becomes more and more pronounced, until the output signal begins to display a bursting behavior (Fig. 5b) in which each burst is followed by a number of rapid and noisy

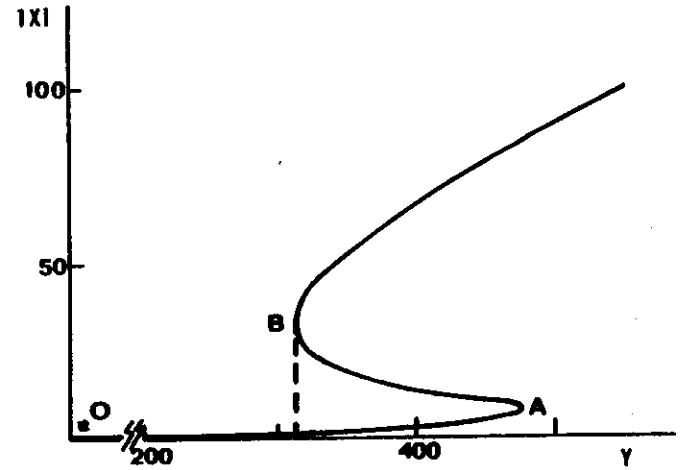

Fig. 4. Laser with injected signal. Steady state equation (eq.(5)), for C = -500, $\Delta = \theta = 5$. The segment OAB is unstable.

oscillations. A further increase in y brings the system out of the chaotic domain through a sequence of period doubling bifurcations in reverse order (examples of period 4 and period 1 oscillations are shown in Figs. 5c,d). At this point, by further increasing y, the system enters a new regime, in which a much longer time scale emerges. Fig. 5e shows the time evolution of the output on a time scale which is much more compressed than that of Figs. 5a-d, so that the simple oscillations can no longer be resolved. In this case, it is easy to see that the envelope of self-pulsing acquires a periodic modulation. This phenomenon is usually referred to as breathing. Larger values of the injected field lead, eventually, to a spiking regime (Fig. 5f) in which very sharp spikes of randomly varying height are followed by long periods of lethargy.

This behavior is typical of a range of values of the incident intensity that immediately preceeds the injection locking threshold y_{thr} in all cases when the upper branch of the state equation is completely stable. On approaching y_{thr}, the temporal separation of the spikes increases, and, apparently, diverges. This type of critical slowing down is similar to the one found in the laser with saturable absorber[36] and in Optical Bistability with three-level atoms[37]. Finally, when y exceeds y_{thr}, after a short transient, the system approaches steady state.

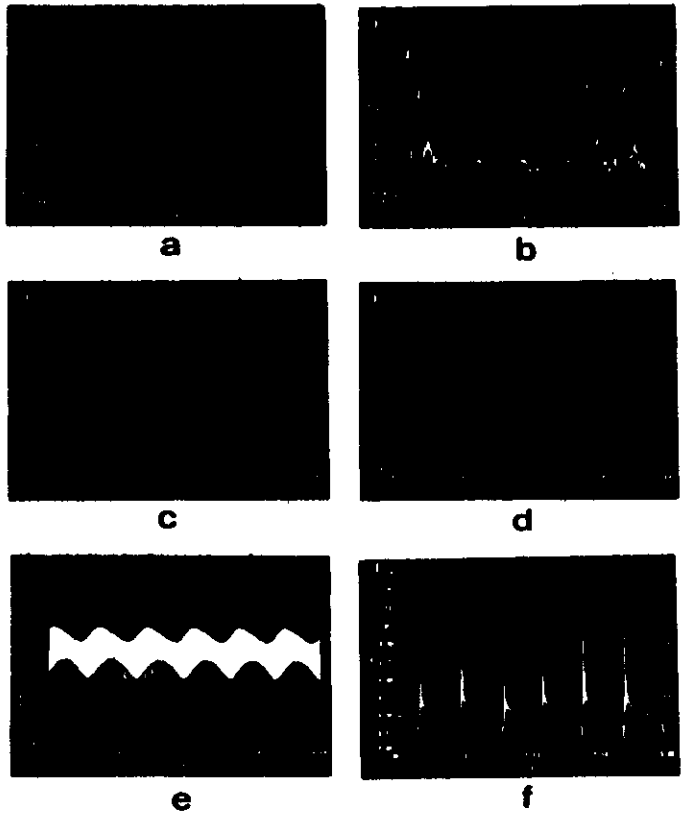

Fig. 5 Time evolution of the normalized output field $|x|$ for the same parameters as used in Fig. 4 and $\kappa/\gamma_\perp = 1$, $\gamma_\parallel/\gamma_\perp = 1$. The horizontal time axis is measured in units of $\gamma_\perp^{-1}$. (a) erratic behavior, y=117; (b) bursting, y=250; (c) 4P-type solution, y=279; (d) 1P-type solution, y=300; (e) envelope breathing, y = 310.3; (f) spiking action, y=311.

For parameter values different from those used in Figs. 5a-f, the injection locking threshold may lie beyond the turning point B, so that also a segment of the upper branch becomes unstable. In this case, breathing and spiking are replaced by a gradual reduction of the self-pulsing amplitude which vanishes at the injection threshold.

The sequence shown in Figs. 5a-f occurs in full only for very large values of $|C|$. When $|C|$ is of the order of 20, the picture remains essentially the same, with the exception of breathing, which appears to be absent, at least in the resonant case ($\omega_a = \omega_c$).

Other results concerning self-pulsing in the laser with injected signal and an analysis of the spectrum of the output intensity with a characterization of the route to chaotic behavior can be found in Refs. 35 and 38.

REFERENCES

1. L. Mandel and E. Wolf, Eds., *Coherence and Quantum Optics IV*, Proceedings of the Fourth Conference on Coherent and Quantum Optics, Rochester, NY, June 1977 (Plenum Press, 1978). See the papers by R. Bonifacio and L.A. Lugiato, p. 249 and by G.S. Agarwal, L.M. Narducci, D.H. Feng and R. Gilmore, p. 281.
2. C.M. Bowden, M. Ciftan and H.R. Robl, Eds., *Optical Bistability*, Proceedings of the International Conference on Optical Bistability, Asheville, NC, June 1980 (Plenum Press, 1981).
3. A. Szoke, V. Daneu, J. Goldhar, and N.A. Kurnit, Appl. Phys. Lett. 15, 376 (1969).
4. H. Seidel, U.S. Patent #3,610,731 (1971).
5. H.M. Gibbs, S.L. McCall, and T.N.C. Venkatesan, Phys. Rev. Lett. 36, 113 (1976).
6. S.L. McCall, Appl. Phys. Lett. 32, 284 (1978).
7. R. Bonifacio and L.A. Lugiato, Lett. al Nuovo Cimento, 21, 510 (1978).
8. H. Haken, *Synergetics - An Introduction*, Springer-Verlag, Berlin, 1977.
9. G. Nicolis and I. Prigogine, *Self-Organization in Nonequilibrium Systems. From Dissipative Structures to Order Through Fluctuations*, Wiley and Sons, NY, 1977.
10. K. Ikeda, Opt. Comm. 30, 257 (1979).
11. H. Haken, Z. Phys. 190, 327 (1966); H. Risken, C. Schmid, and W. Weidlich, Z. Phys. 194, 337 (1966).
12. H. Risken and K. Nummedal, J. Appl. Phys. 39, 4662 (1968); R. Graham and H. Haken, Z. Phys. 213, 420 (1968).
13. J.L. Jewell, H.M. Gibbs, S.S. Tarng, A.C. Gossard, and W. Wiegman, Appl. Phys. Lett. 40, 291 (1982).
14. L.A. Lugiato, *Theory of Optical Bistability*, to appear in Progress in Optics, Vol. XXI, ed. by E. Wolf (North Holland).

15. M. Gronchi, V. Benza, L.A. Lugiato, P. Meystre and M. Sargent III, Phys. Rev. A24, 1419 (1981).
16. L.A. Lugiato, Opt. Comm. 33, 108 (1980).
17. V. Benza and L.A. Lugiato, Zeit. Physik B35, 383 (1979); ibid. 47, 79 (1982).
18. L.A. Lugiato, V. Benza, L.M. Narducci and J.D. Farina, Zeit. Physik B49, 351 (1983).
19. H. Haken, Zeit. Physik, B21, 105 (1975); ibid. 22, 69 (1975).
20. L.A. Lugiato, M.L. Asquini and L.M. Narducci, Opt. Comm. 41, 450 (1982).
21. H.J. Carmichael, R.R. Snapp and W.C. Schieve, Phys. Rev. A26, 3408 (1982).
22. R.M. May and G.E. Oster, Am. Nat. 110, 573 (1976).
23. S. Grossmann and S. Thomae, Zeit. Naturforsch. 32A, 1353 (1973).
24. M.J. Feigenbaum, J. Stat. Phys. 19, 25 (1978); ibid, 21, 669 (1979).
25. K. Ikeda, H. Daido, and O. Akimoto, Phys. Rev. Lett. 45, 709, (1980).
26. H.M. Gibbs, F.A. Hopf, D.L. Kaplan and R.L. Shoemaker, Phys. Rev. Lett. 46, 474 (1981).
27. R. Bonifacio and L.A. Lugiato, Opt. Comm. 19, 172 (1976); Phys. Rev. A18, 1129 (1978).
28. K. Ikeda and O. Akimoto, Phys. Rev. Lett. 48, 617 (1982).
29. L.A. Lugiato, L.M. Narducci, D.K. Bandy and C.A. Pennise, Opt. Comm. 43, 281 (1982); L.M. Narducci, D.K. Bandy, C.A. Pennise and L.A. Lugiato, Opt. Comm. 44, 207 (1983).
30. R. Bonifacio and L.A. Lugiato, Lett. al Nuovo Cimento, 21, 517 (1978); S.S. Hassan, P.D. Drummond, and D.F. Walls, Opt. Comm. 27, 480 (1978).
31. B.L. Hao, Phys. Lett. 86A, 267 (1981).
32. L.A. Lugiato, Lett. al Nuovo Cimento 23, 609 (1978), and references quoted therein.
33. M.B. Spencer and W.E. Lamb, Jr., Phys. Rev. A5, 884 (1972).
34. T. Yamada and R. Graham, Phys. Lett. 53A, 77 (1975); M.J. Scholz, T. Yamada, H. Brand, and R. Graham, Phys. Lett. 82A, 321 (1981).
35. L.A. Lugiato, L.M. Narducci, D,K. Bandy and C.A. Pennise, Opt. Comm., to be published.
36. J.C. Antoranz, J. Gea and M.G. Velarde, Phys. Rev. Lett. 47, 1895 (1981).
37. F.T. Arecchi, J. Kurmann and A. Politi, Opt. Comm. 44, 421 (1983).
38. D.K. Bandy, L.M. Narducci, C. A. Pennise and L. A. Lugiato, this volume, p. 585.

ACKNOWLEDGEMENTS

We are grateful to Mrs. Debbie DeLise-Hughes for her expert advice with the prepration of this manuscript. This research was partially supported by a grant from the Martin-Marietta Research Laboratories and from the Army Research Office under contract #DAAG29-82-K-0021, and also by the Comitato Nazionale delle Ricerche (CNR, Italy) under contract # CT82.00031.02.115.14905.

(71)

Time-Dependent Behavior of a Unidirectional Ring Laser with Inhomogeneous Broadening

Donna K. Bandy, L.M. Narducci
Physics Department
Drexel University
Philadelphia, PA 19104 U.S.A.

Luigi A. Lugiato
Dipartimento di Fisica
Universita di Milano
Milano, Italy

and

Neal B. Abraham*
Istituto Nazionale di Ottica
Firenze, Italy

ABSTRACT

We solve numerically the time-dependent equations of motion for an inhomogeneously broadened single-mode ring laser. As expected from the linear stability analysis, pulsations develop in the output of the laser for appropriate values of the gain parameter. Under resonant conditions, the tendency is for the system to slip from a periodic regime into irregular oscillations; out of resonance, instead, periodic oscillations and period doubling bifurcations are more typical over a large range of gain values. We find that as the ratio of the population to polarization decay rates varies from a value of two (radiative limit) to smaller values, the periodic oscillations turn into a train of well-separated pulses whose peak intensity scales approximately as the square of the atomic density.

*Permanent Address: Physics Department, Bryn Mawr College, Bryn Mawr, PA 19010

INTRODUCTION

It is now well established[1] that even a limited amount of inhomogeneous broadening in the gain profile of a homogeneously broadened laser can induce large qualitative changes in the stability properties of its output intensity. Thus, for example, the instability threshold for the appearance of pulsations is generally low enough that the operation of a laser under experimentally controllable, unstable conditions is feasible with a variety of gaseous media and cavity designs.

The lowering of the instability threshold is accompanied by the replacement of the well known cavity linewidth and laser gain requirements for a homogeneous system[2] with new, less stringent bounds which, on the one hand, allow the selection of a somewhat higher cavity quality factor without the loss of output pulsations, and on the other, permit practical gain levels to be used in the observation of the effect.

The results of detailed studies of the steady state and stability properties of inhomogeneously broadened media have already been reported in numerous contributions, and several updates appear in this special issue[3]. Detailed investigations of the temporal behavior of inhomogeneously broadened lasers, on the other hand, have not kept pace with the recent rapid experimental development[4].

The purpose of this paper is to present the results of our numerical studies of the temporal evolution of a unidirectional ring laser system with a Gaussian inhomogeneously broadened line. Our intention is to survey some of the general features of this problem; fine scans of control parameter space are under investigation and will be discussed in future communications.

In Section 2 we survey the main aspects of our working model. In Section 3 we review the results of our study and compare some of our solutions with the ones derived from an interesting approximate method suggested by Graham and Cho[5]. We reserve Section 4 for a few comments on the numerical method adopted in our simulations and on some relevant accuracy tests.

2. *DISCUSSION OF THE MODEL*

We consider a collection of active two-level systems in a unidirectional ring laser cavity operating in a single mode. The atoms whose spectral profile is inhomogeneously broadened around a central frequency ω_A according to the frequency distribution

$$g(\delta) = \frac{1}{\sqrt{2\pi}\,\sigma_D}\, e^{-\delta^2/2\sigma_D^2} \qquad (2.1)$$

$$-\infty < \delta < +\infty$$

are placed in a ring cavity, adjusted to resonate at the eigenfrequency ω_C with a linewidth κ, and are maintained in a state of inversion by an external pump mechanism.

With reference to the carrier frequency ω_L of the laser system[6], the interaction of the atoms and the cavity field is described within the context of our model by the Maxwell-Bloch equations

$$\frac{d}{d\tau} X(\tau) = -\tilde{\kappa}\left\{(1 - i\,\tilde{\theta}/\tilde{\kappa})\, X(\tau) + 2C \int_{-\infty}^{\infty} d\tilde{\delta}\;\; g(\tilde{\delta})\; P(\tilde{\delta},\tau)\right\} \qquad (2.2a)$$

$$\frac{dP}{d\tau}(\tilde{\delta},\tau) = XD(\tilde{\delta},\tau) + (1 + i(\tilde{\Delta}+\tilde{\delta}))\, P(\tilde{\delta},\tau) \qquad (2.2b)$$

$$\frac{d}{d\tau} D(\tilde{\delta},\tau) = -\tilde{\gamma}\left\{\frac{1}{2}\,(X^{*}\, P(\tilde{\delta},\tau) + XP^{*}(\tilde{\delta},\tau)) \;\; + D(\tilde{\delta},\tau) + 1\right\} \qquad (2.2c)$$

where $\tilde{\theta}$ is the frequency offset of the laser carrier ω_L from the cavity eigenfrequency in units of the polarization relaxation rate, $\gamma_\perp$; $\tilde{\Delta}$ is the displacement of the center of the atomic line from ω_L, also in units of $\gamma_\perp$[7], and $\tilde{\gamma} = \gamma_\parallel/\gamma_\perp$, with $\gamma_\parallel$ the spontaneous relaxation rate of the atomic population difference. The parameter $\tilde{\delta} = \delta/\gamma_\perp$ denotes the position of an arbitrary atomic homogeneous packet away from line center, while $P(\tilde{\delta},\tau)$ and $D(\tilde{\delta},\tau)$ represent the atomic polarization and population difference,

(42)

respectively; finally, $X(\tau)$ is the slowly varying output field amplitude of the laser scaled to the square root of the saturation intensity, and $\tau = \gamma_\perp t$.

For selected values of the cavity and atomic rates, the detuning $\tilde{\delta}_{AC} = (\omega_A - \omega_C)/\gamma_\perp$, the excitation parameter C and the inhomogeneous linewidth $\tilde{\sigma}_D = \sigma_D/\gamma_\perp$, the state equation of the laser defines one, two or three sets of steady state conditions characterized by the field and atomic parameters $|X_{st}|^2$, $\tilde{\Delta}$, $P_{st}(\tilde{\delta})$, $D_{st}(\tilde{\delta})$, whose stability can be assessed with the help of arguments such as developed in Ref. 3a. Initial conditions for the study of the evolution of the equations of motion can be selected in the neighborhood of each of these operating points.

The assignment of an unstable state as the initial condition for the problem, of course, does not match what is actually done in practical situations, where selected control parameters are slowly scanned across the domains of interest. This is, however, a useful way to complement the information provided by the linear stability analysis, so that the long-term behavior of the system can be analyzed in the presence of the nonlinearities. Ultimately, one expects (hopes) that, apart from the initial transient, the comparison between the long-term solutions of the dynamical equations and the output intensity of an unstable laser, whose control parameters are held fixed or varied slowly, should be a fair one.

As background information for the discussion of the time-dependent solutions, it will be useful to review the relevant steady state and linear stability data for this work. The steady state output intensity and the laser frequency offset $\tilde{\Delta}$ as functions of the gain parameter C are shown in Fig. 1

for the two values of the detuning parameter $\tilde{\delta}_{AC} = 0$ and 5 used in the temporal solutions. The state equation is independent of the value of $\tilde{\gamma} = \gamma_{\parallel}/\gamma_{\perp}$ and is single-valued for the range of detuning used here.

The eigenvalues of the linearized equations of motion, however, do depend in a rather sensitive way on $\tilde{\gamma}$ and, for this reason, are displayed separately in Figs. 2 and 3. For the case $\tilde{\gamma} = 2$ (radiative limit), the onset of the instability, as marked by the vanishing of the real part of the first eigenvalue occurs at a ratio $C/C_{thr}^{(0)} = 1.6$ for $\tilde{\delta}_{AC} = 0$ (not shown) and $C/C_{thr}^{(0)} = 1.8$ for $\tilde{\delta}_{AC} = 5$, where $C_{thr}^{(0)}$ denotes the threshold gain for laser action at the center of the atomic line ($C_{thr}^{(0)} = 2$ in this case). For $\tilde{\gamma} = 0.05$, the ratio $C/C_{thr}^{(0)}$ is about 1.2 in resonance and 1.4 at $\tilde{\delta}_{AC} = 5$.

There is a significant difference between the behavior of the eigenvalues displayed in Figs. 2 and 3. In the radiative limit, we observe the existence of a small range of the gain parameter just above threshold for laser action where the largest eigenvalues of the linearized problem are real and negative. Here, the laser is stable and, if slightly perturbed, will relax to steady state monotonically; beyond this small range, the laser displays an additional stable domain where the approach to steady state involves relaxation oscillations. For $\tilde{\gamma} = 0.05$, a pair of complex eigenvalues with a small negative real part, in addition to the real pair, emerge right at threshold for laser action. These complex eigenvalues, as shown in Fig. 3, are responsible for the self-pulsing instability whose dynamical evolution is discussed in the next section. This feature is common, with minor quantitative changes also to $\tilde{\delta}_{AC}$=5 (not shown).

3. *SOLUTION OF THE TIME-DEPENDENT EQUATIONS AND DISCUSSION OF THE RESULTS*

Our numerical analysis has shown the existence of two very different dynamical regimes which will be discussed separately in this section. The first is characterized by the ratio $\tilde{\gamma} \equiv \gamma_{\parallel}/\gamma_{\perp} = 2$ (radiative limit), and the second by $\tilde{\gamma} = 0.05$. On the surface, the main difference between the two is just the rate of incoherent decay of the population difference relative to that of the atomic polarization, but the resulting changes in the observed output patterns are suggestive of considerably more complicated dynamical effects. In both cases discussed in this section, we have chosen an inhomogeneous linewidth $\delta_D = 5$ and selected a bad cavity configuration corresponding to $R = 5$; the same qualitative behavior, however, has been observed, also in the bad cavity limit, for $\delta_D = 2$ and $\delta_D = 7$.

In the radiative limit, $\tilde{\gamma} = 2$, the following general pattern has emerged: above the instability threshold, and over a certain range of the gain parameter, the output oscillations first develop a regular pattern with pulsation frequency that follows rather closely the imaginary part of the unstable eigenvalue. For larger gain values, the resonant laser ($\tilde{\delta}_{AC} = 0$) develops progressively larger irregularities, while, in the presence of detuning, period doubling bifurcations and periodicity appear to be the rule. The same features are apparent also for different values of δ_D and fall in qualitative agreement with the findings of Mandel and Zeglache[8] in the homogeneous broadening case.

We consider now in more detail the results of two typical scans, beginning with the resonant case $\tilde{\delta}_{AC} = 0$; for $|X_{st}| = 2$, somewhat above threshold for self-pulsing, the oscillations are highly periodic with a radian frequency of about 3.7 rad/sec (cfr. Im $s_1 = 3.2$ rad/sec) as shown in Fig. 4; for $|X_{st}| = 2.5$, the output pattern is already strongly irregular (Fig. 5) with

missing "beats" or defects that are suggestive of some kind of intermittency. A finer scan of this region gives evidence for what appears to be a period doubling bifurcation around $|X_{st}| = 2.12$ (Fig. 6). The pattern, however, persists only over a very narrow range of gain values and quickly develops a noisy modulation as shown in Fig. 7.

The output of the off-resonance situation, as mentioned, is far more regular. Periodic oscillations of the 1P-type (Fig. 8) are followed by a clear example of a period doubling bifurcation (Fig. 9) which is then followed, for higher gain values, by a return to simply periodic oscillations with some small amplitude modulation (breathing). Larger values of the cavity linewidth κ have a tendency to reduce the threshold for the onset of oscillations and, in the resonant case, for the appearance of chaos. In the good cavity limit (e.g., $\kappa = 0.5$) instead, the unstable behavior disappears even for values of C that are four or five times larger than the laser threshold.

For small values of γ, the output oscillations begin to take the form of a train of well resolved single pulses with a spacing that grows progressively upon lowering the value of γ. Again, as in the previous case, the existence of detuning favors the occurrence of period doubling bifurcations and stable periodic patterns although, irregular oscillations develop for higher gain values and are considerably less erratic in this case.

A characteristic train of pulses for $|X_{st}| = 1.5$ is shown in Figs. 10a,b. On the expanded scale, the presence of significant ringing is apparent. This feature is in qualitative agreement with some of Casperson's experimental results and numerical simulations in spite of the simplified nature of our model[1a]. For increasing gain, the pulses become sharper, their spacing smaller, and the ringing more pronounced (Fig. 11), while at the same time

irregularities also become more obvious. The out of resonance solutions have much the same appearance as those shown in Figs. 10 and 11, except for larger ringing and their increased regularity, and need not be reproduced here.

Perhaps the most remarkable feature of these solutions is the fact that the emitted intensity is essentially zero between pulses, a feature which is not connected with the individual atomic polarization components becoming zero, but rather with the dephasing action due to the free precession of the dipoles in the absence of the field. This is strictly a feature of the inhomogeneous broadening. Unfortunately, we have not been able yet to identify the mechanism by which the macroscopic polarization periodically returns to a nonzero value, displaying features that are reminiscent of the dipolar rephasing effect in photon echo. The maximum value of $|X|^2$ which is proportional to the peak intensity, somewhat surprisingly, does not scale linearly with the gain, or the number density of atoms. In fact, from the available evidence, it displays a power law dependence of the type $|X_{st}|^2 \propto C^{(\beta>4)}$ which is suggestive of cooperative behavior one finds in superradiance and superfluorescence[9].

In closing, we wish to make a brief comment on an approximate approach for dealing with the solution of the dynamical equation (2.2) that was proposed recently by Graham and Cho[5]. The structure of the field equation (2.2a) suggests that one should consider the total polarization

$$P_o(\tau) = \int_{-\infty}^{+\infty} d\tilde{\delta}\; g(\tilde{\delta})\; P(\tilde{\delta},\tau)$$

as the basic dynamical variable instead of the individual polarization components $P(\tilde{\delta},\tau)$. The difficulty with this viewpoint is that the equation of

motion for $P_0(\tau)$ involves the new variable

$$P_1(\tau) = \int_{+\infty}^{-\infty} d\bar{\delta}\ \bar{\delta}\ g(\bar{\delta})\ P(\bar{\delta},\tau)$$

which is irreducible from P_0, and which, in fact, couples to higher order expressions in an infinite hierarchy. Attempts to insist on a description based on the integrated polarization and population difference variables without introducing drastic approximations have been made without much success; for example, we have managed to transform Eqs.(2.2) into a set of exact partial differential equations involving only collective atomic variables without, however, much clear advantage.

Graham and Cho proposed a clever procedure for truncating the infinite hierarchy of coupled equations based on the introduction of adjustable parameters. As in most similar instances, an assessment of the accuracy of the results is very hard to obtain directly. For this reason, we have decided to compare the results of the truncated Graham-Cho hierarchy with those of the exact Eqs. (2.2). The results, unfortunately, are not very promising, although, roughly, the instability thresholds and self-pulsing frequencies for periodic oscillations in the small gain regime display a reasonable correlation. Away from the instability threshold, on the other hand, the truncated hierarchy develops a sequence of bifurcations that bear little or no resemblance with the exact solutions; the intermittent behavior displayed in Fig. 12, for example, was obtained using the same parameter values and initial conditions used in our earlier Fig. 5.

4. *COMMENTS ON THE NUMERICAL WORK*

The numerical analysis of Eqs. (2.2) presents the usual challenges of any fairly large-scale simulation. The continuous atomic profile must be suitably discretized into a number of components, or "packets", located at frequencies δ_i within the atomic line so that the number of equations to be handled simultaneously is usually rather large. In this work, we have adopted a standard fourth-order Runge-Kutta scheme for the numerical integration of the differential equations and, after several experiments with alternative methods, we have selected the common extended trapezoidal rule for the evaluation of the frequency integral, on the basis of its performance against various other integral routines. The range of integration has been extended to the interval $-4\delta_D$ to $+4\delta_D$ in all our calculations. The selection of the number of packets is a sensitive issue. We have explored this matter at some length not only by comparing with one another time-dependent solutions obtained with different numbers of atomic components but also, and especially, by looking for an accurate match between the results of long term numerical integration under stable conditions with those predicted by the state equation. Since the steady state intensity of the laser is computed from the state equation with a routine based on convenient series representations of the error function, while the direct integration of the equations of motion adopts an entirely different way of calculating $|x_{st}|^2$, the excellent degree of consistency between these results is a good indication of the reliability of our procedure.

In selecting δ_D=5 (as in most of this work) we found that 100 atomic packets was an appropriate compromise between accuracy and speed of execution. This number was varied proprotionally whenever δ_D was varied.

REFERENCES

1. For two recent surveys of theoretical and experimental advances, see, for example, (a) L.W. Casperson, *Lecture Notes in Physics*, *182*, (Springer Heidelberg, 1983) p. 88; and (b) N.B. Abraham, T. Chyba, M. Coleman, R.S. Gioggia, N.J. Halas, L.M. Hoffer, S.N. Liu, M. Maeda and J.C. Wesson, *Lecture Notes in Physics*, *op. cit.*, p. 107.
2. A.Z. Grasiuk and A.N. Oraevskii, *Quantum Electronics and Coherent Light*, Edited by P.A. Miles (Academic Press: NY, 1964) p. 191; H. Makan, Z. Phys. 190, 327 (1966).
3. See, for example, the contributions by (a) N.B. Abraham, L.A. Lugiato, P. Mandel, D.K. Bandy and L.M. Narducci; (b) P. Mandel and (c) S. Hendow and M. Sargent III.
4. Some results of a rather elaborate numerical simulation and a comparison with experimental data appear in Ref. 1a.
5. R. Graham, Y. Cho, Opt. Comm. 47, 52 (1983).
6. ω_L is identified with the carrier frequency of the steady state solution of the laser equations (see, for example, Ref. 3a, Eqs. (2.12)) even when this solution is unstable.
7. Note that $\tilde{\theta}$ and $\tilde{A}$ are not free parameters of the system; $\tilde{A}$ is calculated from the state equation of the laser, and $\tilde{\theta}$ is given by $\tilde{\delta}_{AC}-\tilde{A}$ (see Ref. 3a), where $\tilde{\delta}_{AC}$ is the detuning $(\omega_A - \omega_C)/\gamma_\perp$.
8. P. Mandel and M. Zeglache, J. Opt. Soc. Am. B (this issue).
9. R. Bonifacio and L.A. Lugiato, Phys. Rev. A11, 1507 (1975); A12, 587 (1975).

FIGURE CAPTIONS

1. Steady state output intensity $|X_{st}|^2$ (solid lines) as a function of the gain parameter for $\delta_D = 5$, $\tilde{c} = 5$ and (1) $\tilde{\delta}_{AC}=0$; (2) $\tilde{\delta}_{AC} = 5$; (3) the frequency offset $\tilde{A}$ (dashed line) is also plotted for $\tilde{\delta}_{AC} = 5$.
2. (a) Real parts of the first two eigenvalues as functions of the steady state output intensity $|X_{st}|^2$ for $\delta_D=5$, $\tilde{c} = 5$, $\tilde{\delta}_{AC} = 5$ and $\tilde{\gamma} = 2$.
   (b) The corresponding imaginary parts of the first two eigenvalues for the same values of the parameters as in (a).
3. Real and imaginary parts of the first two eigenvalues as functions of the steady state output intensity $|X_{st}|^2$ for $\delta_D=5$, $\tilde{c}=5$, $\tilde{\delta}_{AC}=0$ and $\tilde{\gamma}=0.05$.
4. Time dependence of $|X(\tau)|$ for $\delta_D=5$, $\tilde{c}=5$, $\tilde{\delta}_{AC}=0$ and $\tilde{\gamma}=2$. The initial unstable state corresponds to $|X_{st}| = 2.0$.
5. Time dependence of $|X(\tau)|$ for $\delta_D=5$, $\tilde{c}=5$, $\tilde{\delta}_{AC}=0$ and $\tilde{\gamma}=2$. The initial unstable state corresponds to $|X_{st}| = 2.5$.
6. The development of a period doubling pattern for $|X(\tau)|$ corresponding to an initial unstable value $|X_{st}| = 2.12$.
7. An erratic modulation of the solution displayed in Fig. 6 develops even by a slight change of the initial unstable value of the field modulus. Here, $|X_{st}| = 2.13$.
8. Period oscillations of $|X(\tau)|$ for $\delta_D=5$, $\tilde{c}=5$, $\tilde{\delta}_{AC}=5$ and $\tilde{\gamma}=2$. The initial unstable state corresponds to $|X_{st}| = 2.0$.
9. Period doubling bifurcation for an out of resonance configuration, $\delta_D=\tilde{\delta}$, $\tilde{c}=5$, $\tilde{\delta}_{AC}=5$, $\tilde{\gamma}=2$ and $|X_{st}| = 3.0$.

Figure Captions (contd.)

10. (a) Regular train of pulses for δ_D=5, $\hat{r}$=5, $\tilde{\delta}_{AC}$=0 and $\hat{\gamma}$=0.05. The initial unstable state corresponds to $|X_{st}|$ = 1.5.
    (b) Expanded view of the same solution displaying pulse details and ringing.
11. (a) An irregular train of pulses for δ_D=5, $\hat{r}$=5, $\tilde{\delta}_{AC}$=0 and $\hat{\gamma}$=0.05. The initial unstable state corresponds to $|X_{st}|$ = 8.0.
    (b) Expanded view of the same solution.
12. Intermittent behavior of $|X(\tau)|$ obtained by solving the equations of Graham and Cho (Ref. 5) using the parameters and initial conditions of Fig. 5.

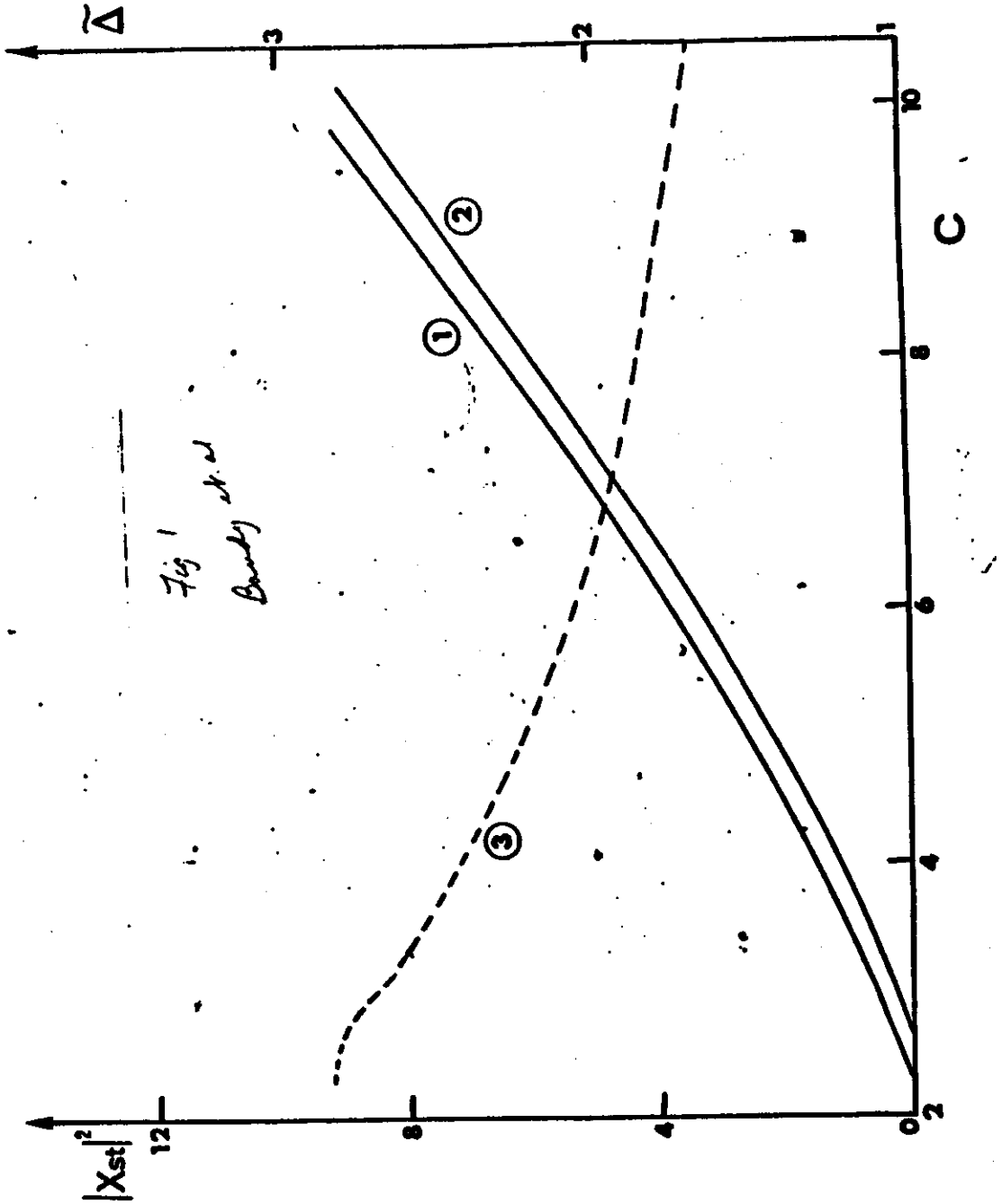

Fig 2a
Bandy et al

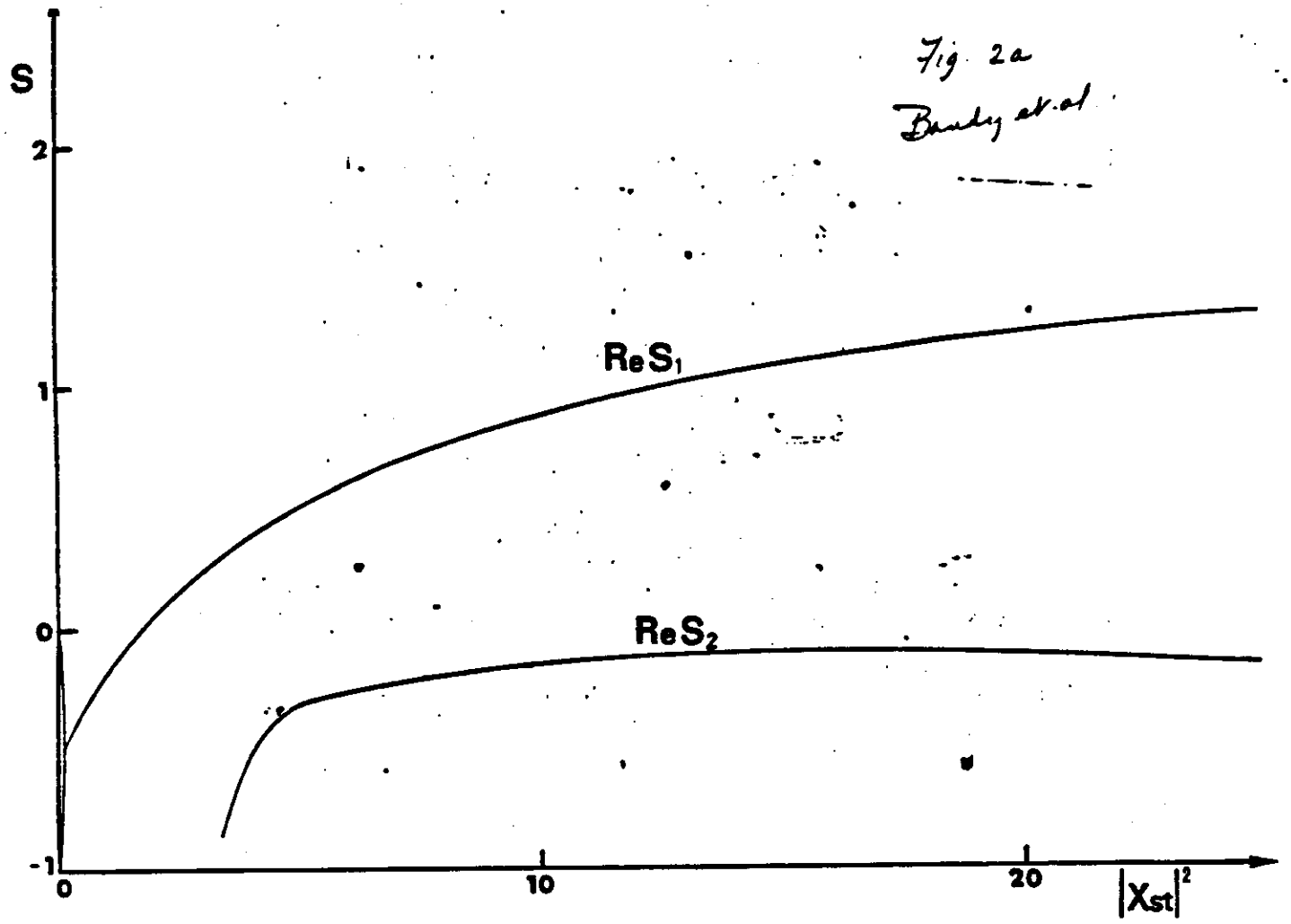

Fig 2b
Bandy et al

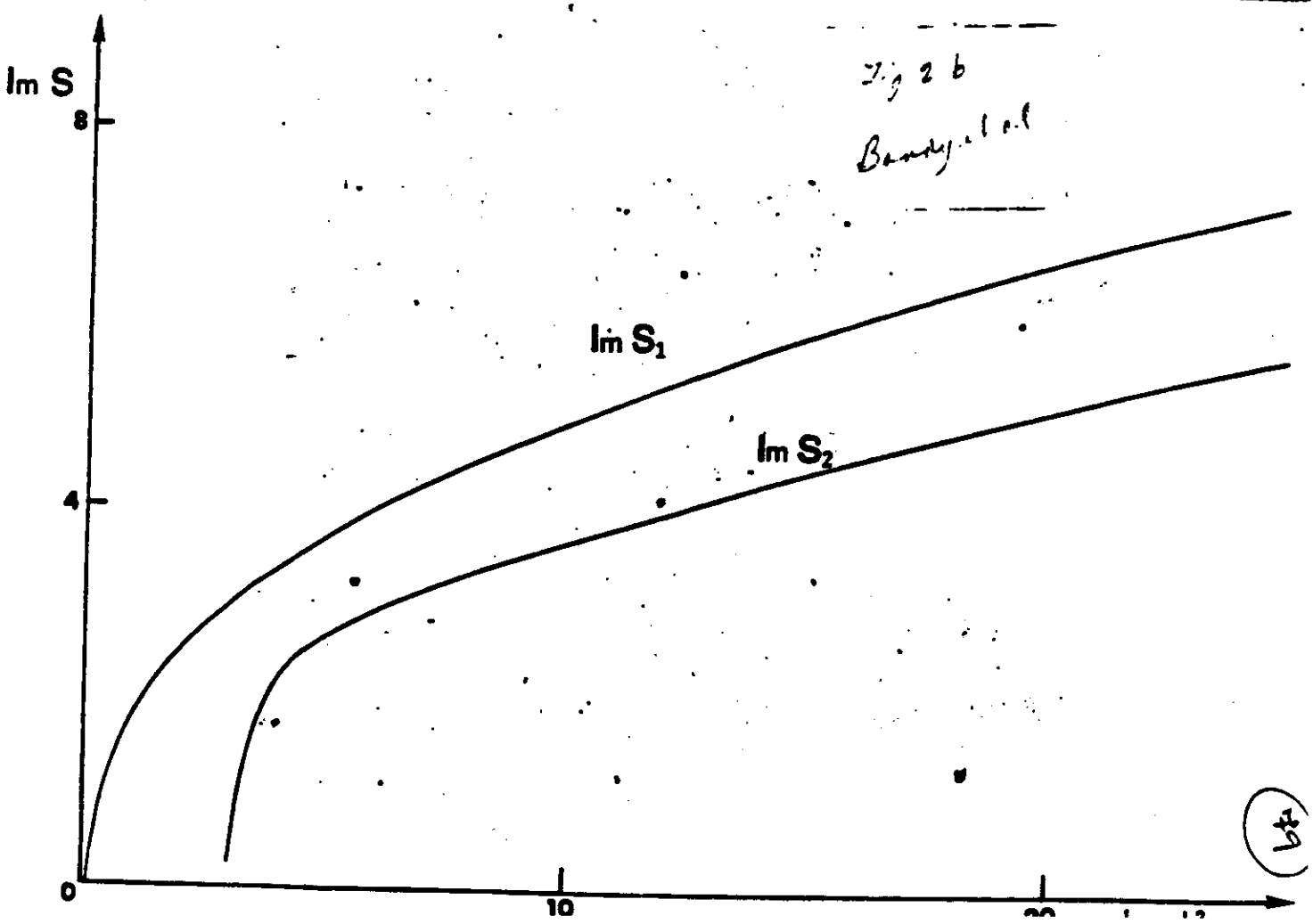

64

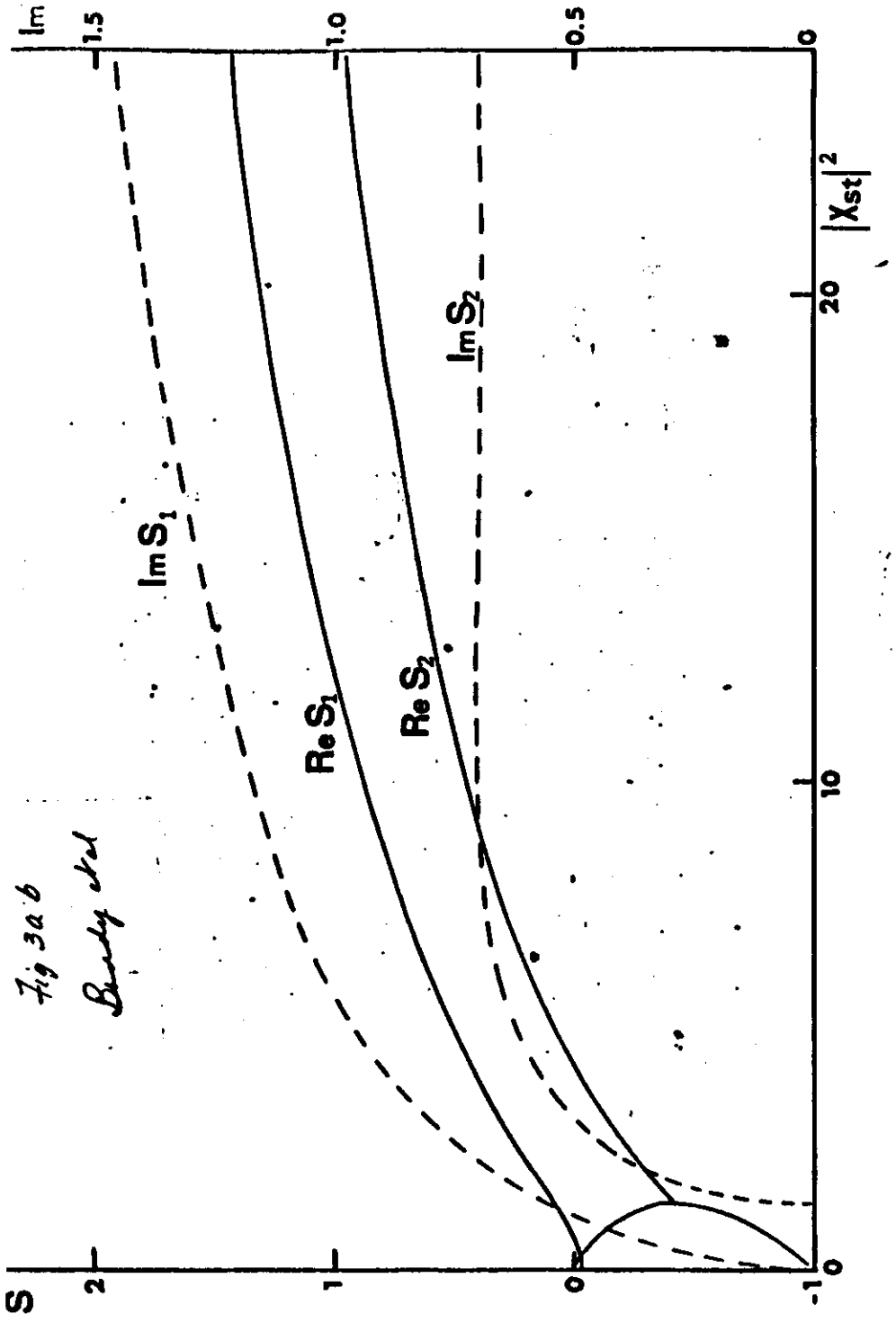

Fig 3a b
Bandy et al

Figure 4
Bandy et al.

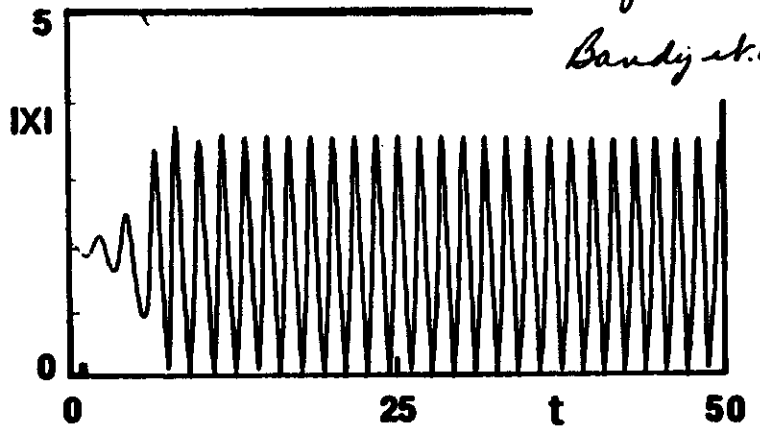

Figure 5
Bandy et al.

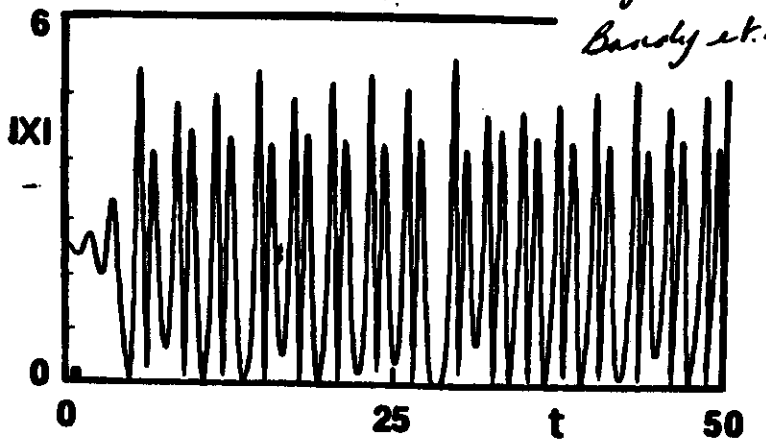

Figure 6
Bandy et al

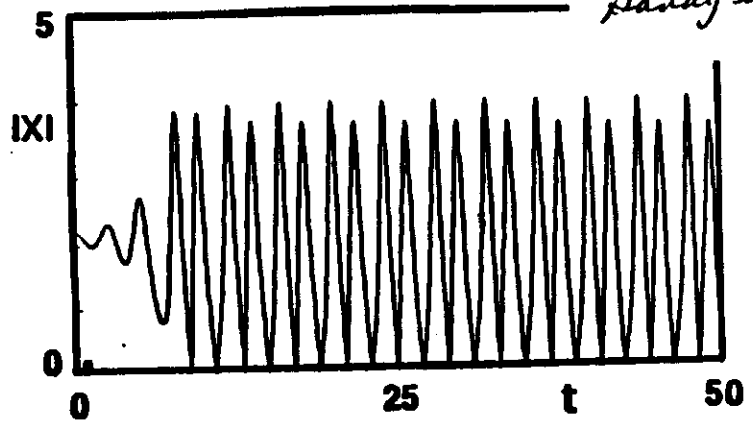

Figure 7
Bandy et al.

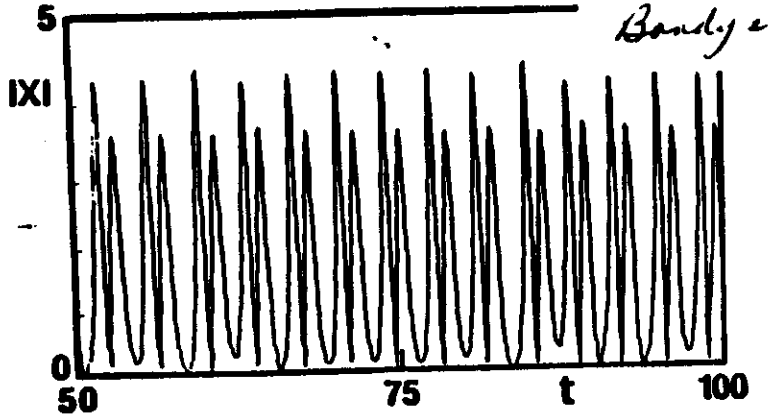

Figure 9
Bandy et

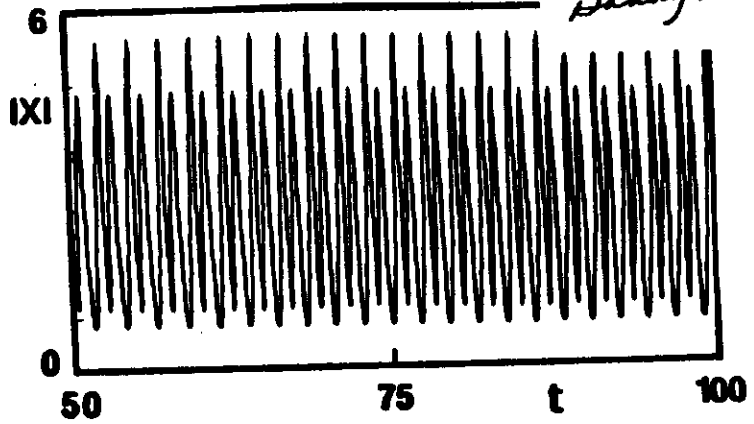

Figure
Bandy et

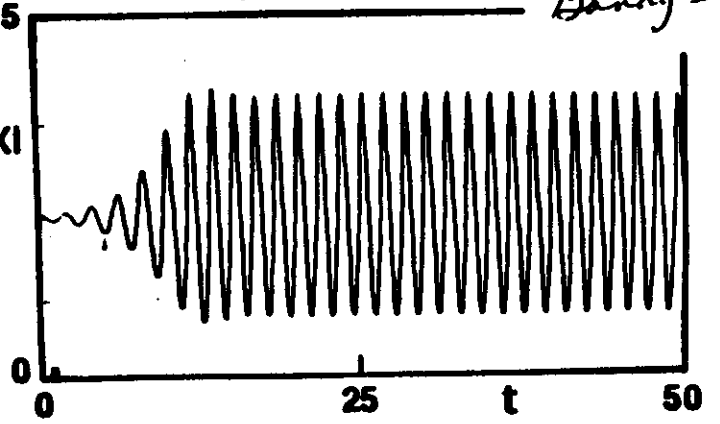

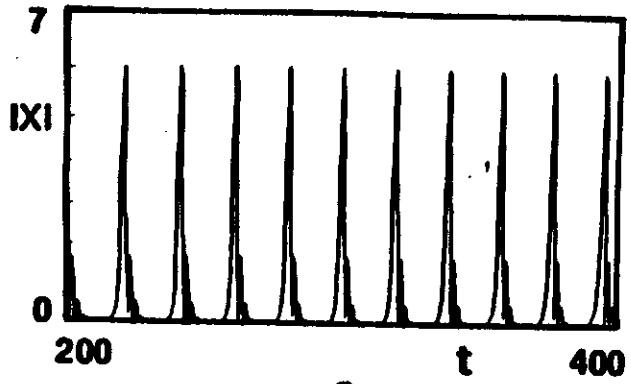

Figure 10a
Bandy et.al.

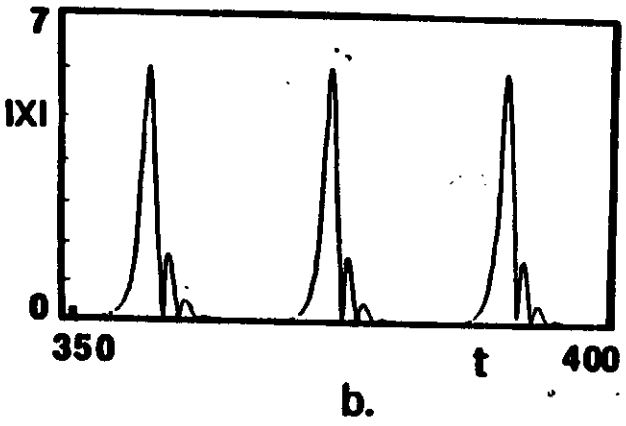

Figure 10b
Bandy et.al.

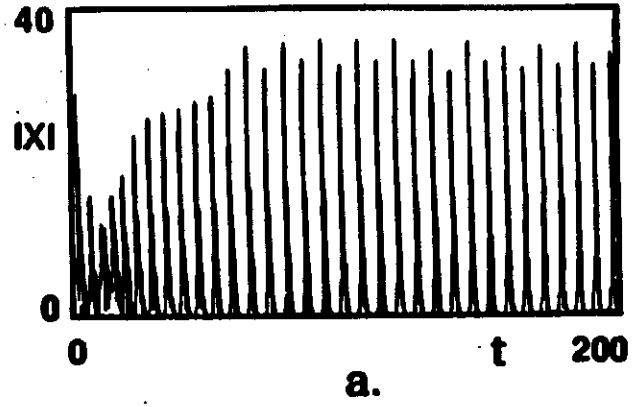

Figure. 11a
Bandy et.a

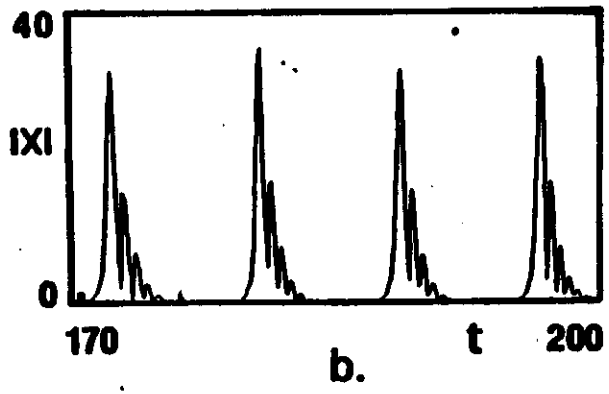

Figure. 11b
Bandy et.

Figure 12
Bondy et al.

L.A. Lugiato - Selected References

1) L.Allen and J.H.Eberly, Optical Resonance and Two-Level Atoms, Wiley, New York 1975.

2) H.Haken, Synergetics - An Introduction, Springer-Verlag, Berlin 1977.

3) O.Svelto, Principles of Lasers, Plenum Press, New York 1982.

4) D.Ruelle, Strange Attractors, Le Recherche n.108, February 1980.

5) R.Bonifacio (ed.), Dissipative Systems in Quantum Optics, Topics in Current Physics n. 27, Springer-Verlag, Berlin 1982.

6) E.Abraham and S.D.Smith, Optical Bistability and related devices, Rep.Progr.Phys. 45, 815 (1982).

7) L.A.Lugiato, Theory of Optical Bistability, in Progress in Optics, Vol. XXI, ed.by E.Wolf, North-Holland 1984.

8) Articles by N.B.Abraham and by L.Casperson in Laser Physics, Lecture Notes in Physics n.182, ed.by J.Harvey and D.F.Walls, Springer-Verlag 1983.